CANADIAN THESES ON MICROFICHE

THÈSES CANADIENNES SUR MICROFICHE

National Library of Canada
Collections Development Branch

Canadian Theses on
Microfiche Service

Ottawa, Canada
K1A 0N4

Bibliothèque nationale du Canada
Direction du développement des collections

Service des thèses canadiennes
sur microfiche

NOTICE

The quality of this microfiche is heavily dependent upon the quality of the original thesis submitted for microfilming. Every effort has been made to ensure the highest quality of reproduction possible.

If pages are missing, contact the university which granted the degree.

Some pages may have indistinct print especially if the original pages were typed with a poor typewriter ribbon or if the university sent us an inferior photocopy.

Previously copyrighted materials (journal articles, published tests, etc.) are not filmed.

Reproduction in full or in part of this film is governed by the Canadian Copyright Act, R.S.C. 1970, c. C-30. Please read the authorization forms which accompany this thesis.

AVIS

La qualité de cette microfiche dépend grandement de la qualité de la thèse soumise au microfilmage. Nous avons tout fait pour assurer une qualité supérieure de reproduction.

S'il manque des pages, veuillez communiquer avec l'université qui a conféré le grade.

La qualité d'impression de certaines pages peut laisser à désirer, surtout si les pages originales ont été dactylographiées à l'aide d'un ruban usé ou si l'université nous a fait parvenir une photocopie de qualité inférieure.

Les documents qui font déjà l'objet d'un droit d'auteur (articles de revue, examens publiés, etc.) ne sont pas microfilmés.

La reproduction, même partielle, de ce microfilm est soumise à la Loi canadienne sur le droit d'auteur, SRC 1970, c. C-30. Veuillez prendre connaissance des formules d'autorisation qui accompagnent cette thèse.

THIS DISSERTATION
HAS BEEN MICROFILMED
EXACTLY AS RECEIVED

LA THÈSE A ÉTÉ
MICROFILMÉE TELLE QUE
NOUS L'AVONS REÇUE

NL 339 (r. 85/09)

Canada

MODELLING MIXING PATTERNS

IN STORMWATER RETENTION PONDS

by

Michel C. Beland
Civil Engineering Department
University of Ottawa
Ottawa, Ontario
K1N 9B4

A thesis
presented to the University of Ottawa
in partial fulfillment of the
requirements for the degree of
Master of Applied Science
in
Civil Engineering

Ottawa, Ontario

December, 1984

UNIVERSITÉ D'OTTAWA
UNIVERSITY OF OTTAWA

ACKNOWLEDGEMENTS

The author expresses his sincerest appreciation to the supervisor of his thesis, Dr. Ronald L. Droste, for his guidance, assistance and encouragement during this study.

Special appreciation is expressed to Dr. R.G. Warnock and Dr. D.R. Townsend for their advice on the scaling aspects presented in this work.

The author would also like to thank Mr. Francisco Aposaga and Mr. Robert Moore for their technical support and assistance with laboratory analysis.

Deep appreciation is felt for my wife, Barb, for her continued support throughout this project and for the typing of the thesis.

Financial assistance for this research was supplied by a grant from the National Research Council, grant # NSERCA 0993.

ABSTRACT

Stormwater treatment ponds have proven to be an effective method of reducing storm-related pollutant loadings on receiving water bodies. Reduction of pollution is achieved by dilution of shock loads as well as by providing a detention volume in which the pollutants are allowed to settle and decay.

The objectives of this study were to characterize mixing patterns, which influence time for treatment, at various length to width ratios, widths of inlet and outlet channels and various flow rates in rectangular ponds.

Many models have been proposed and used in evaluating the treatment efficiency of these ponds. Unfortunately, many are too simplistic and ignore the actual mixing phenomena; or too complicated, and require much experience and knowledge on the part of the modeller. To alleviate these problems, a review of various mixing models was performed. A three-parameter model developed for stabilization ponds was chosen and found to best describe the actual physical mixing pattern in rectangular stormwater retention ponds. The physical model which had a small depth, promoted two dimensional flow, which accounts for the major influences on mixing. The model combines a central active dispersed flow zone and recirculating completely-mixed side sections. Theory was developed and verified to provide a deterministic approach to replace the trial and error method of evaluating

the model's parameters. This enables a modeller to predict flow patterns and effluent concentrations of pollutants given their decay rates. The model's parameters are best derived from the peak concentration and from the ratio of recycled dye to unrecycled dye on the output dye tracer curves.

Model studies were performed following the Froude Law criteria while maintaining turbulent conditions. It was noted that in some instances an exaggerated model may be necessary. Dye tracer curves were obtained for various flow rates, length to width ratios and width of inlet and outlet channels. These curves were then analysed and reproduced by a computer program using a Crank-Nicholson finite difference formulation of the governing partial differential equation.

The principal findings of the model studies are that the width of the active zone increased as the length to width ratio increased, as the width of the inlet and outlet channel increased, and as the flow rate increased. Also, it was found that the dilution ratio in the active zone of the model increased as the length to width ratio increased and as the width of inlet and outlet channels decreased. The dilution ratio appeared to be independent of flow rate. The dispersion coefficient increased as the flow rate increased and as the width of the inlet and outlet channels increased.

I hereby declare that I am the sole author of this thesis. I authorize the University of Ottawa to lend this thesis to other institutions or individuals for the purpose of scholarly research.

Michel C. Beland

I further authorize the University of Ottawa to reproduce this thesis by photocopying or by other means, in total or in part, at the request of other institutions or individuals for the purpose of scholarly research.

Michel C. Beland

The University of Ottawa requires the signatures of all persons using or photocopying this thesis. Please sign below, and give address and date.

TABLE OF CONTENTS

LIST OF TABLES

LIST OF FIGURES

GLOSSARY

C = mass concentration of substance, Chezy's coefficient
C_A = mass concentration of unrecycled dye
Co = area under the dye mass concentration versus reduced time curve, initial concentration
Co_A = area under the unrecycled dye mass concentration versus reduced time curve
CM = complete mix reactor
D = model's depth (m)
D_P = prototype depth (m)
Ds = dilution ratio
E = dispersion coefficient (m^2/s)
E_A = dispersion coefficient in active zone (m^2/s)
F = dimensionless dispersion coefficient
g = gravitational constant (m/s^2)
K = von Karman's constant
k = model's equivalent roughness size (diameter of roughness elements) (m)
Kp = prototype's equivalent roughness size (m)
L = length of basin (m)
Lc = characteristic length (m)
Lr = length scaling ratio
m = number of concentration values
M_R = mass of recycled dye
M_T = total mass of dye
n = model's Manning's roughness coefficient ($s/m^{1/3}$)
Nf = Froude number
Np = prototype's Manning's roughness coefficient ($s/m^{1/3}$)
Nr = Reynolds number
Nr(min) = minimum Reynolds number
PF = plug flow
Q = flow rate (m^3/s)
Q_A = flow rate in active zone (m^3/s)
Q_R = flow rate in recycle zone (m^3/s)
R_h = model's hydraulic radius (m)
R_{hA} = hydraulic radius of the active zone (m)
Rp = prototype's hydraulic radius (m)
Rr = ratio of prototype's hydraulic radius to model's hydraulic radius to the total volume
S = slope of energy grade line (m/m)
s^2 = variance of output dye tracer curve in reduced time
s_A^2 = variance of output dye tracer curve
S_E = standard error of estimate
t = time (s)

T_d = detention time (s)
T_{dA} = detention time in active zone (s)
Tp = time to peak (s)
Tp_A = time to peak in the active zone (s)
U = average flow through velocity (m/s)
U* = bottom shear velocity (m/s)
U_A = flow velocity in active zone (m/s)
V = volume of basin (m), flow velocity (m/s)
V_A = volume of active zone (m^3)
V_R = volume of recycled zone (m^3)
W = model's width (m)
W_A = width of the active zone (m)
Wp = width of prototype (m)
$W_{CHANNEL}$ = width of the model channel (m)
x = distance (m)
Xr = horizontal length scaling ratio
Yr = vertical length scaling ratio

β = ratio of the volume of the active zone
ν = kinematic viscosity (m^2/s)

CHAPTER I

INTRODUCTION

For many years, it has been recognized that urbanization increases the peak flows and the amount of pollutants associated with storm runoff. Stormwater retention ponds (SWRP) have been used with success in attenuating peak flows by temporarily storing runoff. It has also been recognized that these ponds can reduce the amount of pollutants associated with this runoff. Ponds provide a relatively effective method of dealing with runoff because of their low construction and maintenance costs.

Routing rainfall runoff through a pond has been shown to decrease total suspended solids, biochemical oxygen demand (BOD), bacteria and nutrient loadings on the receiving water body, thereby increasing its overall quality. The effectiveness of ponds in treating stormwater has led to the use of stormwater treatment ponds, (SWTP); that is, ponds which are built primarily for mitigating the impacts of runoff pollutants. Reduction of peak flows by these ponds is of secondary importance.

Ponds vary in nature from underground storage tanks to flooded urban lakes. Accordingly, there is great

variability in the geometry of SWTP's, size and their design peak flow. Ponds may be operated as batch processes, or in continuous mode. In continuous mode, the inflow may be steady state or vary with time.

Ponds are an efficient way to reduce storm-associated pollution by providing a detention time which is large enough to allow BOD exhaustion and bacterial dieoff. Also, flow rates and degree of turbulence are low in ponds, thus providing a medium in which suspended solids and nutrients can settle out of the runoff.

Of major importance in the design of SWTP is the evaluation of their treatment capabilities. Studies have been undertaken in which researchers have tried to define these by means of trap efficiency curves, or simple mixing models such as the plug flow (PF) model, the completely mixed (CM) model and the dispersed flow PF model. To date, these analytical methods of assessing the efficiency of ponds in treating runoff pollution are overly simple and results are inaccurate. The difficulty lies in assessing parameters such as runoff quality and treatability of the runoff as well as the hydraulic mixing properties of the pond itself.

The quality of stormwater varies depending on such parameters as the season, time interval since the previous storms, magnitude of the previous storms, physical characteristics of the land, the land uses in the watershed and the intensity and duration of the storm. The

treatability of the pollutants is a function of their nature, origin, quantity, degradability and their settling properties.

The parameters that influence the mixing patterns in SWTP are its geometrical shape, length to width ratio, roughness and type of bottom, inflow and outflow rates, type of inflow and outflow structures, the depth of water and the flow rate. These factors ultimately determine how far the pond's mixing pattern is from the ideal conditions of PF or CM. To account exactly for the non-ideal flow conditions in a SWTP requires detailed knowledge of the flow pattern of the fluid within the basin.

The hydraulic mixing properties of SWTP are also related to the density, temperature, and flow velocity of influent water, seasonal conditions, and wind as well as the pond's mode of operation. In the continuous steady state flow mode, an effective and popular characterization of the mixing properties of basins is by the use of output dye tracer curves. From these, one can easily assess the distribution of residence times of all elemental fractions of the influent which is the most important parameter for determining the pond's capability of treating BOD and bacterial loads. In determining a pond's ability to settle suspended solids and nutrient loads, it is required to know the flow velocities since it is this factor along with the degree of turbulence which controls the rate of settling.

Two more very important parameters to quantify in SWTP are the amount of dead space and short-circuiting that exist under specific conditions. If these are neglected, serious overestimations of a pond's treatment capabilities will result.

The objectives of this research are to characterize the mixing patterns in SWTP by means of a laboratory model. The study has been limited to rectangular ponds of length to width ratios of 3:1, 2:1 and 1:1, with varying widths of the inlet and outlet channels and was conducted at steady flow rates.

The inlet and outlet channels are centered on the longitudinal axis of the pond. This configuration is the most general one although results from these studies cannot be readily extended to other pond configurations.

The depth in the model was maintained small enough to ensure two-dimensional flow which is an improvement over existing one-dimensional models. Three-dimensional flow was not considered. Thus, the effects of density currents, wind currents, channelling, and stratified flow are not investigated. However, lateral and longitudinal transport and mixing are the major influences on dispersion compared to vertical mixing. Therefore, the two-dimensional model is effective.

A suitable mixing model was to be fitted to the laboratory results to define the parameters which allow one to describe the residence time distribution of the effluent

water then, if the treatment kinetics are known, the effluent concentration of a pollutant can be calculated.

The influences of length to width ratio, the width of the inlet and outlet channels and of flow rate on parameters of the mixing model were investigated. The conclusions drawn from these investigations, along with the section on dimensional analysis that is presented enables the extension of this work to actual SWTP, and thus can help in designing more efficient SWTP.

CHAPTER II

LITERATURE REVIEW

2.1 Prototypes

Table 2.1 lists the important parameters obtained from a few SWTP installations. This list is not meant to be exhaustive, but merely to give an overview of the geometries, capacities and peak flow rates of these ponds. It can be easily seen that no correlation among the characteristics of these ponds exists. In some cases, such as in Rolla, Missouri, the pond was developed from an existing lake. The city of Milwaukee built a tank for their stormwater treatment facility.

In this table, the Reynolds number (Nr) is calculated by Eq. (2.1) and the Froude number (Nf) is calculated by Eq. (2.2).

$$Nr = \frac{4\ U\ R_h}{\nu} \qquad (2.1)$$

where: U = flow velocity (m/s)
R_h = hydraulic radius (m)
ν = kinematic viscosity (1.5×10^{-6} m^2/s at 5°C)

$$Nf = \frac{U}{(g\ D)^{1/2}} \qquad (2.2)$$

where: D = depth of water (m)
g = gravitational constant (9.81 m/s^2)

Table 2.1: Important Parameters of Some Stormwater Treatment Ponds

Pond	Kennedy-Burnett Pond[28]	City of Milwaukee[30]	Hawley, Bondelid & McCuen[19]	Rolla, Missouri[32]
Length:Width Ratio	18:1	5:1	1:1*	1:1*
Length (m)	422	128	112*	151*
Width (m)	24	23	112*	151*
Depth (m)	2.4	5.0	0.3	1.0
Volume (m^3)	24,600	14,760	3,800	22,710
Surface Area (m^2)	12,870	2,950	12,460	22,710
Cross-Sectional Area (m^2)	58	115	33.5*	
Hydraulic Radius (m)	1.85	3.5	0.3*	
Peak Flow (m^3/s)	3.5	11	7.1	
Peak Velocity(m/s)	0.060	0.096	0.212	
Reynolds Number	296,000	900,000	170,000	
Froude Number	0.0124	0.0137	0.124	

*Assumed values.

2.2 Methods of Analysing Treatment Efficiency of SWTP

2.2.1 Observation Without Any Model

In their paper, Oliver and Grigoropoulos[32] have simply measured the quality of influent stormwater runoff (BOD, TSS, P, N, Hardness) to a small lake and compared these to the quality of the lake's effluent. Although large reductions in pollutant loadings were noticed, no attempt of predicting treatment efficiency for future storms was made.

2.2.1.1 Sediment Trap Efficiency Curves - I

A general method of evaluating treatment efficiency is by use of performance curves[20,45]. These curves relate the amount of sediment trapped in a basin to the inflow rates and as such, these curves are limited in application to the specific pond for which they were drawn. It is impossible to design ponds from these curves as they can only be drawn once the pond has been built. Also, since no information on the detention time can be obtained from these curves, they have no practical use in evaluating pathogen dieoff.

2.2.1.2 Sediment Trap Efficiency Curves - II

This class of sediment trap efficiency curve is distinguishable from the others in that the amount of sediment trapped is related to the surface overflow rate which is the ratio of the basin's area to the outflow rate[41]. Thus, these curves are more general and can be used

for basins in general. However, flow variation will affect the effective surface overflow rate which is not accounted for in their models.

2.2.2 Uniform Flow Velocity

A simple approach to the analysis of the sedimentation process is to apply discrete particle settling theory to a basin assuming a uniform flow velocity[4,17,28]. This assumption overestimates treatment efficiency since it ignores dead space, short-circuiting and turbulent mixing. Chen[8], however, deals with the turbulent mixing factor by applying the Camp-Dobbins[4] model for discrete particle settling under turbulent conditions.

2.2.3 Completely-Mixed and Dispersed Flow

Medina *et al.*[29] proposed various possibilities for flow conditions in SWTP:

(1) CM, constant volume,

(2) CM, variable volume,

(3) dispersive variable volume.

The latter which is a more likely representation of flow conditions in SWTP implied a discrete convolution of the variable dispersive term and concentrations as the volume and the inflow rate of the basin change with time. This model ignores dead space and, therefore, assumes all ponds of the same volume to behave in the same manner.

Chapter III

THEORY

3.1 Introduction

The SWTP's studied were rectangular in shape with inflow and outflow channels centered on the longitudinal axis of the pond. The general shape of the flow patterns for ponds of this configuration is shown in Fig. 3.1.

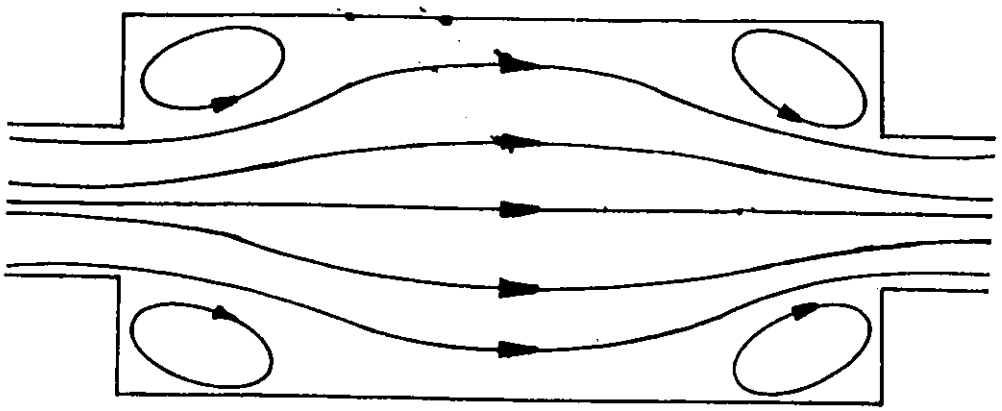

Figure 3.1 Typical Flow Pattern of Rectangular Ponds

Corner circulation is inherent in these ponds. This circulation was described by Abbott and Rasmussen[1] as follows:

> "Since the flow discharge across any section is proportional to the velocity while the resistance is proportional to the square of the velocity, it follows that the flow tends to transform from a flow that is uniformly distributed across its ingoing domain boundary to a flow that is uniformly distributed across its outgoing domain

> boundary. ... However, by virtue of the inertia introduced in the model through the convective momentum terms, the flow cannot follow the wall to the left of the expansion but must expand to meet the wall further along the flow. ... so that a reverse flow is induced along the wall to provide the circulation."

The inflow enters the pond at a relatively high velocity and goes through a jet-type expansion in which significant dispersion of the pollutants occurs. During this expansion, some fluid from the circulation zone flow is entrained. Following this expansion, the main stream continues down the basin where it is subjected to more mixing due to lateral, vertical and turbulent diffusion. As the stream approaches the outlet channel, it is partly contracted and partly split. The part that has split from the stream returns in the recirculation zone.

3.2 The One-Dimensional Conservation of Mass Equation

The one-dimensional conservation of mass equation for a constant flow velocity and a uniformly shaped channel for a conservative substance C can be written as:

$$\frac{\partial C}{\partial t} = - U \frac{\partial C}{\partial x} + E \frac{\partial^2 C}{\partial x^2} \qquad (3.1)$$

where U = average flow velocity (m/s)
C = mass concentration of substance
E = dispersion coefficient (m^2/s)
t = time (s)
x = distance along the longitudinal axis (m)
$\frac{\partial C}{\partial t}$ = mass accumulation term
$U \frac{\partial C}{\partial x}$ = convective term
$E \frac{\partial^2 C}{\partial x^2}$ = diffusion term

The mass accumulation term represents the rate of change of mass with time. The convective term represents the movement of the substance due to bulk flow. The diffusion term quantifies the transport of the substance according to Fick's Law. The dispersion coefficient in this case is mainly representative of turbulent diffusion. Since the flow will be maintained in the turbulent regime, the influence of molecular diffusion on the transport phenomena is negligible.

3.3 Mixing Models

There exist sophisticated three-dimensional finite element and finite difference models which attempt to define the flow velocity vectors at numerous points within a basin and from these, calculate the dispersion of pollutants or other substances as they propagate through it. These methods are very difficult to verify practically and their results are difficult to analyse.

Common practise in evaluating the performance of chemical reactors is to use a suitable mixing model to characterize the mixing pattern in a basin. These models predict the residence times of matter in reactors by making various general assumptions on the flow pattern.

The different mixing models ultimately lead to output residence time curves from which one can readily determine the treatment efficiency of a pond given the reaction model. Today, there exists a vast choice of mixing models varying

in basic principles and in complexity with which one can model most physical situations. The choice of the proper model for the situation must be based on its suitability and its representation of the actual mixing process, while taking into consideration its level of complexity. Other hydrodynamic models worth mentioning are Schamber and Larock's[30] model and Imam and McCorquodale's[23] model. These models are two-dimensional mathematical solutions of velocity profiles in a vertical plane from which the amount of sedimentation can be calculated.

In general, it can be stated that the complexity of a mixing model is directly related to its accuracy of simulating the actual pond's mixing process. However, it is also true that the more complex the model, the more input parameters it requires. As the number of parameters increases, more sophisticated and computationally expensive solution techniques are required.

To choose the most suitable model, a detailed study of them is required. The theory presented below follows procedures outlined in Grady and Lim[14], Levenspiel[24], and Levenspiel and Bischoff[20]. Models utilized to describe reactors can be classified under the following types:

1. PF model,
2. CM model,
3. dispersion model,
4. CM tanks in series model,
5. combined model.

The important characteristics of these models will be briefly discussed.

3.3.1 Plug Flow Model

The PF model assumes that each unit volume of water travels in single file through the basin. Each elemental volume remains in the basin for exactly one detention time. The detention time, T_d, is defined as the volume of the basin divided by the flow through rate. The response output tracer curve for an instantaneous slug of dye from a PF basin is shown in Fig. 3.2. The slug input of dye will tend to propagate through the reactor at the same speed as the fluid and leave the reactor all at once, with very little dispersion, at a time after input equal to T_d. Also shown in Fig. 3.2 is the response output tracer curve

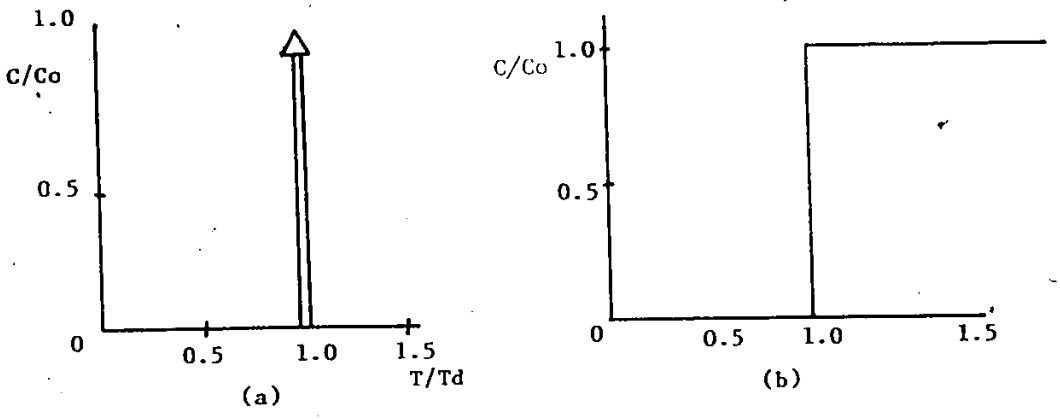

Figure 3.2 Output Dye Tracer Curves for the Plug Flow Model
[(a) Response to a Slug of Dye;
(b) Response to an Input Step Function]

for an input step function. No dye will be detected in the outflow from the reactor until a time equal to T_d.

3.3.2 Completely-Mixed Model

The CM and PF models represent the two simplest mixing models. In a CM model, a unit incoming volume is assumed to be instantaneously dispersed throughout the entire volume of the basin. The detention time of each elemental volume varies although the average detention time is the same as in the PF basin. The response output tracer curve for a slug input of dye is also shown in Fig. 3.3. Since the dye is instantaneously dispersed throughout the volume of the reactor, a portion will immediately leave with the outflow. The output dye concentration will decrease

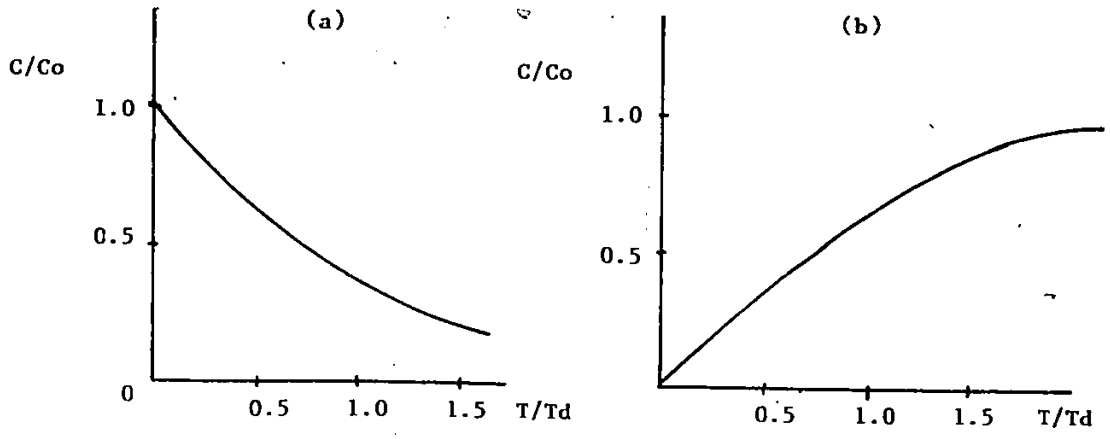

Figure 3.3 Output Dye Tracer Curves for the Completely-Mixed Model [(a) Response to a Slug of Dye; (b) Response to an Input Step Function

exponentially with time.

Also shown in Fig. 3.3 is the response output tracer curve for an input step function to a CM reactor. In this case, it is seen that the concentration of dye leaving the reactor increases exponentially with time. At a time equal to the reactor's detention time, the concentration is equal to 63% of the inflow concentration.

3.3.3 Dispersion Model

The dispersion model is a variation of the PF model in that the slug of dye is assumed to diffuse or disperse as it travels through the vessel. The value of the dispersion coefficient defines the degree of mixing in the vessel. In Fig. 3.4, the effects that the dimensionless dispersion coefficient (F) has on the output tracer curve are shown. It should be noted that as the dispersion coefficient increases, the output tracer curve approaches the CM model curve. Also, a dispersion coefficient of zero results in a PF model. The PF and CM regimes represent the extremes in mixing conditions.

3.3.4 Completely-Mixed Tanks in Series Model

In this model, the total volume of the vessel is simulated by a series of CM tanks of equal volume. The

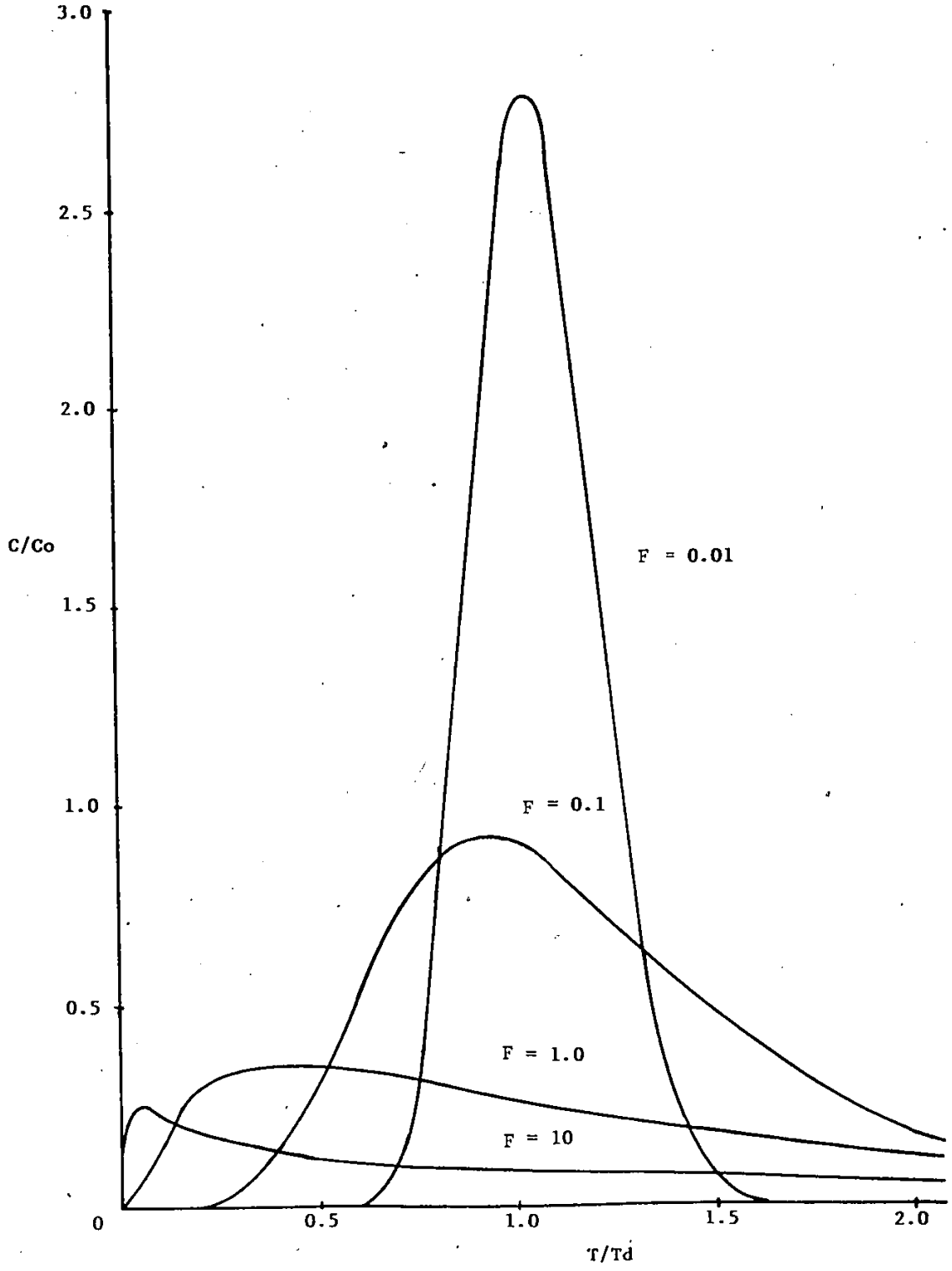

Figure 3.4 Output Dye Tracer Curves to a Slug Input for Various Values of the Dispersion Coefficient of the Dispersion Model

number of tanks to be used depends on the shape of the output tracer curve. In Fig. 3.5, the relationship between the number of tanks in series and the output dye tracer curve is clearly illustrated. As the number of tanks increases, the output dye tracer curve resembles more closely the PF reactor tracer curve. Any degree of dispersion may be represented by dividing the total volume into the appropriate number of CM volumes. If dispersion is uniform throughout the reactor, then each CM tank will have the same volume. If the mixing (dispersion) is not uniform, the CM tanks will have various volumes.

3.3.5 Combined Model

Combined models are mixing models in which one or more of the previous models are combined with short-circuiting and/or deadwater volume to approximate more accurately the true output dye tracer curves. Short-circuited flow is flow which entirely bypasses the basin and appears immediately in the outflow. The deadwater volume of a basin is that portion of the reactor in which no dye enters or leaves. A basin with deadwater volume is similar to a basin with no deadwater but whose volume is smaller by an amount equal to the volume of the deadwater zone. Some of the more notable work in this area follows.

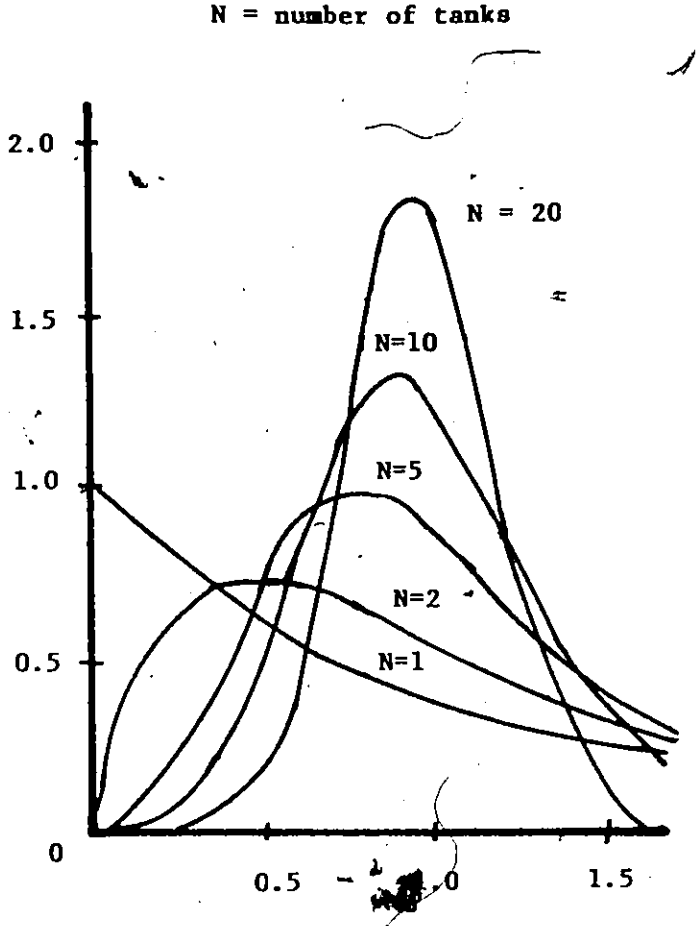

Figure 3.5 Output Dye Tracer Curves to a Slug Input for the Completely-Mixed Tanks in Series Model[26]

3.3.5.1 Wolf and Resnick's Models

These researchers[47] have defined analytical solutions for residence time distributions in PF and CM reactors subject to any combination of the following irregularities:

a) dead space

b) short-circuiting

c) error in average residence time determination

d) lag in response.

Also, the system's volume may be split into varying amounts of PF and CM fractions.

3.3.5.2 Cholette and Cloutier's Model

In their paper, Cholette and Cloutier[9] investigated different arrangements of partial mixing with PF and short-circuiting. The most popular configuration they proposed is shown in Fig. 3.6. This model combines a CM and a dead-water region with a portion of the inflow being short-circuited.

3.3.5.3 Finite Stage Model

Hovorka[22] and Alder[2] have developed this model which combines networks of modules made up of a CM zone, a PF zone and a slow-mixed zone. The slow-mixed zone is considered CM and to be slowly interchanging fluid with the CM zone. Numerous non-ideal flow situations may be represented by varying the number, the volume and the interchange flow rate in each of the zones. A typical representation is shown in

Fig. 3.7. Hovorka and Alder both state that the finite stage model's parameters have physical significance. Any level of dispersion can be modelled by varying respective sizes of the CM and PF zones. To date, however, no predictive method of assessing the parameters exists without performing tracer studies on the pond in question. The PF representation of the entrance condition is not tenable when it is known that this area is subjected to a jet-type expansion of the inflow which is more like a CM situation.

3.3.5.4 Levenspiel's Model

This model[27], which is presented in Fig. 3.8, is divided into two zones: one in which flow passes fairly rapidly (active zone) and the other where flow travels very slowly (dead zone). The model can represent the mixing in reactors whose output dye tracer curves are characterized by a high early peak followed by a long tail.

3.3.5.5 Ryan and Harleman Models

Ryan and Harleman[37] have presented two models to represent flow patterns in cooling ponds which could be used to gauge their performance. The first model (shown in Fig. 3.9) divides the flow into two regions: a CM section followed by a PF section.

The other model is shown in Fig. 3.10. The volume of the pond is divided into three longitudinal sections. The central section is termed the active zone in which the fluid

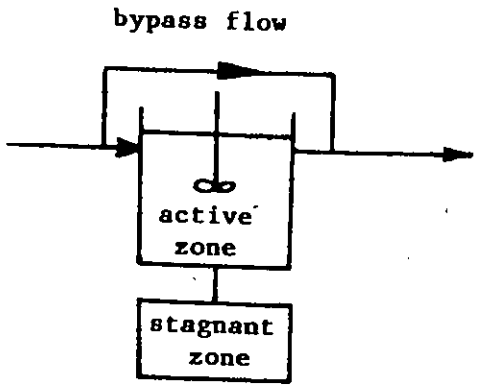

Figure 3.6 Cholette and Cloutier Model

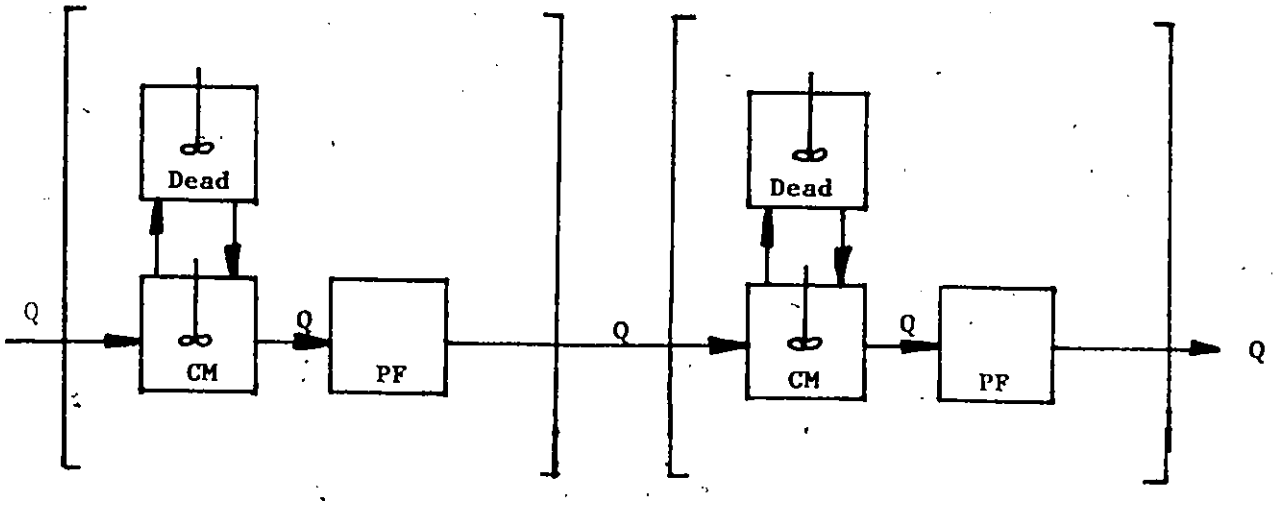

Figure 3.7 Finite Stage Model (CM = completely-mixed; PF = plug flow)

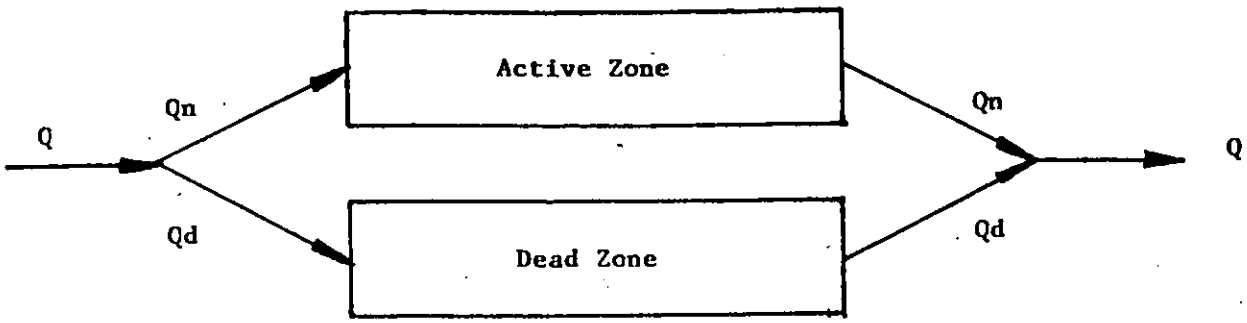

Figure 3.8 **Levenspiel Model**

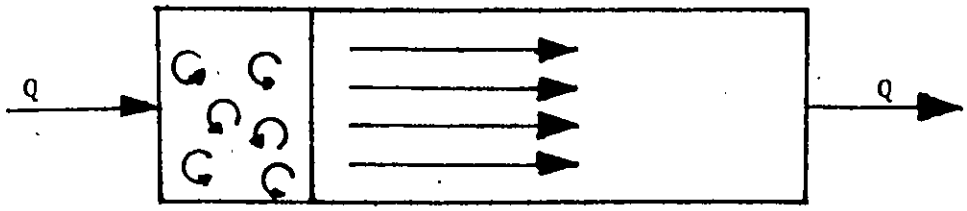

Figure 3.9 **Ryan and Harleman Model**

travels relatively quickly and is modelled according to the dispersion model. The side sections are recirculating zones in which the fluid travels in the opposite direction and is continuously interchanged with fluid in the central zone.

3.3.5.6 Ferrara and Harleman's Model

The second model of Ryan and Harleman presented above was subsequently refined by Ferrara and Harleman[14], who successfully applied it to waste stabilization ponds. They found very good reproduction of the output dye tracer curves could be achieved by limiting the interaction between the different zones to the inlet and outlet of the active zone. They also found the dispersion in the recycle zones to be so high, that practically speaking, it could be modelled as CM. These simplifications have the benefit of reducing the number of parameters to be determined to use the model.

This simplified model is shown in Fig. 3.11. The active zone is narrow relative to the basin's width and handles a flow rate larger than the inflow rate, thus, the diffusing substance appears at the outlet in a shorter time than predicted by the PF or dispersed flow models. Also, some of the tracer enters the CM recycle zones and slowly re-enters the active zone. The model is very applicable to ponds whose dye output tracer curves are characterized by an early peak followed by a long tail.

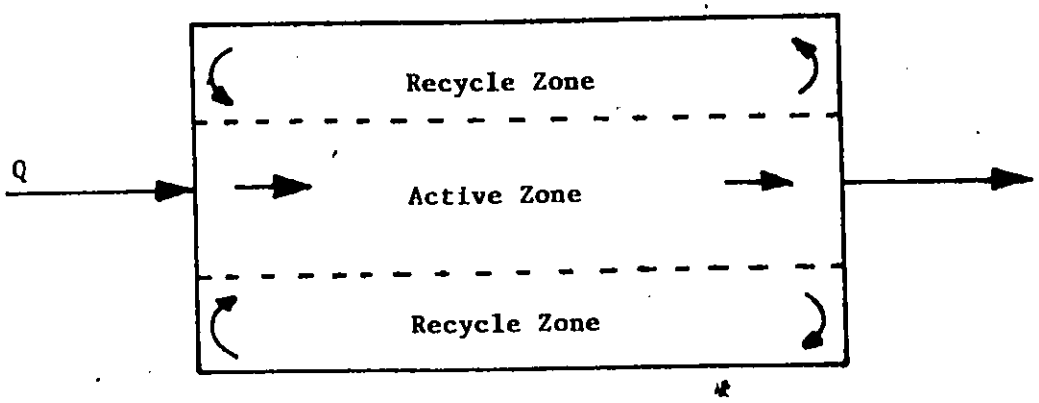

Figure 3.10 **Ryan and Harleman. Recycle Model**

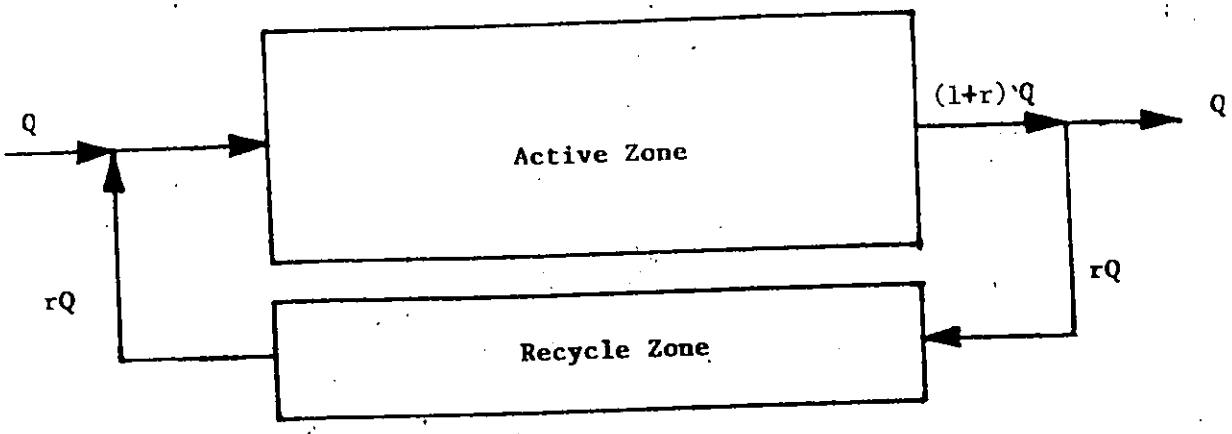

Figure 3.11 **Ferrara and Harleman's Model**

3.4 Mixing Model Chosen for Simulation

To simulate the output dye concentration curves, it was desirable to employ a mathematical model that meets the following criteria:

1) ability to reproduce experimental output dye concentration curves.
2) physically meaningful parameters.
3) parameters for the scaled pond should be applicable to prototype ponds.
4) easy to apply.

It is believed that the model used by Ferrara and Harleman[14] best meets these criteria. The model employs an active zone with recirculating zones which can be combined.

The model's parameters are:

1) width of the active zone.
2) amount of circulation.
3) dispersion coefficient in the active zone.

The first two parameters physically represent the flow pattern whereas the dispersion coefficient defines the degree of mixing in the active zone. Thus, the model does meet the criteria of physically representing the mixing pattern in the pond, described in Fig. 3.1.

The model is also easily applied when one of the parameter estimation techniques presented later is used. The parameters can then be inserted into Ferrara and Harleman's steady state solution for treatment efficiency of a substance which has a first order decay rate[14]. Under

these conditions, the need for finite difference simulations of the dye tracer curves is eliminated.

It should also be noted that these types of models with central active zones and "dead" CM side zones, have been successfully applied to natural streams[5].

In Section 3.5, it will be shown how results from these model studies can be extended to full-size SWTP's.

3.4.1 Detailed Model Description

A general description of the model was presented in Section 3.3.5.6. Under steady-state conditions, the inflow is assumed to be instantaneously mixed with recycle flow at the inlet to the active zone. The resulting stream travels down the active zone and is subjected to axial dispersion. At the end of the active zone, the flow is split: an amount equal to the inflow rate exits the pond and the remainder returns into the recycle zone where it is assumed to instantaneously mix throughout that zone. This assumption was used by Ferrara and Harleman to model stabilization ponds. Since flow rates in a SWTP are normally much higher than in a stabilization pond, Reynolds numbers in the recycle zones will be higher, thereby increasing the validity of the assumption of CM conditions there.

3.4.1.1 Boundary Conditions

For axial dispersion along the longitudinal axis only, the one-dimensional conservation of mass equation (Eq.

(3.1)) applies to the active zone (subscript A added to indicate this).

$$\frac{\partial C_A}{\partial t} = E_A \frac{\partial^2 C_A}{\partial x^2} - U_A \frac{\partial C_A}{\partial x} \qquad (3.1)$$

The boundary conditions to be satisfied have been discussed in Ferrara and Harleman[13] and Wehner and Wilhelm[44]. At the inlet, a concentration discontinuity exists such that the concentration on the upstream side of the inlet boundary [*i.e.*, $C(0^-)$] is equal to the concentration of the dye on the downstream side of the boundary [*i.e.*, $C(0^+)$] minus the rate at which the dye is diffusing away from the boundary:

$$C(0^-) = C(0^+) - \frac{E_A(0^+)}{UL} \frac{\partial C(0^+)}{\partial x} \qquad (3.2)$$

where L = length of the basin

No dye diffusion is assumed to occur on the upstream side of the boundary.

At the outlet, the boundary condition is set up so that the concentrations of dye on either side of the boundary are equal. Since it is again assumed that no diffusion takes place on the downstream side of the boundary, the boundary condition also implies that no diffusion takes place on the upstream side of the boundary:

$$C(L^-) = C(L^+) \qquad (3.3)$$

Therefore,

$$\frac{E_a(L^-)}{UL} \frac{\partial C(L^-)}{\partial x} = 0 \qquad (3.4)$$

3.4.1.2 Dispersion in the Active Zone

Several formulae have been developed to estimate the dispersion coefficient under various flow conditions[12,15,43]. The one most suitable in this case[13] is Fischer's expression.

$$E\ (m^2/s) = 0.225 \frac{U^* L_c^2}{K^2 R_h} \qquad (3.5)$$

where U^* = bottom shear velocity (m/s)
L_c = characteristic length (m)
K = von Karman's constant = 0.4

The essence of Ferrara and Harleman's[13] arguments for using Fischer's equation are as follows. This equation was developed for application in natural streams where higher flow velocities exist in the central portion of the stream than along the banks. The flow pattern in the laboratory model, with its fast flowing central active zone and slow return flow zones, is similar.

3.4.1.3 Mathematical Formulation of the Model

The following parameters must be defined to solve the one dimensional conservation of mass equation:

1) volume of the basin (length, width, depth);

2) volume of the active and recycle zones;

3) inflow rate and flow rates in the active and recycle zones;

4) dispersion coefficient in the active zone.

The volume of the basin and the inflow rates are readily obtainable from the laboratory setup. The other parameters are determined by the flow pattern and are expected to vary from one set of conditions to another. However, several relationships already exist among these parameters. The volume of the active zone plus the volume of the recycle zone must be equal to the total volume.

$$V = V_A + V_R \tag{3.6}$$

where V = volume of pond (m^3)
V_A = volume of active zone (m^3)
V_R = volume of recycle zone (m^3)

β is defined to be the ratio of the active zone volume to the total volume:

$$\beta = \frac{V_A}{V} \tag{3.7}$$

The flow rate in the active zone must be equal to the sum of the inflow rate plus the flow rate from the recycle zone.

$$Q_A = Q + Q_R \tag{3.8}$$

where Q_A = flow rate in the active zone (m^3/s)
Q = inflow rate (m^3/s)
Q_R = flow rate of recycle zone (m^3/s)

D_m is defined as a dilution factor which may be expressed as:

$$D_m = \frac{Q_A}{Q} \tag{3.9}$$

The dispersion coefficient in the active zone can be defined by making the proper substitutions into Fischer's equation (Eq. (3.5)). These are:

$$L_c = \frac{W_A}{2} \quad \text{(from Ferrara and Harleman[22])} \tag{3.10}$$

where W_A = width of the active zone (m)

$$U^* = (g\, R_{hA}\, S)^{1/2} \tag{3.11}$$

where R_{hA} = hydraulic radius of active zone (m)
S = slope of energy grade line (m/m)

Substituting Eqs. (3.10) and (3.11) into (3.5) and simplifying, the following expression is obtained for the dispersion coefficient in the active zone:

$$E_A = \frac{1.101126\, S^{1/2} W_A^2}{R_{hA}^{1/2}} \tag{3.12}$$

Another expression for E_A (Eq. (3.14)) may be obtained by substituting Manning's equation (Eq. (3.13)) into the above.

$$S^{1/2} = \frac{U_A \cdot n}{(R_{hA})^{2/3}} \tag{3.13}$$

where U_A = flow velocity in active zone (m/s)
n = Manning's roughness coefficient (s/m$^{1/3}$)

$$E_A = \frac{1.101126\, U_A \cdot n \cdot W_A^2}{R_{hA}^{7/6}} \tag{3.14}$$

The time required to reach the peak output concentration after injecting a slug of dye (Tp) in the pond is the same as the time to peak in the active zone (Tp_A).

$$Tp_A = Tp \tag{3.15}$$

For small values of the dimensionless dispersion coefficient ($F < 0.01$),

where $F = \frac{E_A}{U_A L}$ (3.16)

the time to peak in the active zone is approximately equal to the detention time in the active zone. In Section 3.4.3.1, a method is presented in which the detention time in the active zone is corrected for any dispersion coefficient.

$$T_{dA} = Tp_A \quad (3.17)$$

The detention time in the active zone is also related to the volume and flow rate in the active zone:

$$T_{dA} = \frac{V_A}{Q_A} \quad (3.18)$$

Substituting from Eq.'s (3.7) and (3.9):

$$T_{dA} = \frac{\beta V}{D_m Q} \quad (3.19a)$$

$$= \frac{\beta T_d}{D_m} \quad (3.19b)$$

3.4.2 Ferrara and Harleman's Method of Optimizing the Values of β, D_m and E_A

Ferrara and Harleman[14] employ a trial and error method for finding the correct values of β, D_m and E_A. The detention time in the active zone is initially assumed to be:

$$T_{dA} = \frac{Tp_A}{0.9} \quad (3.19c)$$

Substituting Eq. (3.18) for T_{dA} and solving for V_A:

$$V_A = \frac{Q_A Tp_A}{0.9} \quad (3.20)$$

and using Eq. (3.9) one obtains:

$$V_A = \frac{D_m Q Tp_A}{0.9} \quad (3.21)$$

An initial estimate of D_m is made. Tp_A is known from the experimental output dye tracer curve. Then, Eq. (3.21) can be solved for V_A; Eq. (3.7) for β; and, Eq. (3.14) for E_A. The model is then completely defined and a finite difference solution technique can be used to obtain the output dye tracer curve. Various values of D_m were assumed by Ferrara and Harleman to find the best fit to their experimental data. During this procedure, the relationship between T_{dA} and Tp_A (Eq. (3.19c)) was adjusted as required.

3.4.3 Determination of the Values of β, D_m and E_A

In the conclusions from their work, Ferrara and Harleman[14] express the need for research which may be used to derive predictive relationships for the model's parameters. The trial and error procedure for defining the model's parameters is tedious and lengthy. The following methods for estimating the model's parameters are proposed.

3.4.3.1 Estimation of the Dispersion Coefficient from the Peak Concentration

Levenspiel and Smith[28] have written an article which completely characterizes the dispersion model analytically. Useful mathematical relationships may be extracted from this paper for the active zone which has the characteristics of the dispersion model.

The dispersion coefficient may be estimated from the peak value on the output dye tracer curve:

$$(C_A/C_{oA})_{max} = \frac{\exp\,[1-(F^2+1)^{1/2}/2F]}{2(\pi F)^{1/2}[(F^2+1)^{1/2}-F]^{1/2}} \qquad (3.22)$$

where $(C_A/C_{oA})_{max}$ = largest relative concentration on the output dye tracer curve

C_{oA} is defined as the area under the unrecycled dye concentration versus reduced time curve (Eq. 3.23). Unrecycled dye is defined as the dye that passes through the basin into the outflow via the active zone without ever entering the recycle zone.

$$C_{oA} = \frac{\int_0^{\infty} C_A(t)\,dt}{T_{dA}} \qquad (3.23)$$

Where $C_A(t)$ is the concentration of unrecycled dye in the outflow at any time, t.

At the outset, the detention time of the active zone is not known. However, if T_{dA} is initially assumed to be equal to the time to peak, Eq. (3.22) may be solved for the dispersion coefficient, F. Levenspiel and Smith also present the following equation:

$$\frac{T_{pA}}{T_{dA}} = (F^2+1)^{1/2} - F \qquad (3.24)$$

Substituting for the estimate of F and for the known value of T_{pA} in the above equation leads to a second estimate of T_{dA} which can again be substituted into Eq. (3.23). The above procedure should converge to the proper values of F and T_{dA}.

3.4.3.2 Estimation of the Dispersion Coefficient from the Variance

Also, the variance of the output dye tracer curve may be used to estimate the dispersion coefficient:

$$F = \frac{(8\ s^2+1)^{1/2}-1}{8} \qquad (3.25)$$

Where s^2 is the variance of the output dye tracer curve in reduced time units.

$$s^2 = \frac{s_A^2}{T_{dA}^2} \qquad (3.26)$$

$$\text{Where } s_A^2 = \frac{\int_0^\infty t^2 C_A(t)dt}{C_{A0}} - \frac{\left[\int_0^\infty tC_A(t)dt\right]^2}{C_{A0}} \qquad (3.27)$$

or in finite sums:

$$s_A^2 = \frac{\Sigma\ t^2\ C_A(t)}{\Sigma\ C_A(t)} - \left[\frac{\Sigma tC_A(t)}{\Sigma\ C_A(t)}\right]^2 \qquad (3.28)$$

This method also requires that T_{dA} be known but, again, the same procedure outlined previously in which Eq. (3.24) is used with an initial estimate of T_{dA} equal to Tp_A should converge to the correct values of T_{dA} and F.

It should be noted that in the above two equations a knowledge of the portion of the output dye tracer curve which represents unrecycled dye is required. This requires an estimation of the cut-off point on the curve by the modeller. A cut-off point is used to separate the unrecycled dye from the recycled dye portions of the output dye tracer curve. This is shown in Fig. 3.12 where in one case the cut-off point is easy to determine; and in the

other, it is quite difficult. In this second case, some of the recycled dye appears in the outflow before all of the unrecycled dye has passed through it.

This occurs when the flow pattern is unsymmetrical and there exist small recirculating zones in the corners of the basin. The dye enters these zones and is quickly re-released into the active zone before all of the unrecycled dye passes through the outflow (see Fig. 3.13). Whether or not the dye which enters the small recirculation zones is to be considered part of the unrecycled dye remains a point of contention, however, the fact remains that this portion of the dye can create errors in the estimation of the dispersion coefficient for the active zone.

It is important to determine the cut-off point accurately because it is only the unrecycled dye that should be used in evaluating the dispersion coefficient. It can also be seen that errors in the estimate of the dispersion coefficient would be negligible in the case shown

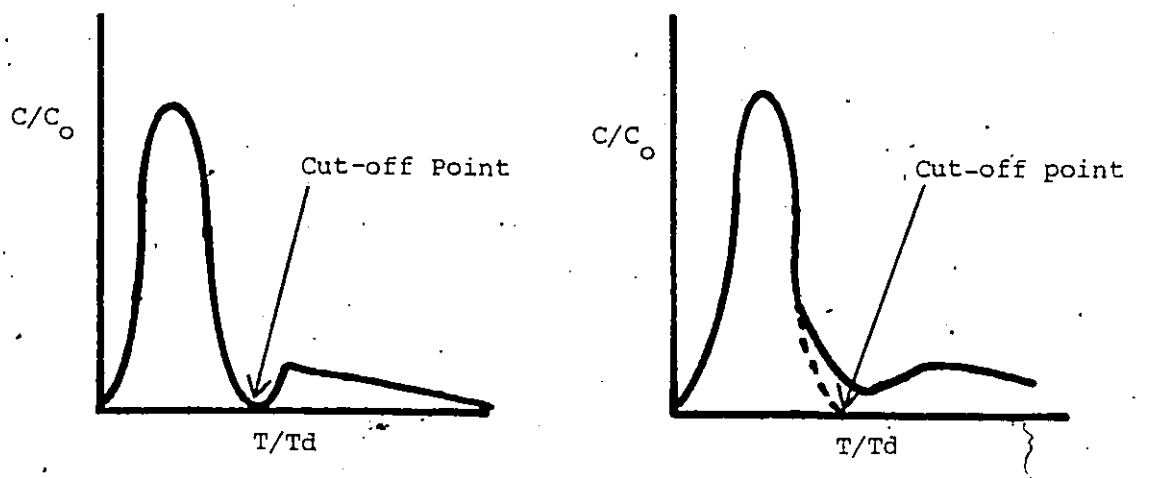

a) Cut-off easily determined b) Cut-off not well-defined

Figure 3.12 Cut-off Point for Unrecycled Dye on the Output Dye Tracer Curves

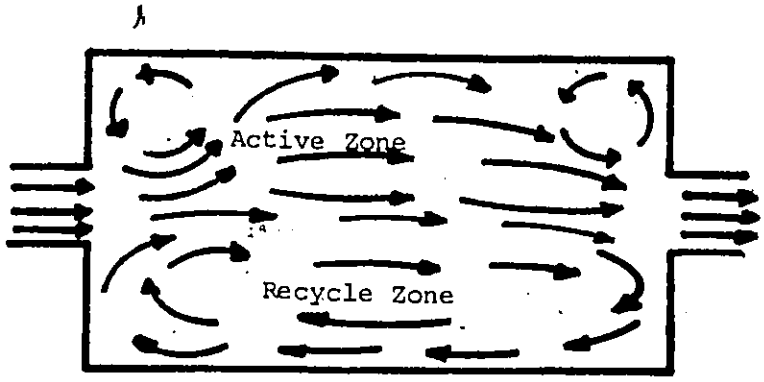

Figure 3.13 Unsymmetrical Flow Pattern Showing Small Recirculating Zones.

in Fig. 3.12(a), but may become very significant in the case of Fig. 3.12(b). However, if the dispersion coefficient was to be estimated from Eq. (3.22), a fairly accurate value of the dispersion coefficient could be obtained by locating the cut-off point by neglecting the extra recycled mass (see Fig. 3.14). In this method, (C/Co)max is obtained by dividing the maximum dye concentration by the total amount of unrecycled dye, therefore, the relocation of the cut-off point can lead to a more accurate estimate of the dispersion coefficient in the active zone.

At first, this method of locating the cut-off point may seem rather crude, but it should be noted that at small values of the dimensionless dispersion coefficient (F < 0.01) the dye output tracer curve for the unrecycled dye is

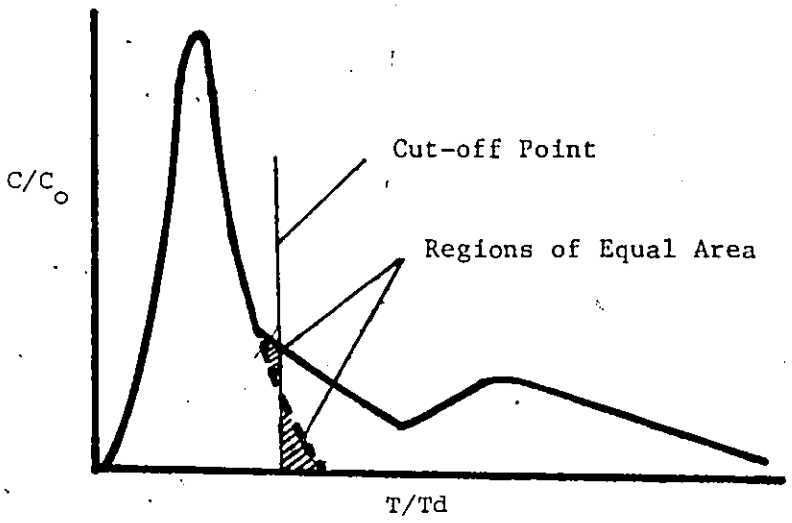

Figure 3.14 A Judicial Placement of the Cut-off Point

symmetrical. Thus, the modeller can quite accurately locate the required position of the cut-off point. As F increases the estimate of the cut-off point becomes more difficult.

However, this method of relocating the cut-off point does not help when it comes to using Eq. (3.25) since it does not correct the variance in any way. Although it may seem that using Eq. (3.22) would always be better than using Eq. (3.25) for calculating the dispersion coefficient, this is not true when the output dye tracer curve is as shown in Fig. (3.12a). In this instance, Eq. (3.25) would be more accurate since the variance considers all points influencing the maximum concentration which may be adversely affected by experimental errors.

The expressions given in Eq.'s (3.22) and (3.25) give two alternative methods for evaluating the dispersion coefficient. Ferrara and Harleman[14] relied solely on Fischer's equation (Eq. (3.14)), and made no attempt to verify the accuracy of their dispersion coefficient, except that reasonably accurate reproductions of the dye tracer curves were obtained.

An advantage of using Eq.'s (3.22) and (3.25) for determining F is that it enables one to use the methods outlined in the following subsection for determining the other two parameters, β and D_m.

3.4.3.3 Determination of β and D_m from Fischer's Equation

As noted above, Ferrara and Harleman[13,14] have found that reasonably accurate results could be obtained for the dispersion coefficient of the active zone by using Fischer's equation (Eq. (3.12) or (3.14)). Since the dispersion coefficient can also be obtained from Eq. (3.22) and Eq. (3.25), back-substitution into Eq. (3.12) or Eq. (3.14) leads to the values of β and D_m.

(i) Method I

One can combine Eq.'s (3.12) and (3.16):

$$F = \frac{1.101126\ S^{1/2} W_A^2}{R_{hA}^{1/2} L\ U_A} \tag{3.29}$$

and from Eq. (3.18):

$$T_{dA} = \frac{V_A}{Q_A} = \frac{L}{U_A} \tag{3.30}$$

which can be substituted into Eq. (3.29) to give:

$$F = \frac{1.101126\ S^{1/2} T_{dA} W_A^2\ (W_A + 2D/W_A\ D)^{1/2}}{L^2} \tag{3.31a}$$

The only unknown in the above equation is W_A which can be found by Newton's Method[7]:

$$W_{A,i+1} = W_{A,i} - \frac{f(W_{A,i}) - F}{f'(W_{A,i})} \tag{3.32}$$

where $W_{A,i}$ = initial estimate of W_A
$W_{A,i+1}$ = next estimate of W_A

$$f(W_{A,i}) = \frac{1.101126\ S^{1/2} T_{dA} W_{A,i}^2}{L^2} \frac{W_{A,i} + 2D}{W_{A,i} D}^{1/2} \tag{3.31b}$$

$$f'(W_{A,i}) = \frac{1.101126 S^{1/2} T_{dA}\ W_{A,i}^{1/2} (2W_{A,i} + D)}{L^2 \qquad (W_{A,i} + 2D)^{1/2}} \tag{3.33}$$

Using Newton's Method, the solution is easily obtained by iterating. Once W_A is known, it is a simple matter to

obtain β from Eq. (3.7):

$$\beta = \frac{V_A}{V} = \frac{W_A}{W}$$

D_m can then be calculated from Eq. (3.19b):

$$D_m = \frac{\beta T_d}{T_{dA}}$$

Thus, a complete solution of the model can be obtained by using Eq. (3.22) or Eq. (3.25) with Eq.'s (3.31), (3.32), (3.7) and (3.19b).

(ii) Method II

One can also combine Eq.'s (3.14) and (3.16):

$$F = 1.101126 \frac{n W_A^2}{L (R_{hA})^{7/4}}$$

$$= \frac{1.101126\, n\, W_A^{5/4} (W_A+2D)^{7/4}}{L\, D^{7/4}} \qquad (3.34)$$

Again, the only unknown is W_A which can be solved by Newton's Method (Eq. (3.32)) where:

$$f(W_{A1}) = \frac{1.101126\, n\, W_{A1}^{5/4} (W_{A1}+2D)^{7/4}}{L\, D^{7/4}} \qquad (3.34a)$$

and

$$f'(W_{A1}) = \frac{1.101126\, n}{L} \frac{W_{A1}}{6} (1/R_{hA1})^{7/4} [5 + 7R_{hA1}/D]$$

$$= \frac{1.101126\, n\, W_{A1}}{6\, L\, (R_{hA1})^{7/4}} (5+7\, R_{hA1}/D) \qquad (3.35)$$

Using Eq.'s (3.32), (3.34a) and (3.35), the value of W_{A1} can be arrived at by iteration. As before, this procedure along with Eq.'s (3.7) and (3.19b) completely defines the model.

3.4.3.4 Estimation of β and D_m from the Ratio of Unrecycled Mass to Recycled Mass

The distinction between recycled and unrecycled mass was made previously. This method is based on the assumption that the flow coming out of the active zone and going into the outlet has the same dye concentration as the flow coming out of the active zone and entering the recycle zone at any instant of time. It is also assumed that all the dye has been through the active zone once before the cut-off point occurs. Thus, the ratio of the active zone flow rate to the influent flow rate must be equal to the ratio of the total mass of dye injected in the basin to the mass of unrecycled dye.

$$\frac{Q_A}{Q} = \frac{M_T}{M_A} \qquad (3.36)$$

where M_R = mass of recycled dye
M_T = total mass of dye injected

Since Eq. (3.36) deals with ratios, the relative units used for M_A and M_T are not important. M_T can be taken as the total area under the output dye concentration versus time curve and M_A can be taken as the area under the output dye concentration curve before the cut-off point.

Rearranging Eq. (3.36),

$$Q_A = Q(M_T/M_R) \qquad (3.37)$$

Thus, D_m can be calculated from Eq. (3.9) and β from Eq. (3.19b). This method does not rely on Fischer's equation or on the determination of the dispersion coefficient.

Nevertheless, it does require knowledge of the detention time in the active zone which, as was shown above, is obtained in the determination of the dispersion coefficient.

It is important to note at this time that the various methods developed above for estimating the model's parameters demonstrate how this rather sophisticated three-parameter model can be simply defined by a careful analysis of the output dye tracer curve. Therefore, the modeller does not need to bother with tedious trial and error solutions to find the "best fit" values of R_v, D_m and E_A. These methods also provide some understanding of the significance of the various portions of the output dye tracer curve which is useful in extending the results of model studies to prototype ponds.

The programming details of the model are presented in the Appendix.

3.5 Scaling of Ponds

For model studies to be used to predict the performance of stormwater treatment ponds, it is necessary to abide by the proper scaling laws. These laws must be chosen by consideration of the forces that control the phenomena which affect the performance of a pond.

The mixing properties of a pond are a direct consequence of its flow pattern and of the level of turbulence that exists in it. The flow pattern ultimately controls the amount of short-circuiting, dead space in the

pond and the size of the circulation zones. The level of turbulence dictates the amount of dispersion which takes place. In the following subsections, a brief discussion of these phenomena and their controlling forces will be presented, followed by the selection of the scaling laws.

3.5.1 Pond's Flow Pattern

For simplicity, it is assumed that the flow pattern representation given by the Ferrara and Harleman model[14] is sufficiently accurate. The model allows for short-circuiting by its fast flowing, narrow active zone, and dead space and circulation are modelled by the size and flow rate in the recycle zones.

Ponds of the configuration shown in Fig. 3.1 are subjected to circulation in the corners[1]. The amount of circulation generated is dependent on the convective momentum of the influent stream as well as the level of resistance to which it is subjected as it enters the basin. These will control the expansion of the stream across the width of the basin as well as the degree of circulation. Since the amount of resistance is a function of depth, the flow pattern will vary with depth. The momentum term is directly related to the flow velocity, therefore, it is easy to understand why flow rates and the width of the inlet and the outlet channels can influence the flow pattern.

The influence of the corner circulation zones on the overall flow pattern of a basin is a function of the length

of the basin. In a short basin, the circulation zone can be expected to occupy a large portion of the length of the basin whereas in a very long basin, the circulation zones become proportionally insignificant (see Fig. 3.15).

To assess the amount of recirculation and the size of the recycle zones, it is first necessary to determine the flow rates to be used in the experiment model. It is, therefore, necessary to determine the scaling law (Froude and/or Reynolds) that applies. Abbott[1] concludes that under steady state, "resistance effects finally come to dominate over the dynamic effects". Unfortunately, the operating Reynolds numbers were not mentioned in their paper. However, it is noted that although the bottom's roughness numbers are space constant, they vary with the flow rate. This implies that the flow rates used did not generate fully turbulent flow for which the roughness coefficients become constant. This is well illustrated in Fig. 3.16.

In Table 2.1, it was shown that the Reynolds numbers for the prototypes are greater than 100,000, thus fully turbulent flow conditions exist. Therefore, in the scaling process, it will not be necessary to abide by Reynolds' Law as long as turbulent conditions are maintained and Froude's Law determines the scaling ratios to be applied. This is supported by many researchers: Ploeg[33], Pratte[34], and Townsend[44]. Also, in mixing models of estuaries, rivers and lakes, Froude's law is always used[18,21,33,34,39,40,48]. It should be noted, however, that in most cases it is

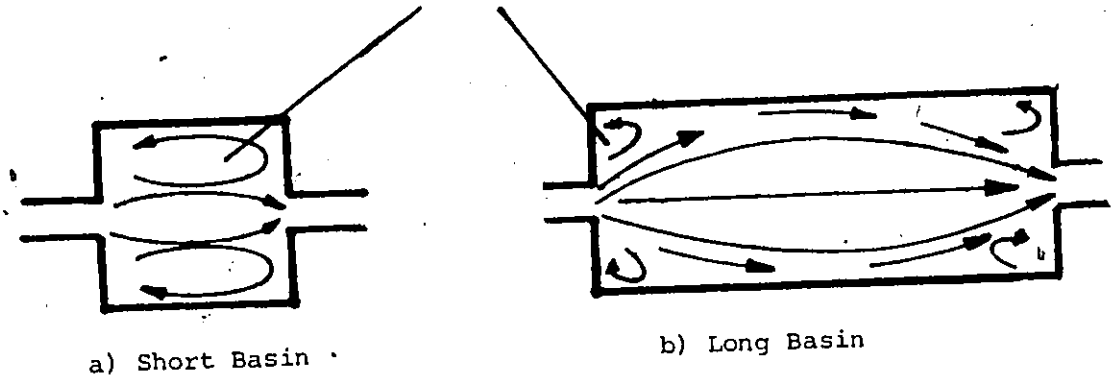

Figure 3.15 Circulation Zones in Short and Long Basins

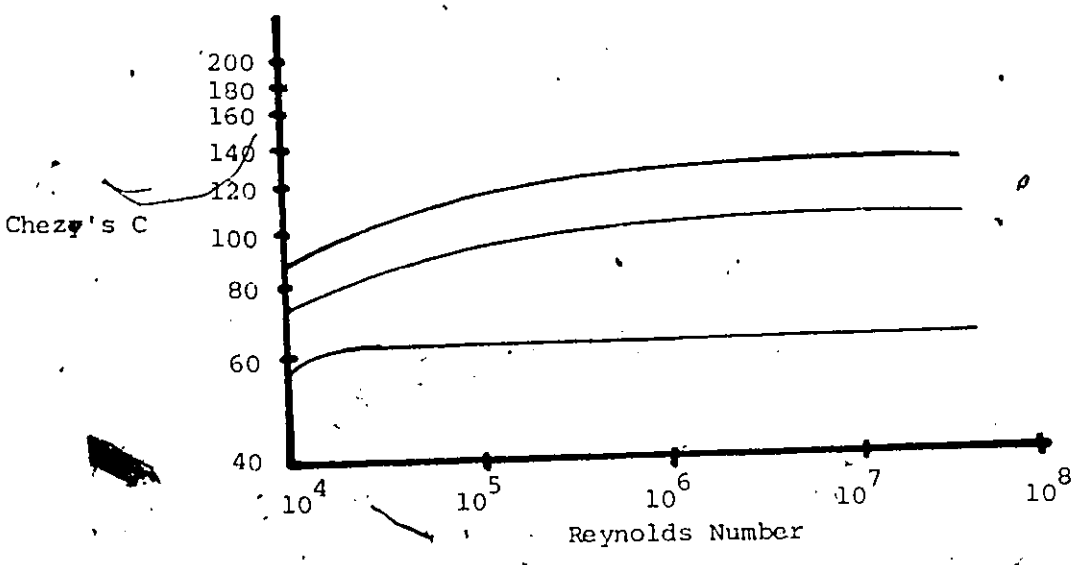

Figure 3.16 Variation of Chezy's C with Reynolds Number for Various Surface Roughnesses[21]

necessary to use a distorted or vertically exaggerated model to obtain Reynolds numbers in the turbulent regime[21,24,31,37]. This is shown to be the case, if it is desired to scale down a specific prototype such as the Kennedy-Burnett pond to a laboratory model with a width limited to 1.5 meters.

3.5.2 Prototype Modification

Prototype data is required to determine the model flow rates for the experimental model. For geometric similarity, the prototype ponds must have the same length to width ratio as the laboratory setup. Since no data from prototype ponds of the length to width ratios desired for testing were available, the data from two of the ponds in Table 2.1 was used as a guide to generate typical prototype data for the model. The modification of prototype data to satisfy the modelling needs is justifiable, since the major objective of this study was to characterize the variation of mixing properties with changes in flow and geometry of the SWTP. Also, it should be kept in mind that the objective of this study is to represent SWTP in general, not only one SWTP in particular.

The present study involved ponds of three different length to width ratios: 3:1; 2:1; and 1:1. The parameters describing the Kennedy-Burnett pond and the Milwaukee tank along with the length to width ratios required by this study are shown in Tables 3.1 and 3.2 respectively. The original

depths, volumes, surface areas, and design peak flows were not changed but the different length to width ratios resulted in modified hydraulic radii, peak velocities, Reynolds and Froude numbers. These modifications can be justified by the fact that in most cases ponds are designed on the basis of volume and detention time alone, the configuration of the pond usually being defined by physical constraints, costs and other considerations.

Table 3.1: Original and Modified Kennedy-Burnett Pond Data

	Original	Modified		
Length:Width Ratio	18:1	3:1	2:1	1:1
Length (m)	422	198	160	113
Width (m)	24	65	80	113
Depth (m)	2.4	2.4	2.4	2.4
Volume (m^3)	24,600	24,600	24,600	24,600
Surface Area (m^2)	12,870	12,870	12,870	12,870
Cross-Sectional Area (m^2)	58	156	192	271
Hydraulic Radius(m)	1.85	2.23	2.26	2.30
Peak Flow (m^3/s)	3.5	3.5	3.5	3.5
Peak Velocity(m/s)	0.060	0.022	0.018	0.013
Reynolds Number	296,000	134,000	110,000	79,300
Froude Number	0.0124	0.0045	0.0038	0.0027

Table 3.2: Original and Modified City of Milwaukee Tank Data

	Original	Modified		
Length:Width Ratio	5:1	3:1	2:1	1:1
Length (m)	128	93	76	54
Width (m)	23	31	38	54
Depth (m)	5.0	5.0	5.0	5.0
Volume (m^3)	14,760	14,760	14,760	14,760
Surface Area (m^2)	2,950	2,950	2,950	2,950
Cross-Sectional Area (m^2)	115	155	190	270
Hydraulic Radius (m)	3.50	3.78	3.96	4.22
Peak Flow (m^3/s)	11.0	11.0	11.0	11.0
Peak Velocity (m/s)	0.096	0.071	0.05	0.041
Reynolds Number	900,000	715,000	611,000	458,000
Froude Number	0.0137	0.0101	0.0083	0.0059

3.5.3 Froude Law Model

Table 3.3 lists the various scaling ratios for Froude's Law. The third column in this table is a simplification of the second column assuming that the model and prototype are run with water at the same temperature and that the gravitational constant is also the same in both cases. These scaling ratios have been applied to the Kennedy-Burnett pond and the City of Milwaukee tank. The results are tabulated in Tables 3.4 and 3.5, respectively, for a laboratory model whose width is fixed at 1.50 meters due to physical constraints.

Table 3.3: Froude's Law Scaling Factors

Parameter	Dimension	Froude Scaling Ratio	Simplified Froude Scaling Ratio
Length	L	Lr	Lr
Area	L^2	$(Lr)^2$	$(Lr)^2$
Volume	L^3	$(Lr)^3$	$(Lr)^3$
Time	T	$(Lr)^{1/2}\ g^{-1/2}$	$(Lr)^{1/2}$
Velocity	L^{-1}	$(Lr\ g)^{1/2}$	$(Lr)^{1/2}$
Discharge	$L^3\ T^{-1}$	$(Lr)^{5/2}\ g^{1/2}$	$(Lr)^{5/2}$

Table 3.4: Laboratory Model's Parameters (Scaled from Kennedy-Burnett Pond)

Length:Width Ratio	3:1	2:1	1:1
Length Scaling Ratio (Lr)	43	53	74
Length (m)	4.57	3.05	1.50
Width (m)	1.50	1.50	1.50
Depth (m)	0.056	0.045	0.032
Volume (m^3)	0.3890	0.209	0.074
Surface Area (m^2)	6.95	4.64	2.31
Cross-Sectional Area (m^2)	0.085	0.068	0.049
Hydraulic Radius (m)	0.052	0.041	0.031
Peak Flow (m^3/s)	289×10^{-4}	171×10^{-4}	74×10^{-4}
Peak Velocity (m/s)	0.0034	0.0025	0.0015
Reynolds Number	470	270	125
Froude Number	0.0046	0.0038	0.0027

In Table 3.4 it can be seen that the models' Reynolds numbers that would be obtained from scaling down the Kennedy-Burnett pond are not high enough to maintain turbulent flow conditions.

Table 3.5: Laboratory Model's Parameters (Scaled from Milwaukee Tank)

Length:Width Ratio	3:1	2:1	1:1
Length Scaling Ratio (Lr)	20	25	36
Length (m)	4.57	3.05	1.52
Width (m)	1.52	1.52	1.52
Depth (m)	0.25	0.20	0.14
Volume (m^3)	1.74	0.93	0.32
Surface Area (m^2)	6.95	4.64	2.31
Cross-Sectional Area (m^2)	0.38	0.30	0.21
Hydraulic Radius(m)	0.19	0.16	0.12
Peak Flow (m^3/s)	0.0061	0.0035	0.0014
Peak Velocity (m/s)	0.0162	0.0117	0.0067
Reynolds Number	8,200	5,000	2,200
Froude Number	0.0103	0.0084	0.0057

The scaling of the Milwaukee tank would result in model flow rates high enough to generate turbulent conditions. However, one of the parameters whose influence on the mixing pattern was to be investigated was the flow rate. It was desired to examine a flow rate of one-third the design peak flow rate. This permits the analysis of mixing patterns resulting from storms of different peak flows. However, these flow rate reductions also lead to proportional reductions in the tabulated values of the Reynolds number which then become too low to maintain fully turbulent conditions. Thus, a vertically exaggerated model is needed to increase the Reynolds numbers in the model.

3.5.4 Vertically Exaggerated Model

This type of model enables the use of higher flow rates at greater depths, thereby increasing the Reynolds number while maintaining the Froude number constant. Note that the dispersion coefficient as calculated by Fischer's equation is dependent on the hydraulic radius and on the width of the active zone, thus accounting for variations due to a distorted model.

The following is a theoretical development of mathematical equations which one can use for determining the flow rate and degree of distortion required in model studies of a specific pond. The distorted model's scaling ratios are presented in Table 3.6.

Table 3.6: Distorted Model Law Scaling Ratios

Parameter	Dimension	Scaling Ratio
Horizontal Length	L	Xr
Vertical Length	L	Yr
Volume	L^3	$(Xr)^2$ Yr
Time	T	$Xr/(Yr)^{1/2}$
Velocity	$L\ T^{-1}$	$(Yr)^{1/2}$
Discharge	$L^3\ T^{-1}$	$Xr\ (Yr)^{3/2}$

A proper Reynolds number criterion must be chosen to calculate the required degree of distortion. Sharp[39] suggests that the most reliable criterion is to specify the minimum Reynolds number in terms of the bottom shear velocity (U^*) and the equivalent roughness size (k). This criterion is of the form of Eq. (3.38).

$$Nr(min) = \frac{U^* k}{\nu} \qquad (3.38)$$

where k = equivalent roughness size (m)

The stipulated minimum Reynolds number varies from researcher to researcher (see Table 3.7).

With appropriate substitutions, Eq. (3.38) was modified to contain the required model flow velocity and hydraulic radius. This development follows.

The shear velocity is the ratio of bed shear stress to fluid density and may be expressed as in Eq. (3.39):

$$U^* = (g\ R_h\ S)^{1/2} \qquad (3.39)$$

Table 3.7: Minimum Reynolds Number to Maintain Turbulent Flow

Researcher	Formula for Reynolds Number	Minimum Reynolds Number
Allen[2]	$\frac{U\ D}{\nu}$	1,400
Chow[10]	$\frac{U\ R_h}{\nu}$	500
de Vries[11]	$\frac{U\ D}{\nu}$	400 to 800
Henderson[21]	$\frac{U^*\ k}{\nu}$	100
Russel[34]	$\frac{U\ R_h}{\nu}$	1,000
Yalin[40]	$\frac{U^*\ k}{\nu}$	approximately 70

The slope of the energy line can be expressed by re-arranging Manning's equation as shown in Eq. (3.40).

$$S^{1/2} = \frac{U\ n}{(R_h)^{2/3}} \qquad (3.40)$$

Substituting Eq. (3.39) and Eq. (3.40) into Eq. (3.38) and simplifying, one obtains:

$$Nr(min) = \frac{g^{1/2} U\ n\ k}{R_h^{1/4}} \qquad (3.41)$$

Chow[12] expresses the model's roughness size (k) in terms of Manning's roughness coefficient in the prototype as:

$$k = (n/Np)^4\ Kp \qquad (3.42)$$

where Np = prototype's Manning roughness coefficient ($s/m^{1/3}$)
Kp = prototype's diameter of roughness elements (m)

Eq. (3.43) is obtained by substituting Eq. (3.42) for k in Eq. (3.41).

$$Nr(min) = \frac{g^{1/2}\ U\ n\ Kp\ (n/Np)^4}{R_h^{1/4}} \qquad (3.43)$$

Henderson[21] uses Eq. (3.44) to relate hydraulic radius to the Manning's roughness coefficient in a distorted model.

$$(n/Np) = (R_h/Rp)^{2/3}\ Xr^{1/2} \qquad (3.44)$$

where Rp = prototype's hydraulic radius (m)
Xr = horizontal length scaling ratio

Eq. (3.45) is obtained by introducing Eq. (3.44) into Eq. (3.43) and simplifying.

$$Nr(min) = \frac{g^{1/2}\ U\ R_h^{7/2}\ Np\ Kp\ Xr^{7/2}}{\nu Rp^{14/3}} \qquad (3.45)$$

This equation is dimensionally correct.

For a smooth earth channel with no weed growth, Henderson[21] relates Kp to Np by the following equation:

$$Kp = (26.3\ Np)^4 \qquad (3.46)$$

The value of the constant in Eq. (3.46) ranges from about 3.5 to 50 depending on the smoothness of the channel surface and weed growth.

Substituting Eq. (3.46) for Kp in Eq. (3.45), and simplifying results in:

$$U\ R_h^{7/2} = \frac{Nr(min)\ \ Rp^{14/3}\ \nu}{g^{1/2}\ \ (26.3)^4\ \ Np^7\ \ Xr^{7/2}} \qquad (3.47)$$

The depth can be expressed in terms of the width and the hydraulic radius:

$$D = (W \cdot R_h)/(W-2R_h) \qquad (3.48)$$

The Froude law criterion can be expressed as follows when Eq. (3.48) is substituted for the depth.

$$U\,[(W-2R_h)/(W R_h)]^{1/2} = Nf\, g^{1/2} \qquad (3.49)$$

Eq. (3.47) and Eq. (3.49) can be solved simultaneously for the values of the model's velocity and hydraulic radius which satisfy the minimum Reynolds number criterion (taken from Table 3.7) and also achieve the desired Froude number. Two other unknowns in the above equations are Xr and W. However, these are related by Eq. 3.50:

$$W = \frac{Wp}{Xr} \qquad (3.50)$$

where W = model's width (m)
Wp = prototype's width (m)
Xr = horizontal length scaling ratio.

Thus, the horizontal length scaling ratio must be chosen before Eq. (3.47) and Eq. (3.49) can be solved. The horizontal length scaling ratio's value is limited on the one hand by costs, and availability of space, and on the other by the minimum aspect ratio. The aspect ratio is defined as the ratio of the width to the depth of the model. Yalin[40] suggests a minimum aspect ratio of five for maintaining two dimensional flow. At this ratio or higher, the side wall effects on the flow pattern are negligible. However, other researchers[31,39] suggests a minimum aspect ratio of ten when modelling dispersion. Thus, to maintain the model study's costs at a minimum, Eq. (3.47) and Eq. (3.49) should be solved for various values of Xr until the desired minimum aspect ratio is achieved.

Once the flow rate and hydraulic radius are known, the model's depth can be obtained from Eq. (3.48). The flow rate may be obtained as follows:

$$Q = U \cdot W \cdot D \qquad (3.51)$$

The vertical exaggeration can be calculated as follows:

$$Vr = \frac{Lr \cdot D}{Dp} \qquad (3.52)$$

where Vr = vertical exaggeration
Dp = prototype's depth (m)

The above procedure may be used by any researcher whose main objectives are to reproduce the mixing patterns of a particular SWTP. As with any modelling technique, care should be exercised in evaluating the factors which affect the particular pond's mixing properties and the model's capabilities of reproducing mixing pattern. Also, in some cases, the model may be built large enough to ensure that there will be no need for vertical distortion.

CHAPTER IV

EXPERIMENTAL SETUP

The model was built in an existing channel in the hydraulics laboratory at the Department of Civil Engineering of the University of Ottawa.

Figure 4.1 shows the model setup. The basin width was fixed at 1.50 m. The sides of the model were approximately 1.0 m high. The existing channel sidewalls were utilized in the model. The endwalls consisted of sheets of plywood mounted on angle iron frames. The inlet and outlet to the model pond consisted of plywood channels that ran the entire depth of the model. An endwall and an overflow weir were attached to the inlet and outlet channels, respectively. Water was supplied to the model by a PVC (50 mm diameter) pipe assembly connected to a constant head tank. The discharge end of the pipe was fitted with a slotted diffuser.

4.1 Length of the Model

The length of the model was varied by moving the outflow endwall closer to the inflow endwall. Length to width ratios of 3:1, 2:1 and 1:1 were investigated for their effects on mixing properties in ponds.

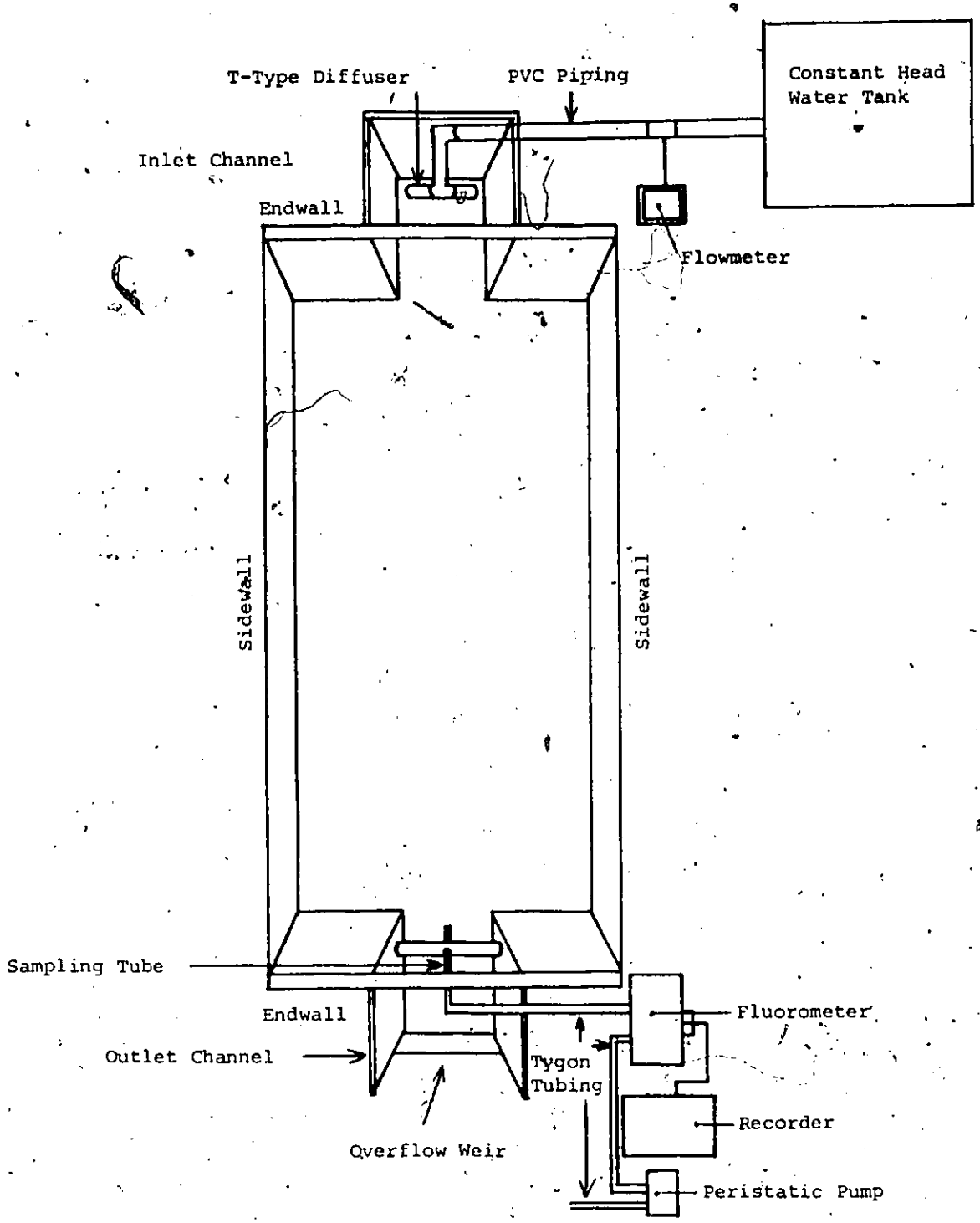

Figure 4.1 Schematic of the Laboratory Setup (Plan View)

4.2 Floor of the Model

The floor of the model was finished in concrete and made level to a tolerance of 5.0 mm to prevent the flow pattern from being affected by floor irregularities.

4.3 Endwalls

The endwalls were constructed of plywood panels mounted on angle iron frames. The plywood panels were interchangeable to permit the testing of various widths of inlet and outlet channels. Three widths of these channels were used, 0.20 m, 0.30 m and 0.50 m. The far end of the inlet channel was blocked off with a screwed on plywood panel so that no water could leave the model at that end. An overflow weir was attached to the far end of the outlet channel. This weir was required to maintain the depth of water in the model.

4.4 Flow Rates

Table 4.1 shows the modified minimum Reynolds numbers given by various researchers as expressed by Eq. (2.1). This table was obtained by modifying Table 3.7. In that table, two researchers (Allen[3] and de Vries[11]) express the minimum Reynolds number in terms of the depth (D) instead of the hydraulic radius (R_h). This is most likely due to the fact that in most cases, the width to depth ratio of models of rivers or channels are so large that the hydraulic radius

is approximately equal to the depth. It is therefore assumed that the depth is fully interchangeable with the hydraulic radius in the Reynolds number equation. Also, to be consistent with Eq. (2.1), all the values are multiplied by a factor of four.

Table 4.1: Minimum Reynolds Number Values

Researcher	Nr(min)
Allen[3]	5,600
Chow[10]	2,000
de Vries[11]	1,600 to 3,200
Russel[34]	4,000

To maintain two-dimensional flow while not adversely affecting the dispersion, the minimum aspect ratio (*i.e.*, W/D) was set at 10. Three flow rates were to be tested which would result in Froude numbers found in prototypes. For simplicity, flow rates of one, two and three litres per second were chosen. The overflow weir was set at a height of 0.10 meters. Thus, the Froude and Reynolds numbers were as shown in Table 4.2.

The Froude numbers in Table 4.2 are representative of the prototype Froude numbers which were tabulated in Table 2.1. It should be kept in mind that the Froude numbers in

Table 4.2: Model's Froude and Reynolds Numbers

Flow Rate (l/s)	1.0	2.0	3.0
Flow Velocity (m/s)	6.7×10^{-3}	13.3×10^{-3}	20.0×10^{-3}
Froude Number	0.007	0.0135	0.0201
Reynolds Number	1,570	3,100	4,700

Table 2.1 represent design peak flows. In this study, it was desired to evaluate the performance of SWTP under different flow rates and not only at the design peak values.

The lowest Reynolds number in Table 4.2 is 1,570. This value is somewhat lower than the allowable minimum. However, this is not too significant since, as discussed in the previous chapter, the active zone flows at a velocity much higher than the average velocity through the pond because of recirculating flow and also because the zone was relatively narrow. The actual Reynolds number for that zone is much greater than the values shown in Table 4.2. It can also be expected that in the jet expansion area very large Reynolds numbers exist. Therefore, turbulent conditions exist in the area where the momentum transfer from the active zone to the recirculation zone occurs.

The same flow rates were utilized in all three model length to width ratios. This was done to facilitate the evaluation of the influence of the Froude number on the flow pattern. The model's various length to width ratios

produced different detention times which were easily compensated for by dealing with relative time (T/Td).

4.5 Water Supply

The water for the model was supplied by a constant head tank through a system of PVC pipe 50 mm in diameter. A 1.0 m length of the pipe assembly was made interchangeable with pipes of 25 and 12.5 millimeters in diameter to accommodate measuring different ranges of flows with a flow meter.

The flow meter consisted of a paddlewheel flow sensor (Cole-Parmer # K-5618-10) which is accurate for flow velocities ranging from 0.30 to 15.0 m/s (1% maximum deviation over the full range). This paddlewheel was connected to a self-powered analog flow meter (Cole-Parmer # K-5621-30). The flow meter was calibrated by using the tank weighing method. Once it was calibrated, the accuracy of the meter proved to be very good, after being checked over the entire range of flows (0.70 to 8.50 l/s, 1% maximum deviation over the full range).

The end of the pipe assembly was fitted with a tee-type diffuser to spread the flow evenly across the width of the inlet channel (see Fig. 4.2).

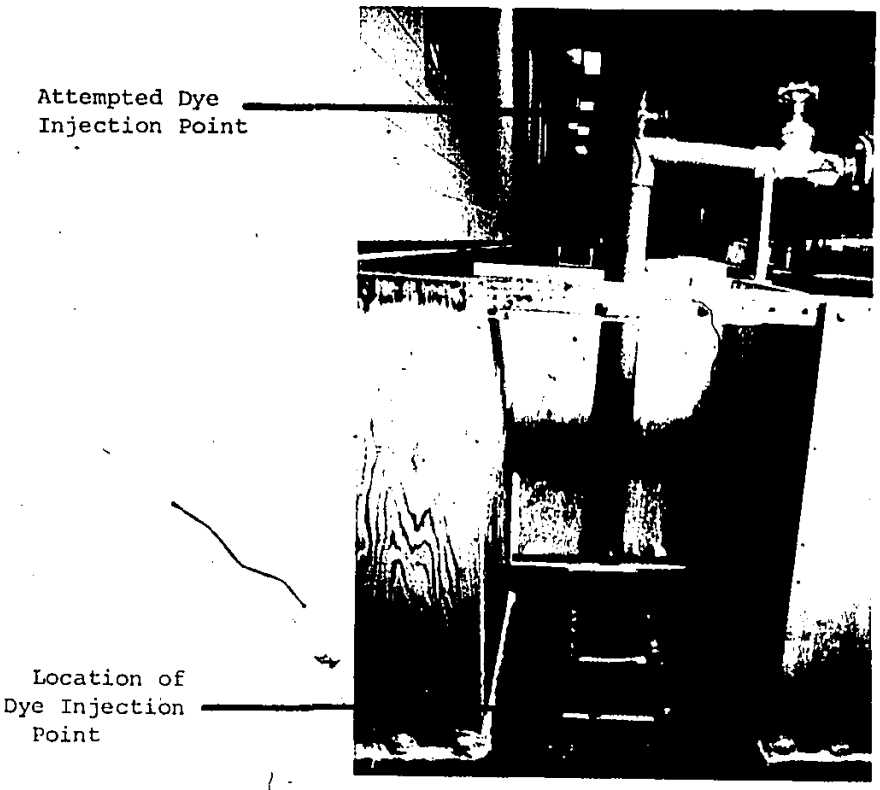

Figure 4.2 Photo of Inlet Channel Showing Location of T-type Slotted Diffuser

4.6 Dye Injection

The dye used in the study was Rhodamine B which is detectable by a fluorometer. The fluorometer calibration and linearity were verified. The change in fluorescence of Rhodamine B is insignificant over the time span of the studies. Initially, it was attempted to inject the dye into the water supply at the last elbow before the tee-type diffuser (see Fig. 4.2). This permitted good instantaneous mixing of the dye with the incoming water while reducing the chances for longitudinal mixing of the dye within the pipe. This method was, however, unsuccessful because a significant amount of dye remained in the inlet channel for more than a minute in some cases. It was preferred to quickly inject an amount of dye across the mouth of the inlet channel with a syringe. With this method, all the dye was out of the inlet channel within a few seconds, thus providing a slug of dye approaching that of an ideal Dirac impulse.

4.7 Outflow Sampling

Two methods of sampling the outflow were considered consisting of one tube and five tube samplers located in the outflow channel. The one-tube sampler is shown in Fig. 4.3.

The five tubes in the five-tube sampler were connected together by Tygon tubing leading to a collector. The flow rate in each of the five tubes was measured and found to be

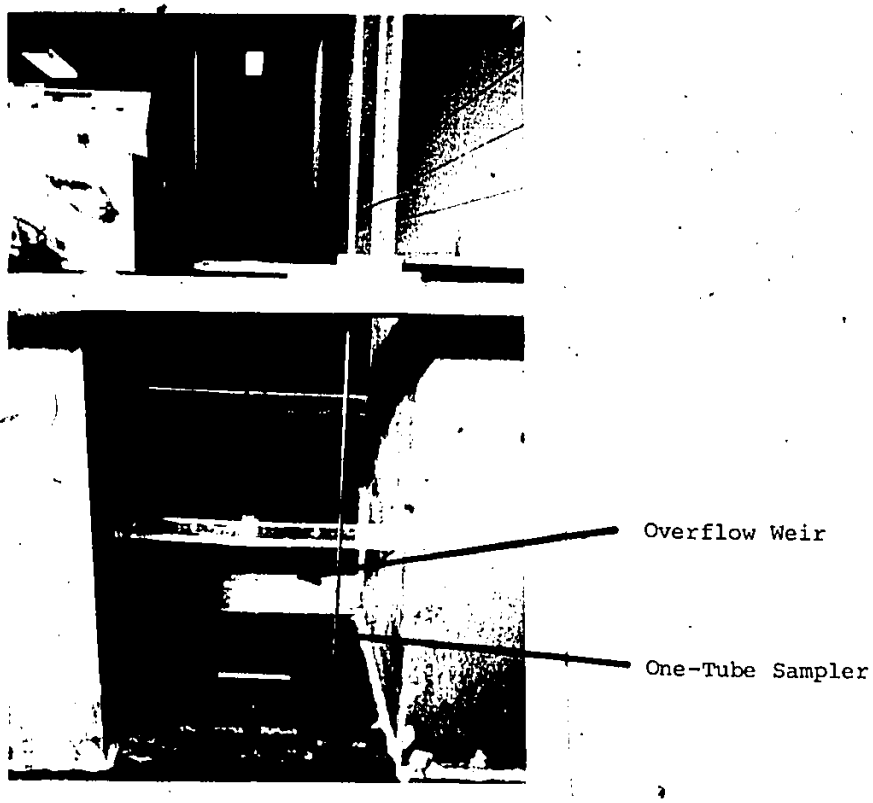

Figure 4.3 Photo of Outflow Channel Showing Location of One-Tube Sampler and of Overflow Weir

equal within limits of accuracy of the graduated cylinders used for measurement. The length of Tygon tubing was kept as short as possible to minimize the amount of longitudinal mixing within them. The five-tube sampler had the advantage of sampling more points along the width of the outlet channel which would be helpful if the concentration of dye varied laterally across the channel.

The suction of the samples from the outflow was accomplished by means of a peristaltic pump. The pump had two main components which were the Masterflex variable speed drive and the Masterflex pump head. The variable speed drive and the the pump head used were Cole-Parmer # K-7553-00 and # K-7017-00, respectively. This is a positive displacement type pump which reduced the chance of air entrainment in the samples which can produce errors in the fluorometer readings.

Both samplers were tested for their response to a slug injection. The dye tracer curves for each are given in Fig. 4.4. It is observed that the dye in the five-tube sampler diffused much more and did not respond as quickly to a slug input compared to the one-tube sampler which quickly responded and returned to zero concentration. The five-tube sampler, because of its difficulties in returning to a zero concentration, would have distorted the output dye tracer curves during the experiments.

DYE TRACER CURVES

FOR ONE-TUBE AND FIVE-TUBE SAMPLE COLLECTORS

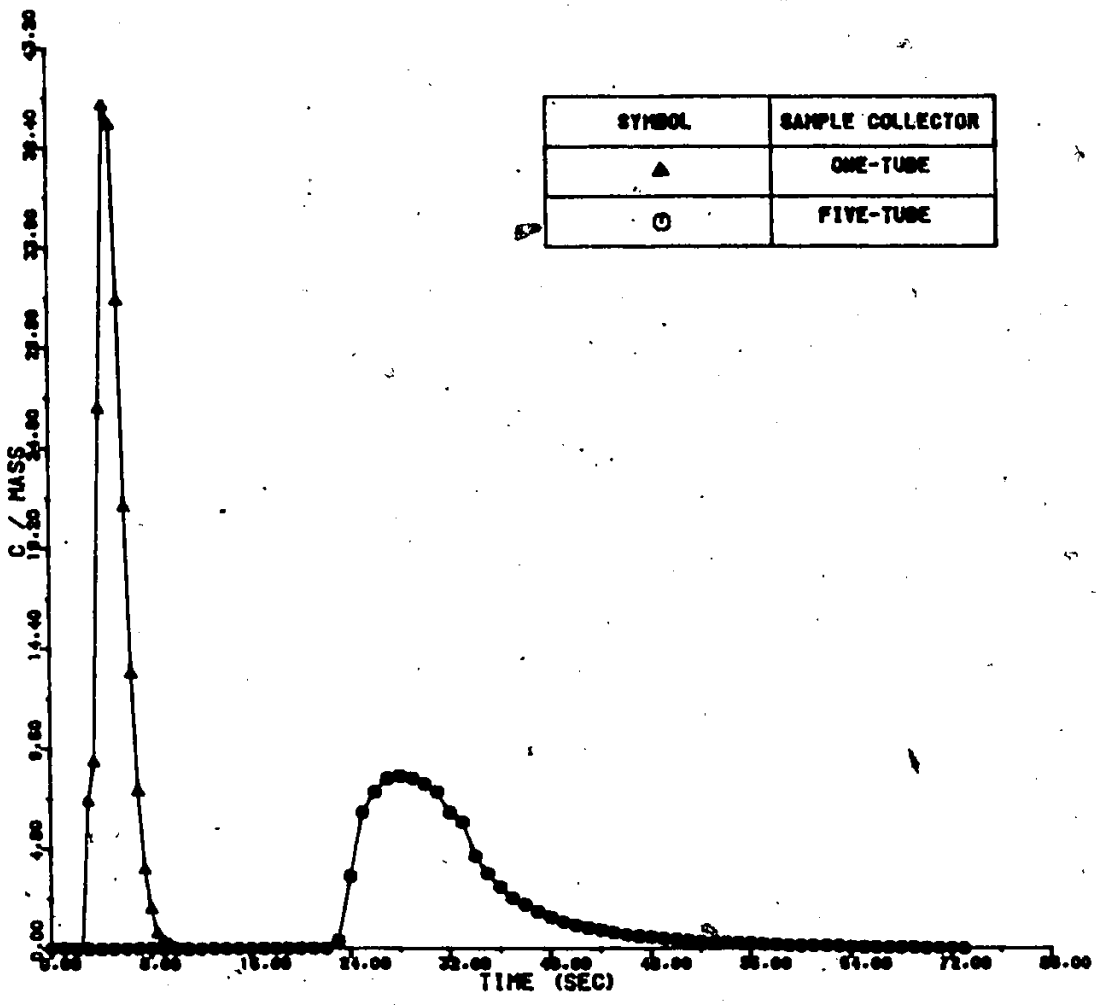

Figure 4.4 Response Dye Tracer Curves to a Slug Injection of Dye

To check dye concentration variation across the width of the outlet channel, five runs were performed under the same conditions while varying the position of the outflow one-tube sampler. The results from these five runs are shown in Fig. 4.5. The curves not only show the repeatability of the tests, but also demonstrate that the outflow dye concentration does not vary significantly across the width of the outflow channel. Therefore, the one-tube sampler could be used without significant error in the experiments.

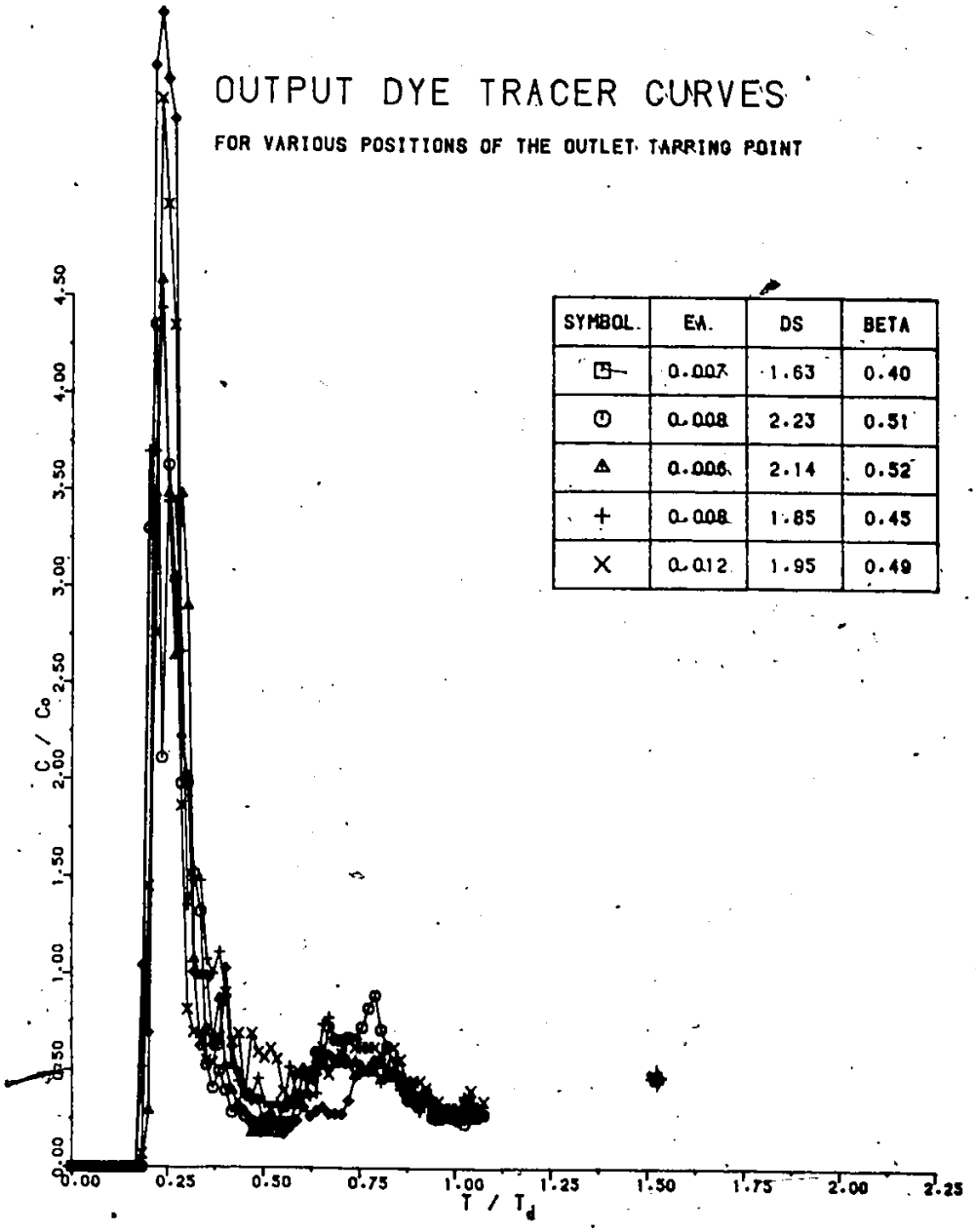

Figure 4.5 Output Dye Tracer Curves for Various Positions of the One Tube Collector

CHAPTER V

EXPERIMENTAL DATA

The data from the experimental model runs is shown in Table 5.1. For ease of reference, the run identification code (ID) is a three digit variable; the first digit refers to the model's length to width ratio; the second identifies the width of the inlet and outlet channels; and, the third defines the flow rate.

The response output dye tracer curves to slug injections into the model are presented in Fig.'s 5.1 to 5.27. These curves are those on which no symbol occurs. The other curves on these figures resulted from the various methods of estimating the parameters of the mixing model. Two plots of each run were made so that the results from the various parameter estimation methods could be presented more clearly. These curves will be discussed in the next chapter.

Fig.'s 5.28 to 5.48 are photos of the flow patterns in various runs. These photos were taken by time exposures (3 to 10 seconds) from a remote camera. Unfortunately, only photos from 21 of the 27 runs were successful.

It can be seen on the photos that the flow pattern for the longer basins (L:W ratios of 3:1 and 2:1) is unsymmetrical. This occurs because the symmetrical flow

pattern that is normally expected is metastable. The resistance to flow in an unsymmetrical flow pattern is less than in a symmetrical flow pattern because the number of recycle zones is reduced from two to one.

Table 5.1: Experimental Data

Run ID	Depth of Water (m)	Width of Basin (m)	Length of Basin (m)	Basin Volume (m^3)	Flow Rate (m^3/s)	Detention Time (s)	Width of Inlet & Outlet Channels (m)
A1A	0.123	1.50	4.56	0.838	0.0010	838	0.20
A1B	0.133	1.50	4.56	0.910	0.0020	455	0.20
A1C	0.142	1.50	4.56	0.971	0.0030	324	0.20
A2A	0.115	1.50	4.56	0.788	0.0010	788	0.30
A2B	0.122	1.50	4.56	0.837	0.0020	418	0.30
A2C	0.130	1.50	4.56	0.888	0.0030	296	0.30
A3A	0.114	1.50	4.56	0.781	0.0010	781	0.50
A3B	0.119	1.50	4.56	0.815	0.0020	408	0.50
A3C	0.123	1.50	4.56	0.841	0.0030	280	0.50
B1A	0.121	1.50	2.98	0.541	0.0010	541	0.20
B1B	0.132	1.50	2.98	0.589	0.0020	294	0.20
B1C	0.140	1.50	2.98	0.628	0.0030	209	0.20
B2A	0.114	1.50	2.98	0.508	0.0010	508	0.30
B2B	0.121	1.50	2.98	0.541	0.0020	270	0.30
B2C	0.128	1.50	2.98	0.574	0.0030	191	0.30
B3A	0.113	1.50	2.98	0.504	0.0010	504	0.50
B3B	0.118	1.50	2.98	0.527	0.0020	263	0.50
B3C	0.121	1.50	2.98	0.543	0.0030	181	0.50
C1A	0.121	1.50	1.53	0.278	0.0010	278	0.20
C1B	0.132	1.50	1.53	0.304	0.0020	152	0.20
C1C	0.140	1.50	1.53	0.322	0.0030	107	0.20
C2A	0.121	1.50	1.53	0.277	0.0010	277	0.30
C2B	0.121	1.50	1.53	0.279	0.0020	140	0.30
C2C	0.129	1.50	1.53	0.296	0.0030	99	0.30
C3A	0.113	1.50	1.53	0.260	0.0010	260	0.50
C3B	0.118	1.50	1.53	0.272	0.0020	136	0.50
C3C	0.122	1.50	1.53	0.280	0.0030	93	0.50

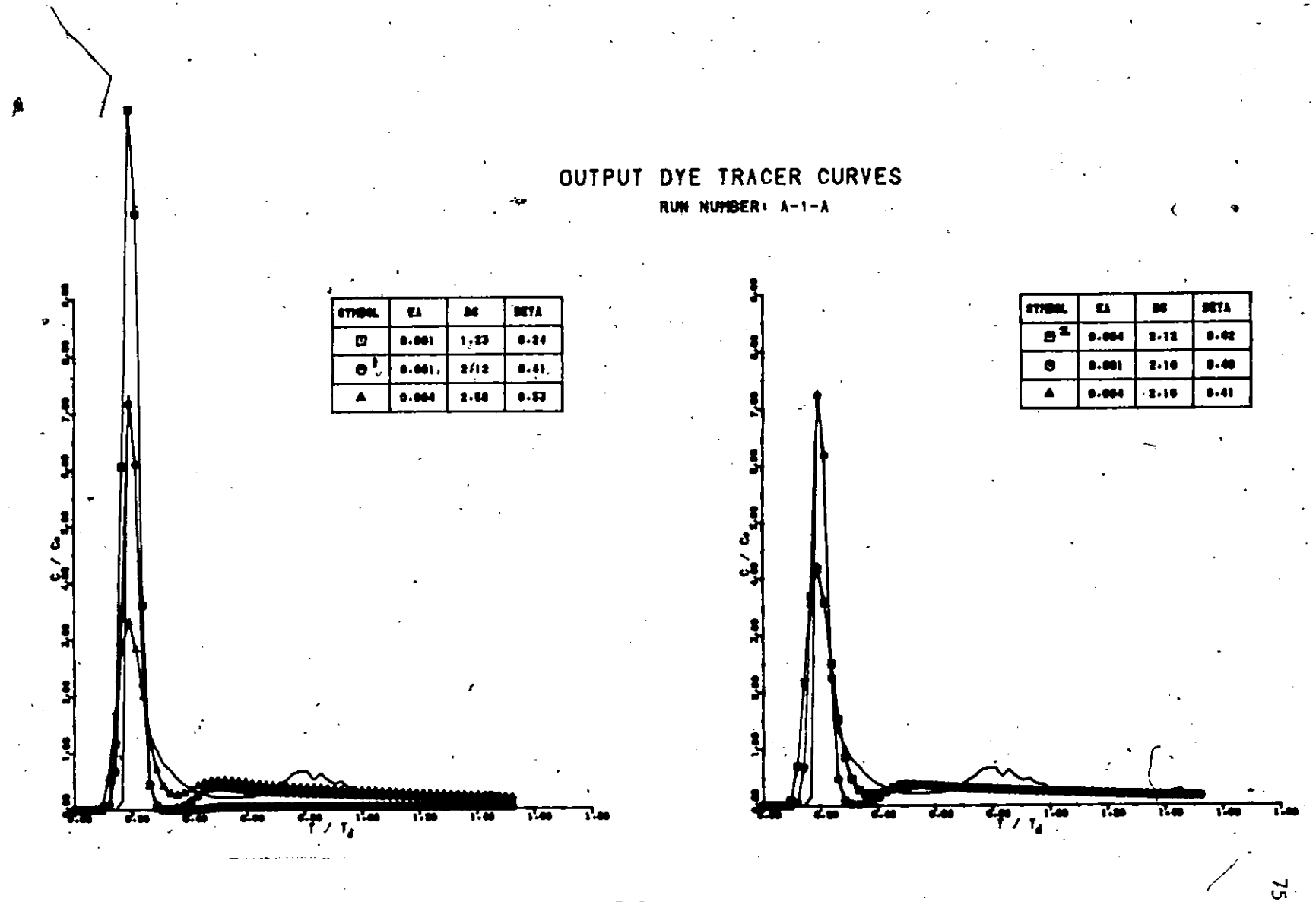

Figure 5.1

1 E_A, D_S and Beta calculated using Method II
2 E_A, D_S and Beta calculated using Method IV
Note: Experimental Curve has no symbol

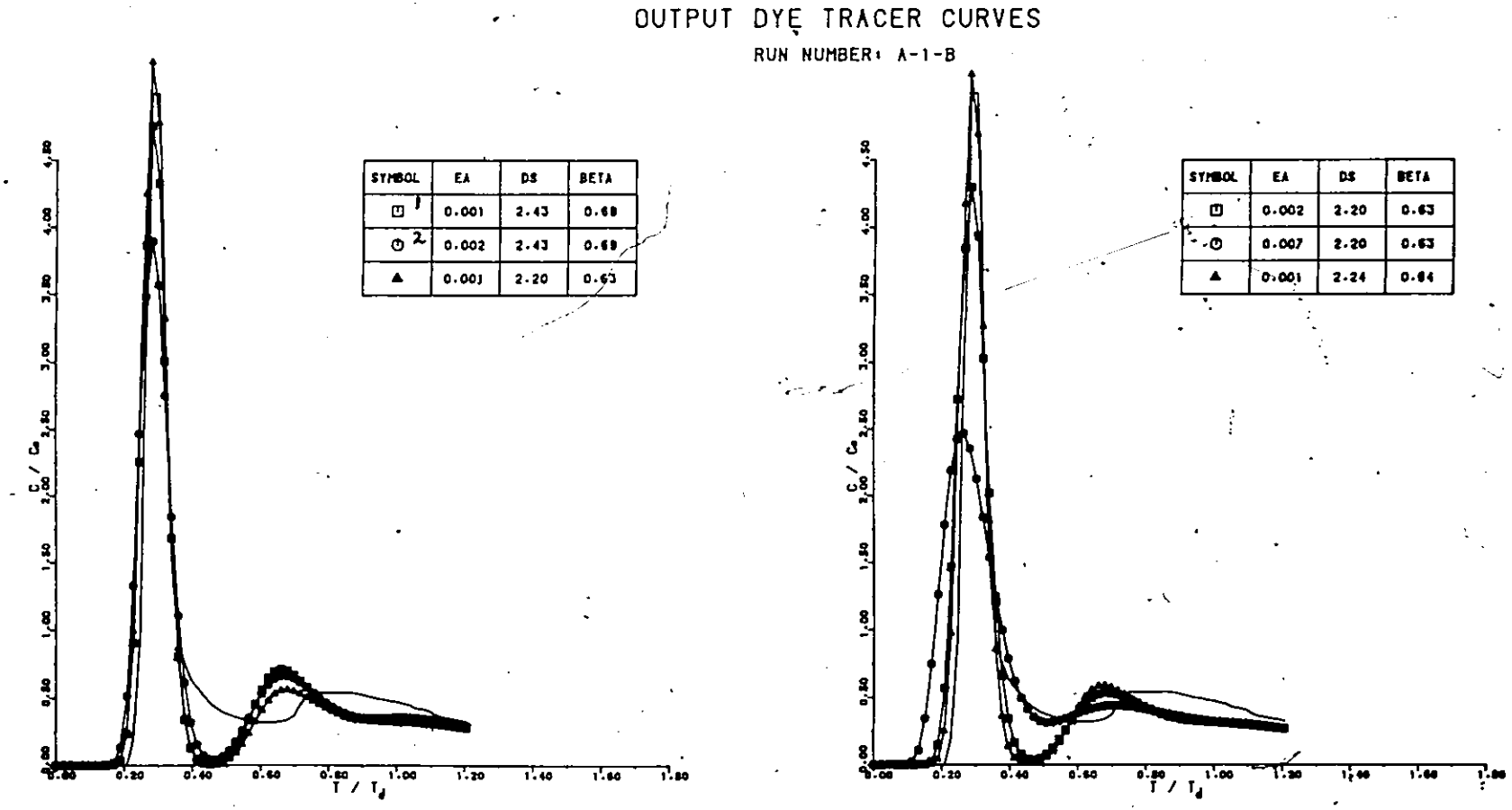

Figure 5.2

1 E_A, D_S and Beta calculated using Method II
2 E_A, DS and Beta calculated using Method IV
Note: Experimental Curve has no symbol

OUTPUT DYE TRACER CURVES

RUN NUMBER: A-1-C

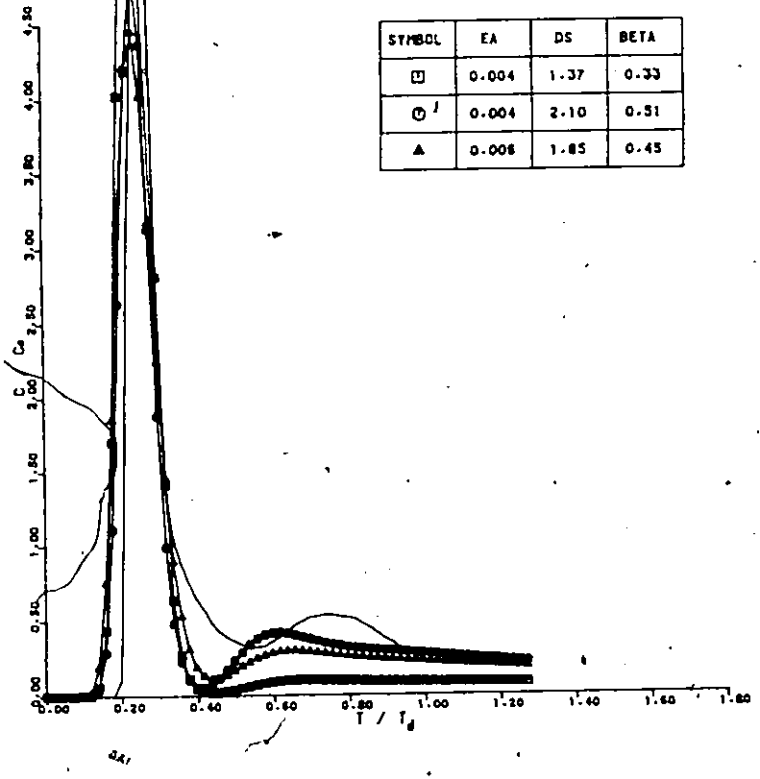

SYMBOL	EA	DS	BETA
□	0.004	1.37	0.33
○ 1	0.004	2.10	0.51
▲	0.006	1.85	0.45

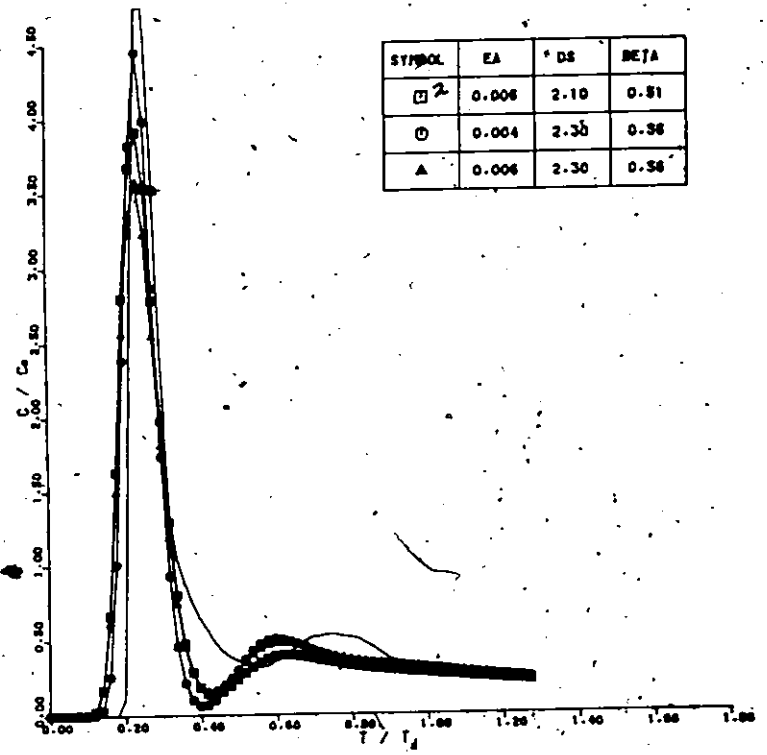

SYMBOL	EA	DS	BETA
□ 2	0.006	2.10	0.51
○	0.004	2.30	0.56
▲	0.006	2.30	0.56

1 E_A, D_S and Beta calculated using Method II
2 E_A, D_S and Beta calculated using Method IV
Note: Experimental Curve has no symbol

Figure 5.3

Peak at 11.50

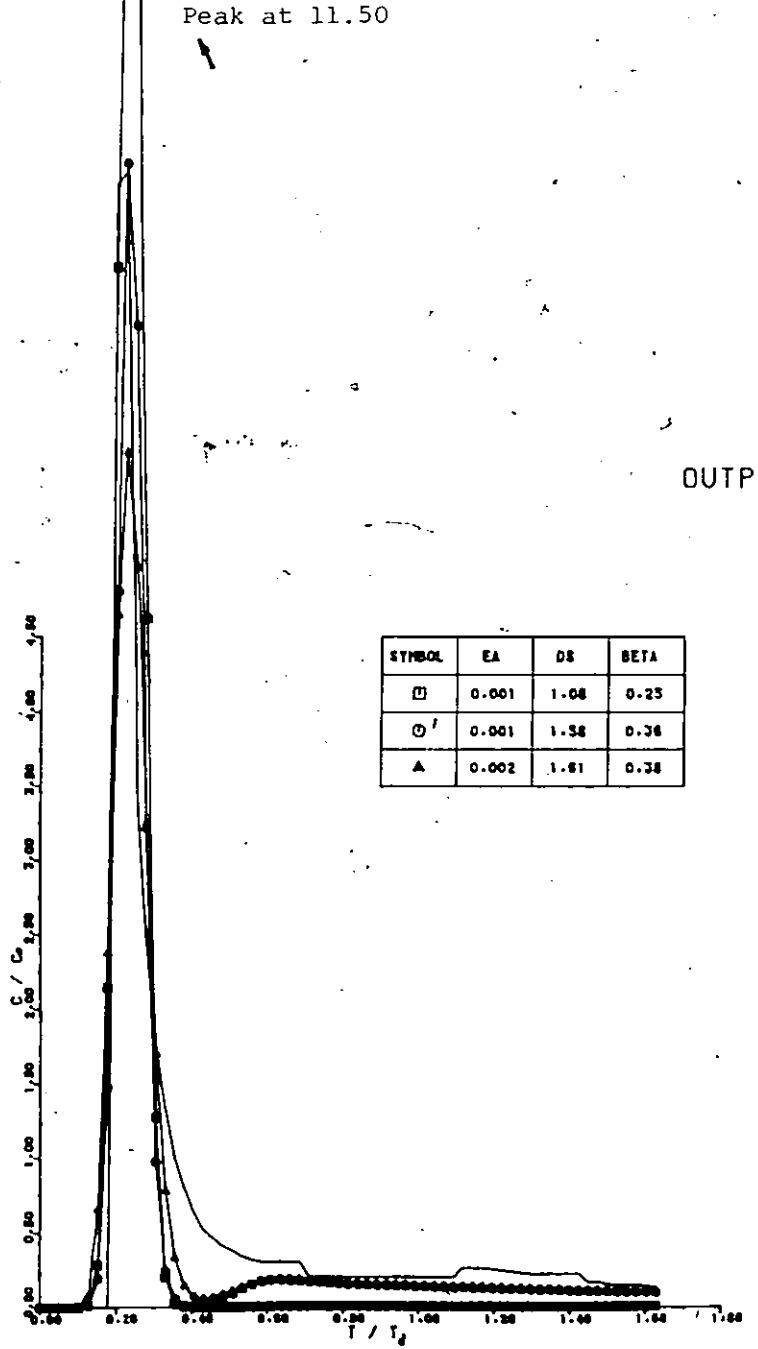

SYMBOL	EA	DS	BETA
□	0.001	1.08	0.25
○	0.001	1.58	0.36
△	0.002	1.61	0.38

OUTPUT DYE TRACER CURVES

RUN NUMBER: A-2

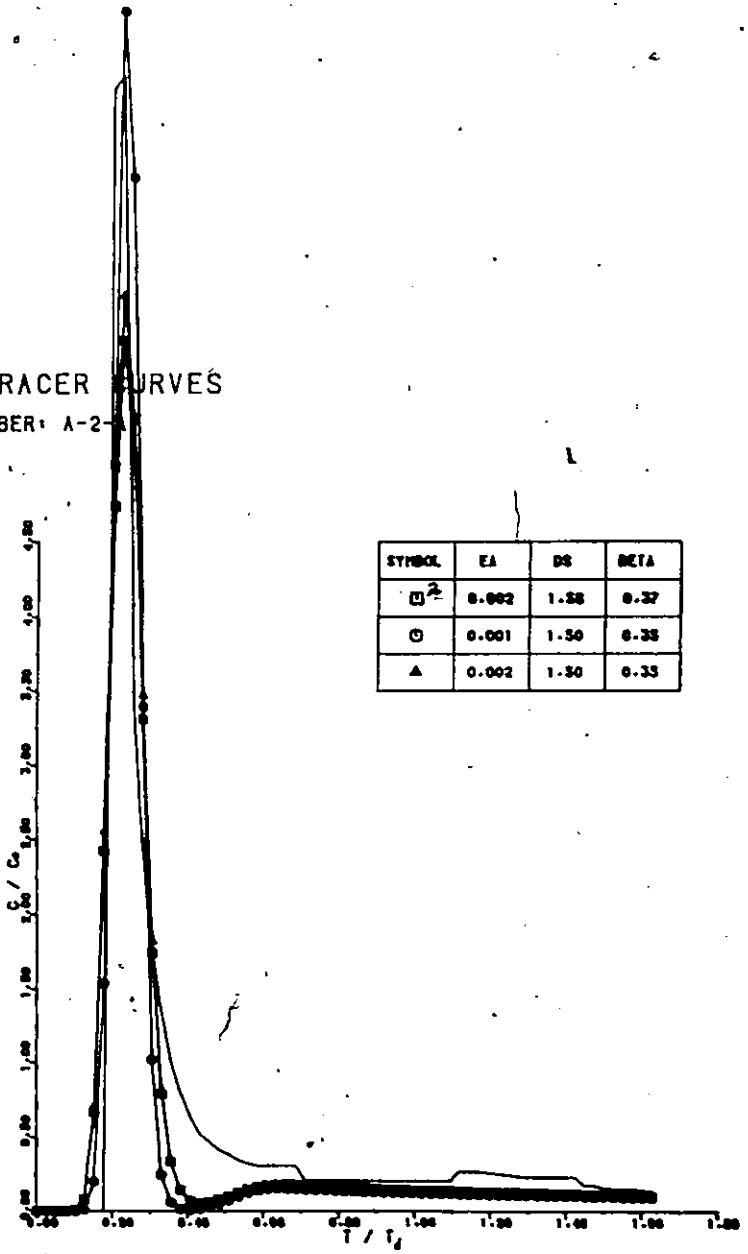

SYMBOL	EA	DS	BETA
□	0.002	1.38	0.37
○	0.001	1.50	0.35
△	0.002	1.50	0.33

1 E_A, D_S and Beta calculated using Method II
2 E_A, D_S and Beta calculated using Method IV
Note: Experimental Curve has no symbol

Figure 5.4

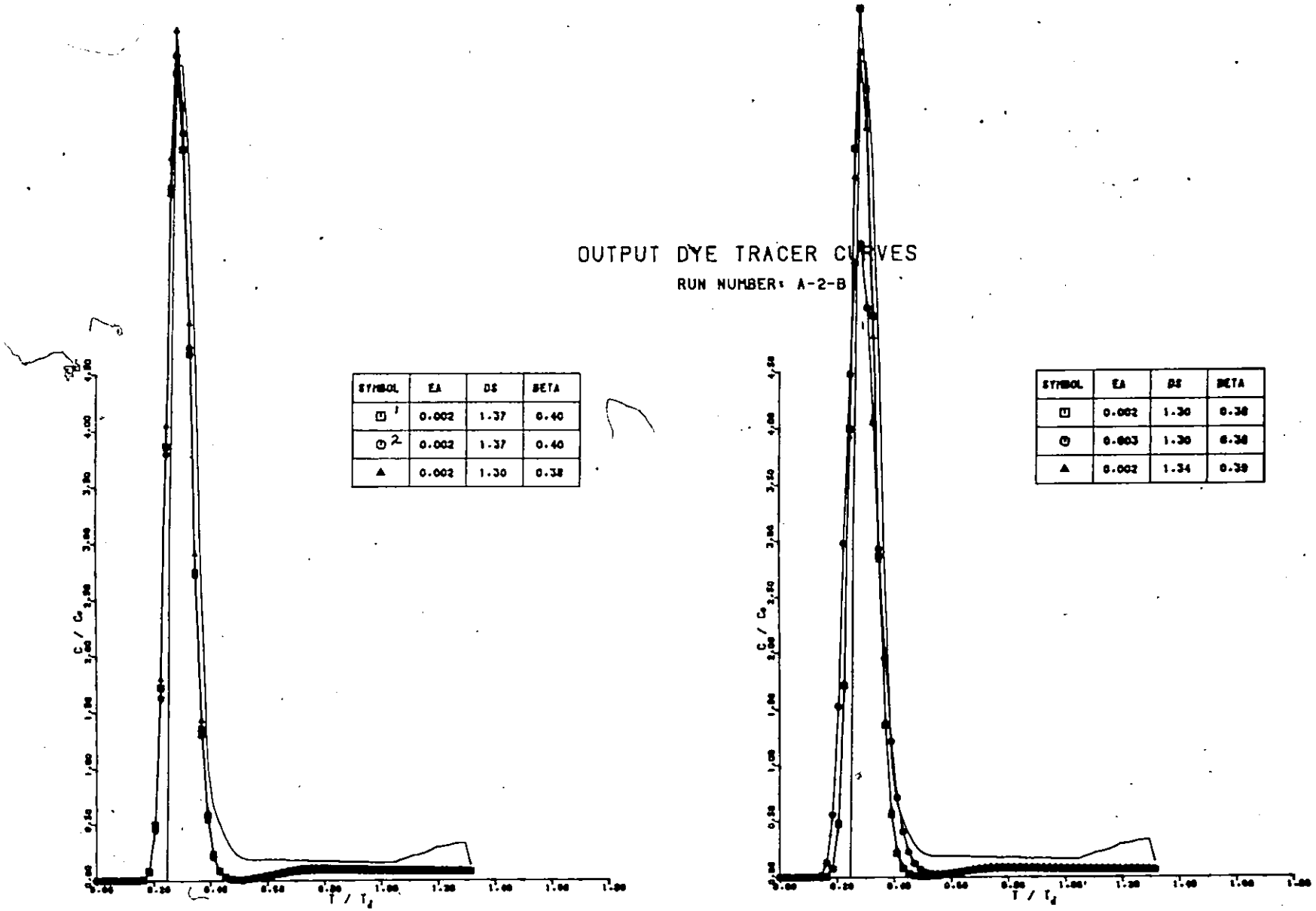

Figure 5.5

1 E_A, D_S and Beta calculated using Method II
2 E_A, D_S and Beta calculated using Method IV
Note: Experimental Curve has no symbol

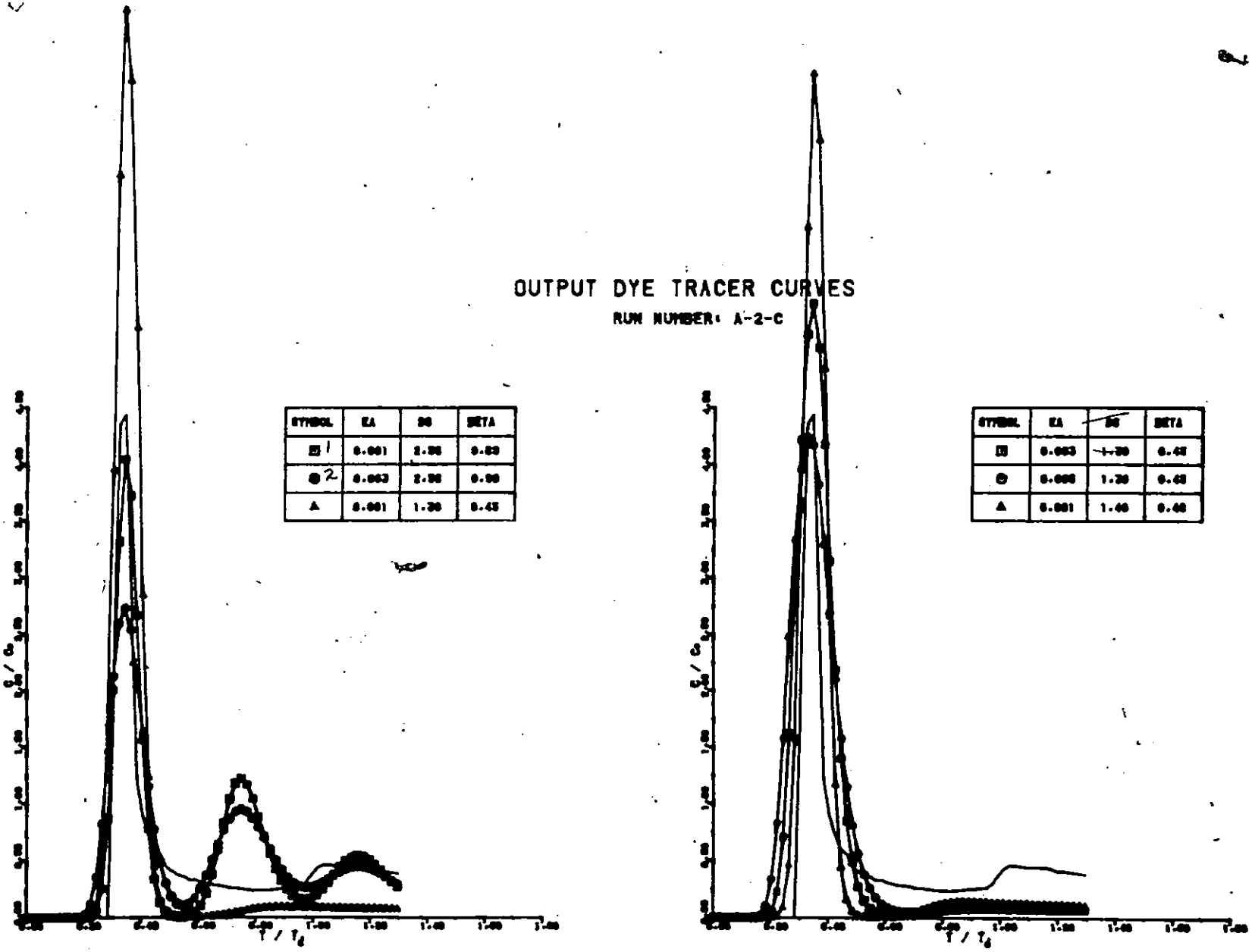

Figure 5.6

1 E_A, D_S and Beta calculated using Method II
2 E_A, D_S and Beta calculated using Method IV
Note: Experimental Curve has no symbol

OUTPUT DYE TRACER CURVES

RUN NUMBER: A-3-A

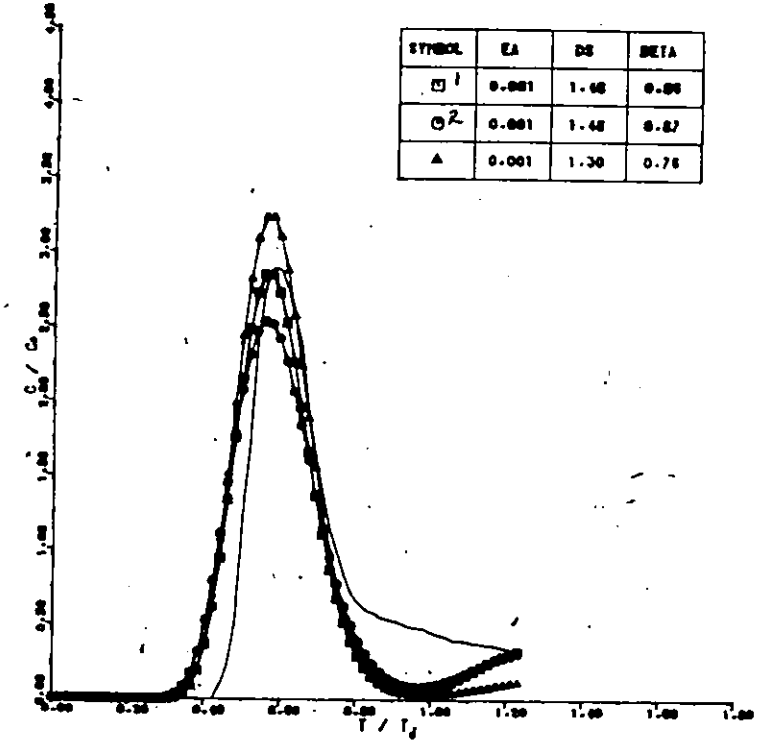

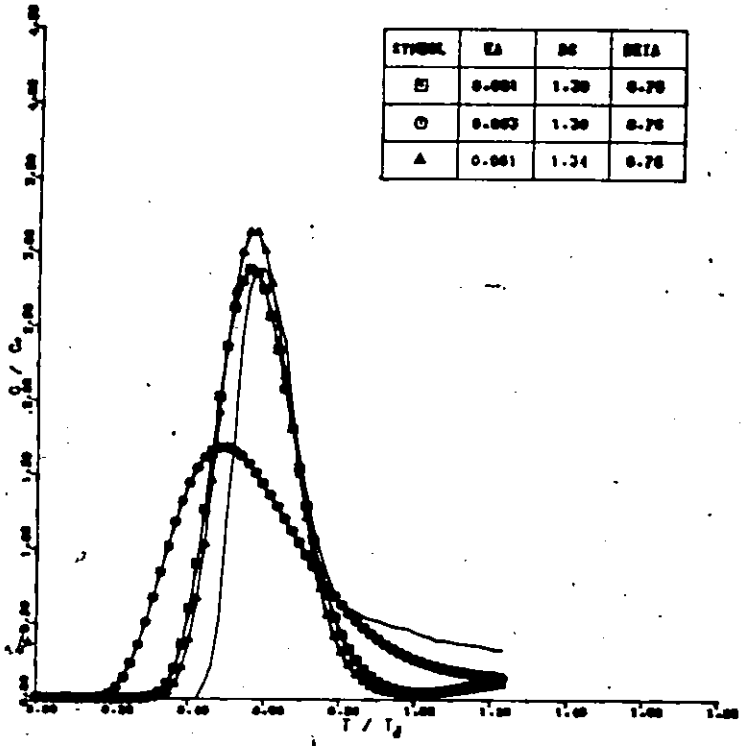

Figure 5.7

1 E_A, D_S and Beta calculated using Method II
2 E_A, D_S and Beta calculated using Method IV
Note: Experimental Curve has no symbol

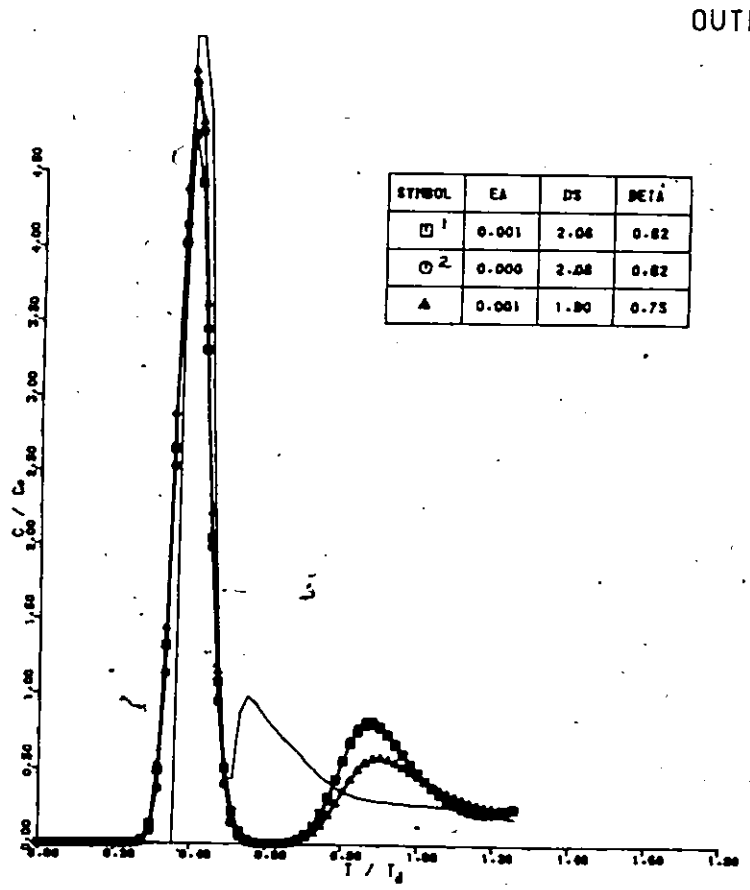

OUTPUT DYE TRACER CURVES

RUN NUMBER: A-3-B

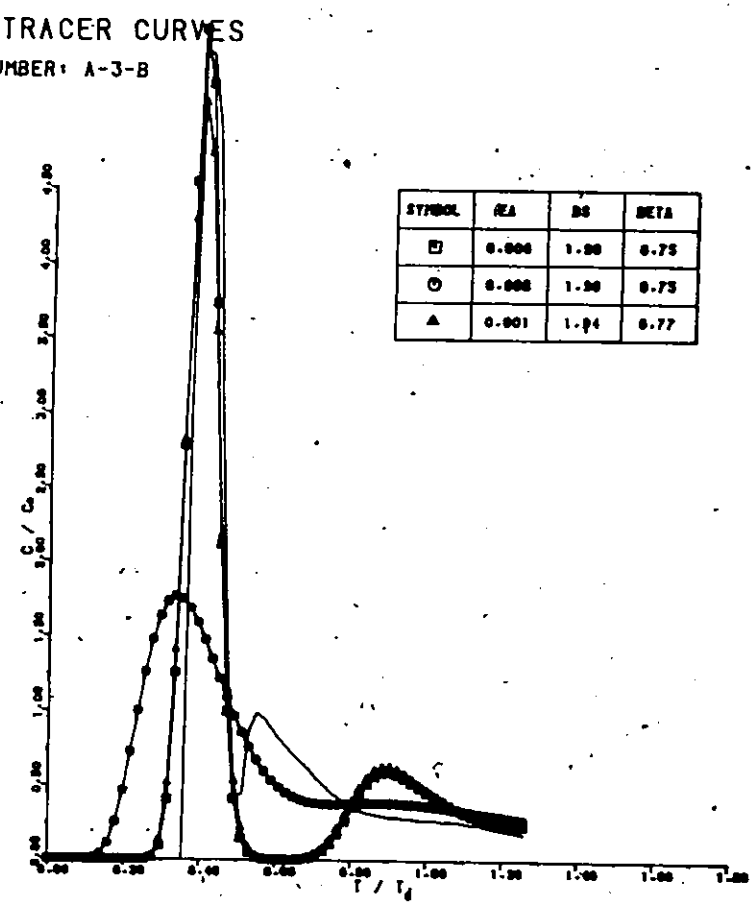

Figure 5.8

1 E_A, D_S and Beta calculated using Method II
2 E_A, D_S and Beta calculated using Method IV
Note: Experimental Curve has no symbol

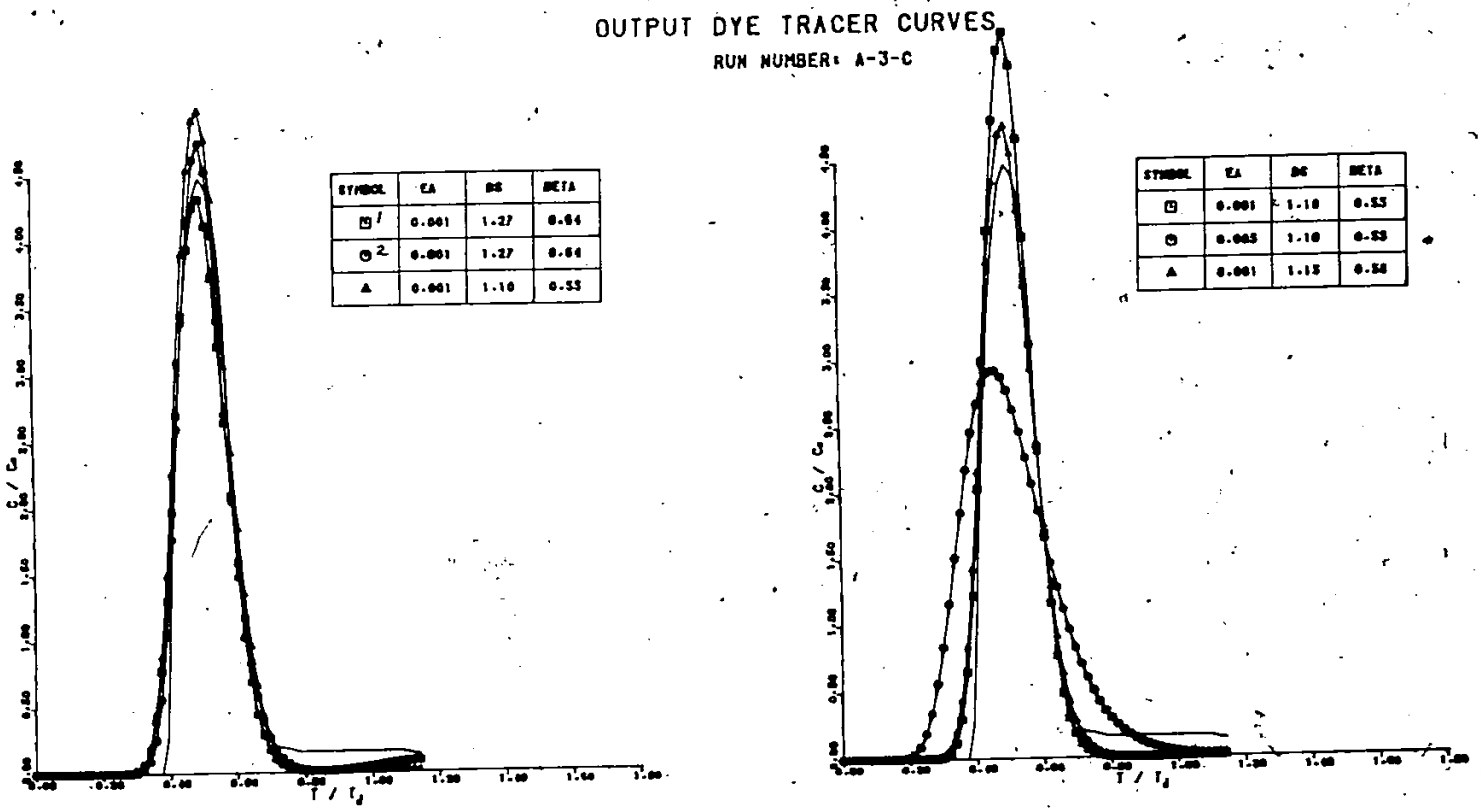

Figure 5.9

1 E_A, D_S and Beta calculated using Method II
2 E_A, D_S and Beta calculated using Method IV
Note: Experimental Curve has no symbol

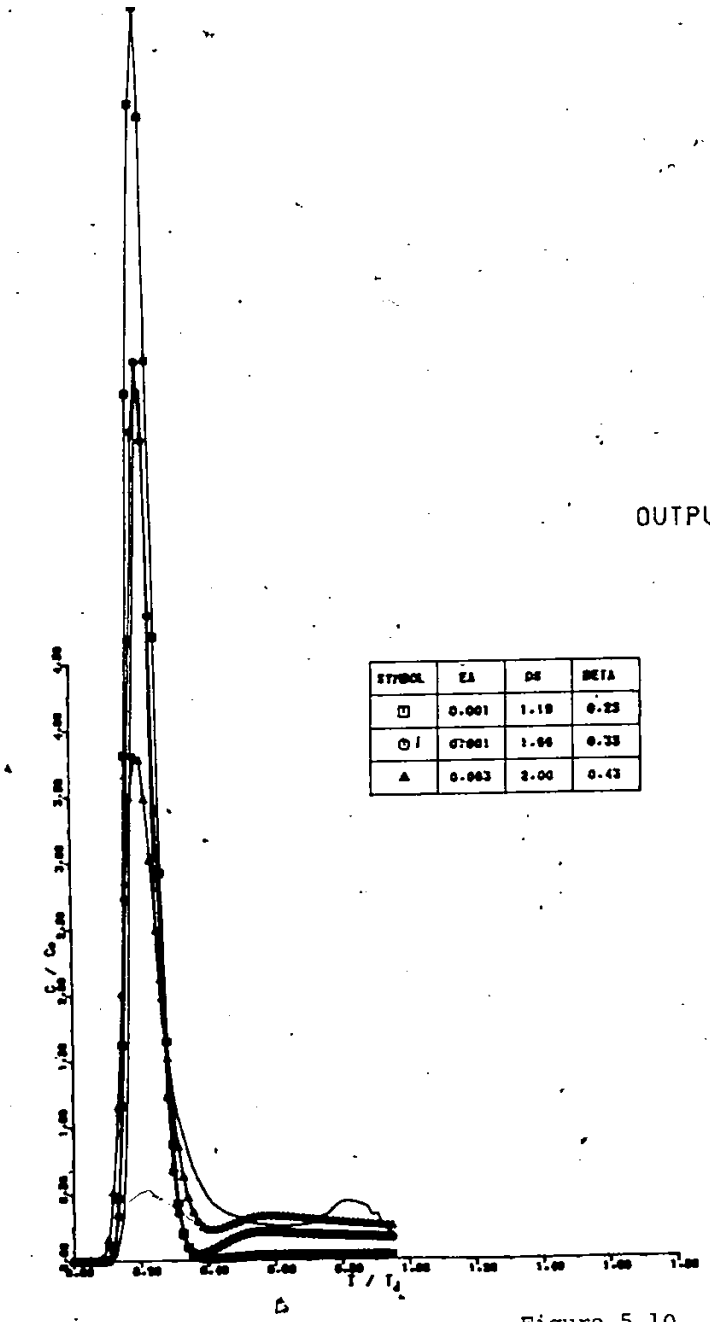

Figure 5.10

1 E_A, D_S and Beta calculated using Method II
2 E_A, D_S and Beta calculated using Method IV
Note: Experimental Curve has no symbol

OUTPUT DYE TRACER CURVES

RUN NUMBER: B-1-B

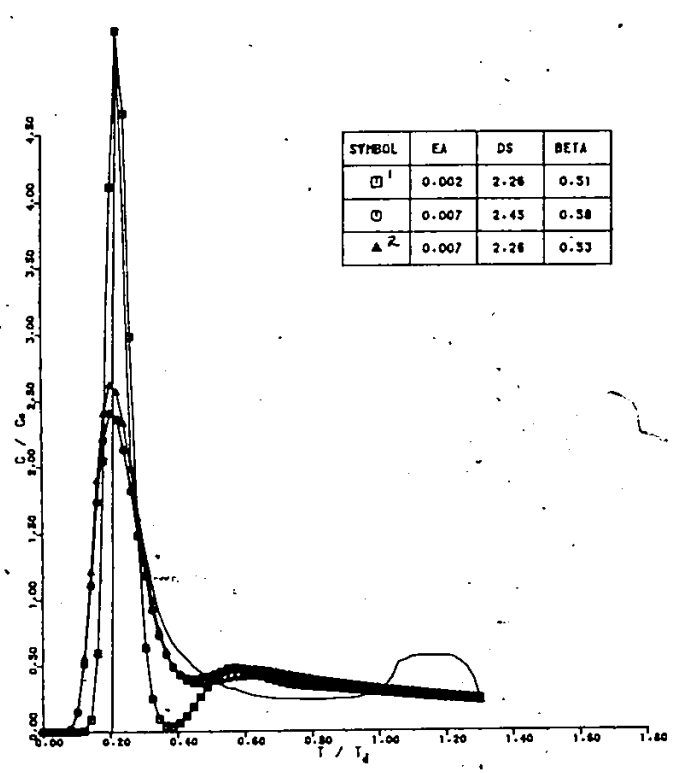

SYMBOL	EA	DS	BETA
□ [1]	0.002	2.26	0.51
○	0.007	2.45	0.58
△ [2]	0.007	2.26	0.53

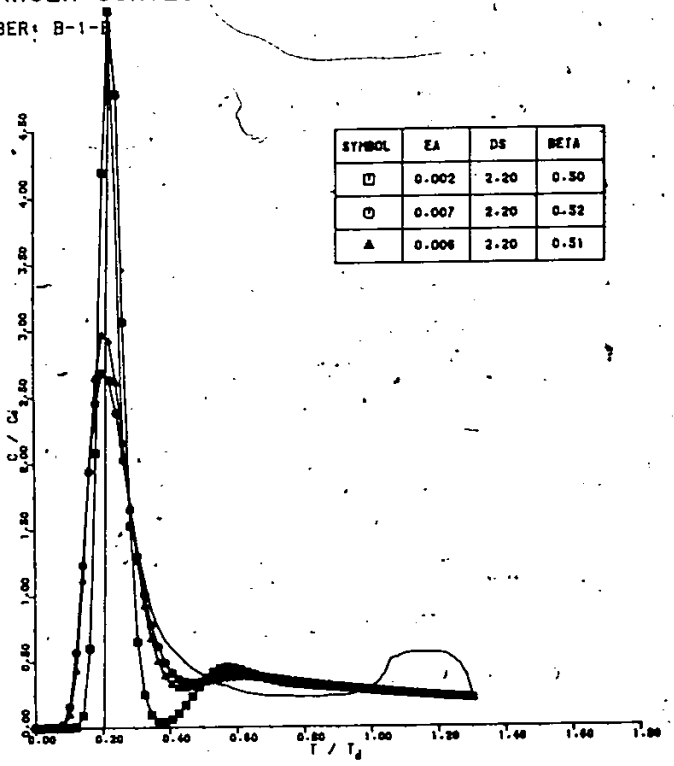

SYMBOL	EA	DS	BETA
□	0.002	2.20	0.50
○	0.007	2.20	0.52
△	0.006	2.20	0.51

Figure 5.11

1 E_A, D_S and Beta calculated using Method II
2 E_A, D_S and Beta calculated using Method IV
Note: Experimental Curve has no symbol

OUTPUT DYE TRACER CURVES

RUN NUMBER: B-1-C

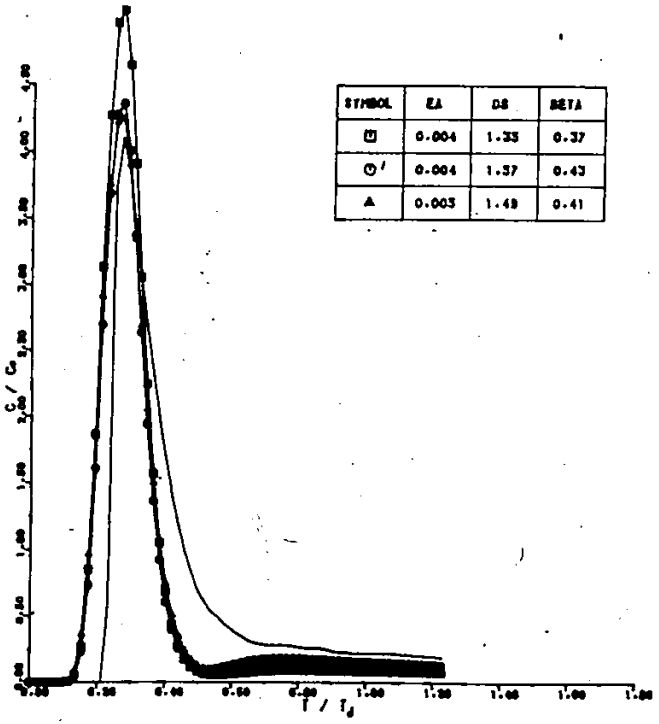

SYMBOL	EA	DS	BETA
☐	0.004	1.33	0.37
⊙ [1]	0.004	1.57	0.43
△	0.003	1.49	0.41

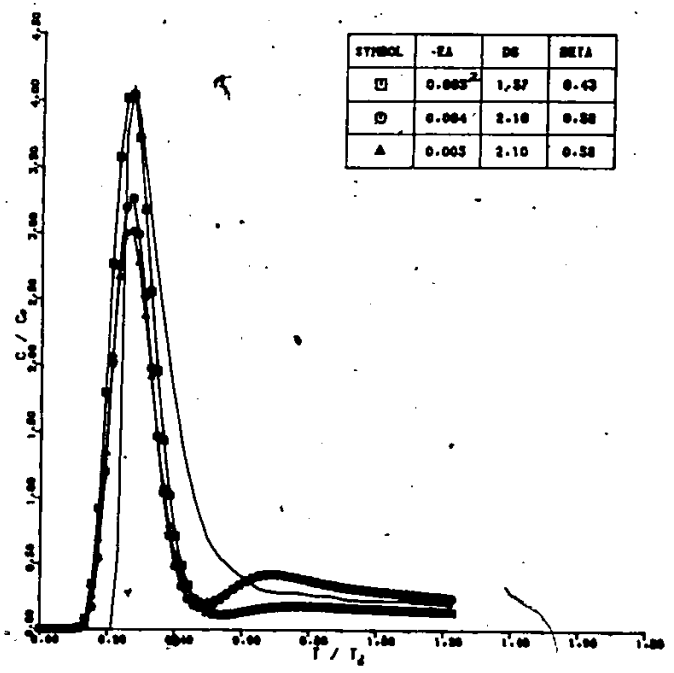

SYMBOL	-EA	DS	BETA
☐	0.003 [2]	1.57	0.43
⊙	0.004	2.18	0.58
△	0.003	2.10	0.58

Figure 5.12

[1] E_A, D_S and Beta calculated using Method II
[2] E_A, D_S and Beta calculated using Method IV
Note: Experimental Curve has no symbol

OUTPUT DYE TRACER CURVES

RUN NUMBER: B-2-A

SYMBOL	EA	DS	BETA
□	0.001	1.14	0.25
○[1]	0.001	2.18	0.49
△	0.002	1.58	0.36

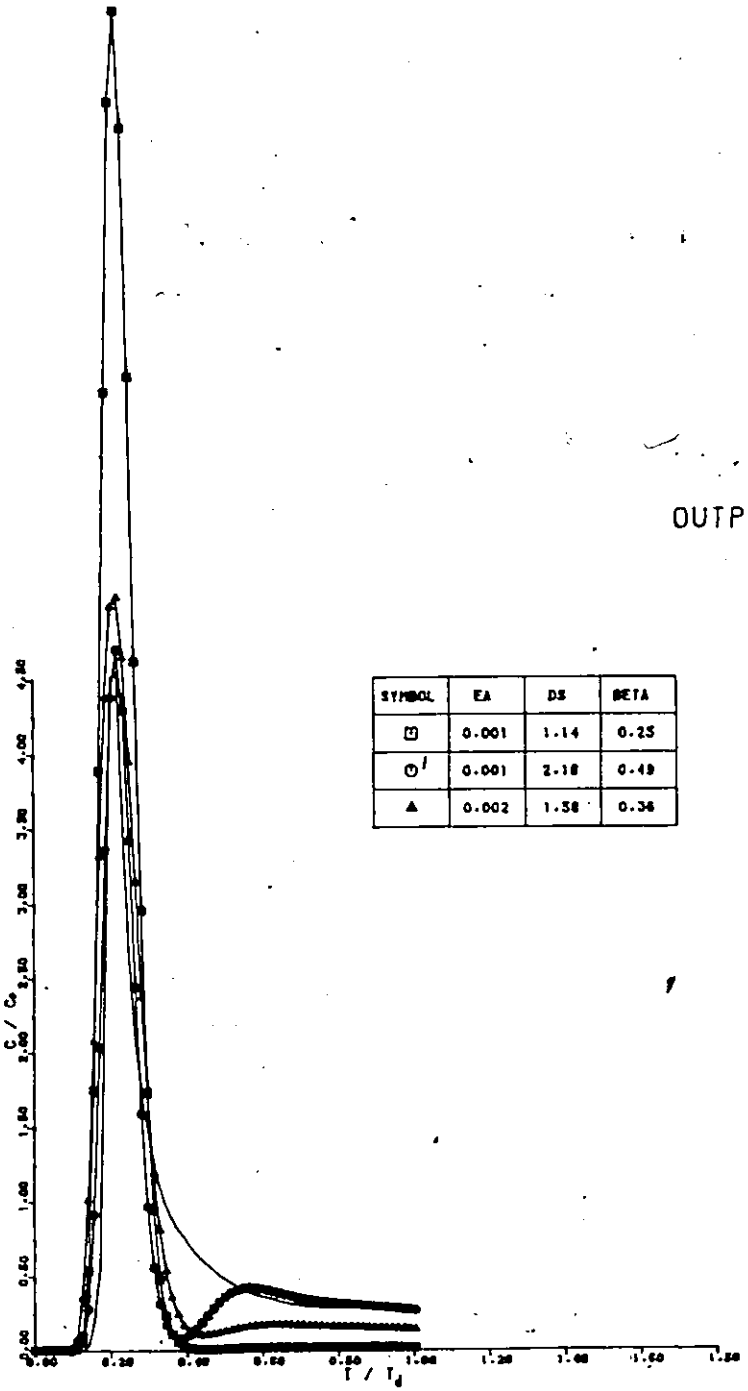

SYMBOL	EA	DS	BETA
□[2]	0.002	2.18	0.49
○	0.001	2.30	0.51
△	0.002	2.30	0.52

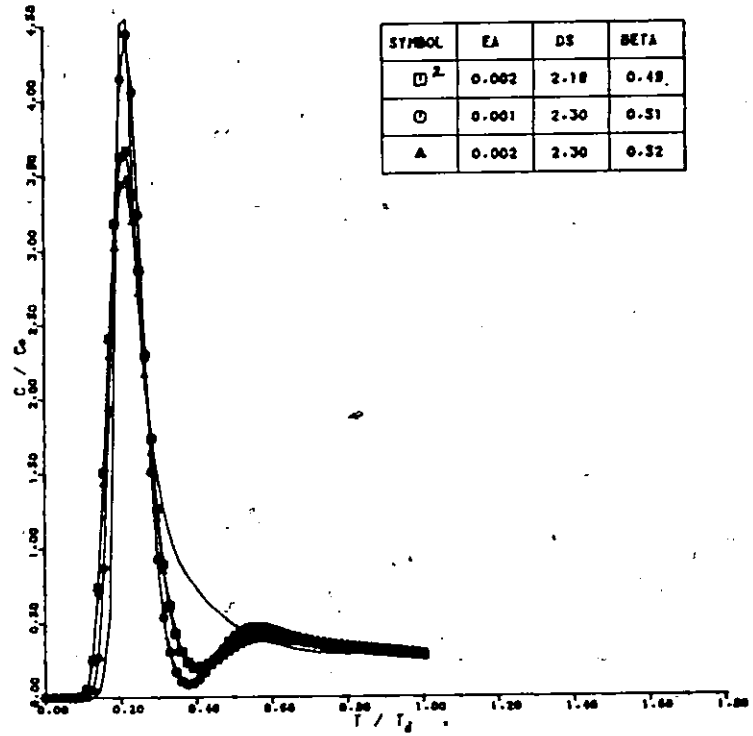

Figure 5.13

1 E_A, D_S and Beta calculated using Method II
2 E_A, D_S and Beta calculated using Method IV
Note: Experimental Curve has no symbol

OUTPUT DYE TRACER CURVES

RUN NUMBER: B-2-B

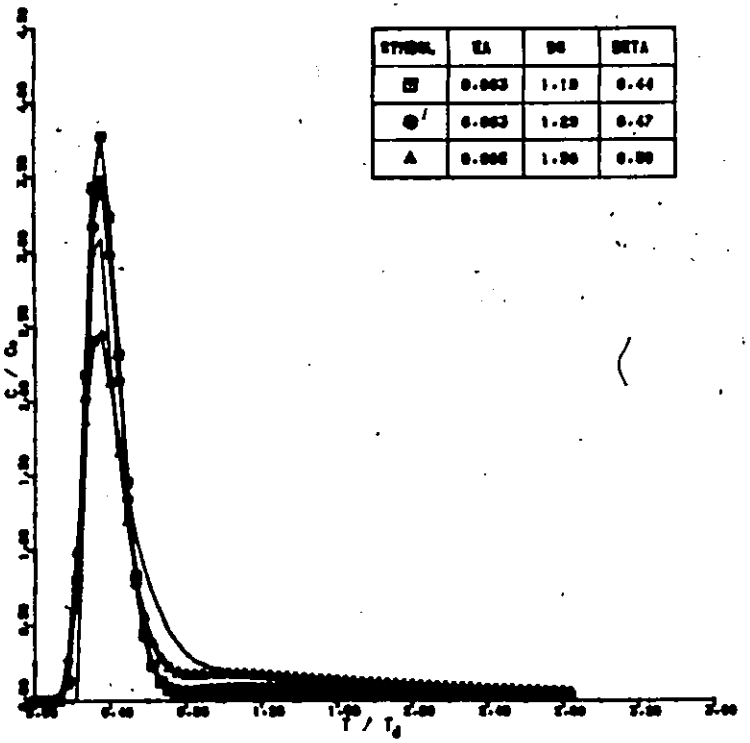

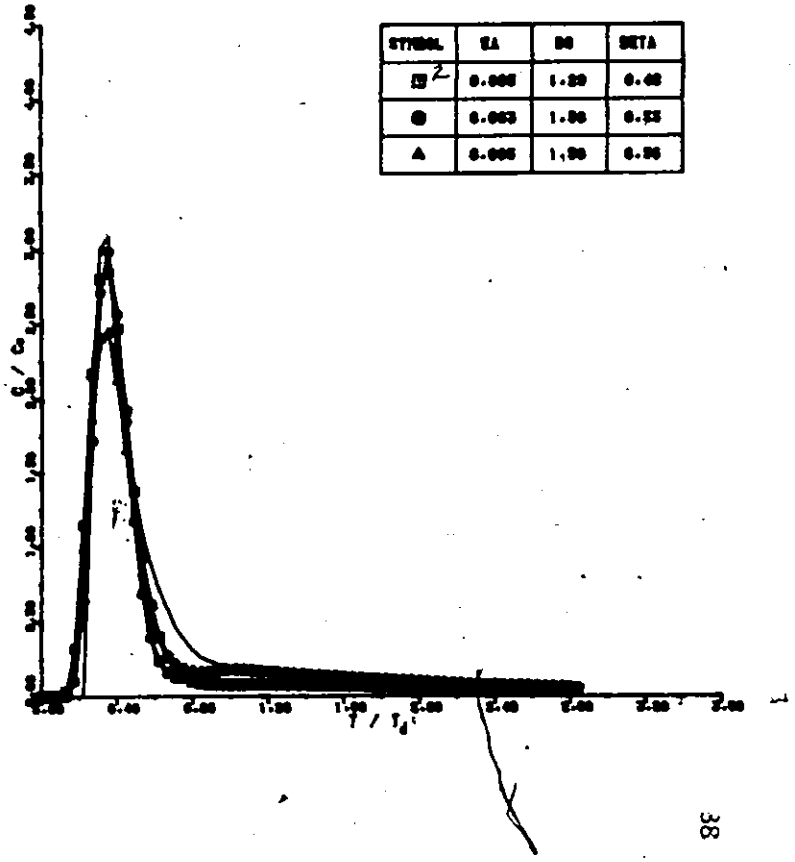

1 E_A, D_S and Beta calculated using Method II
2 E_A, D_S and Beta calculated using Method IV
Note: Experimental Curve has no symbol

Figure 5.14

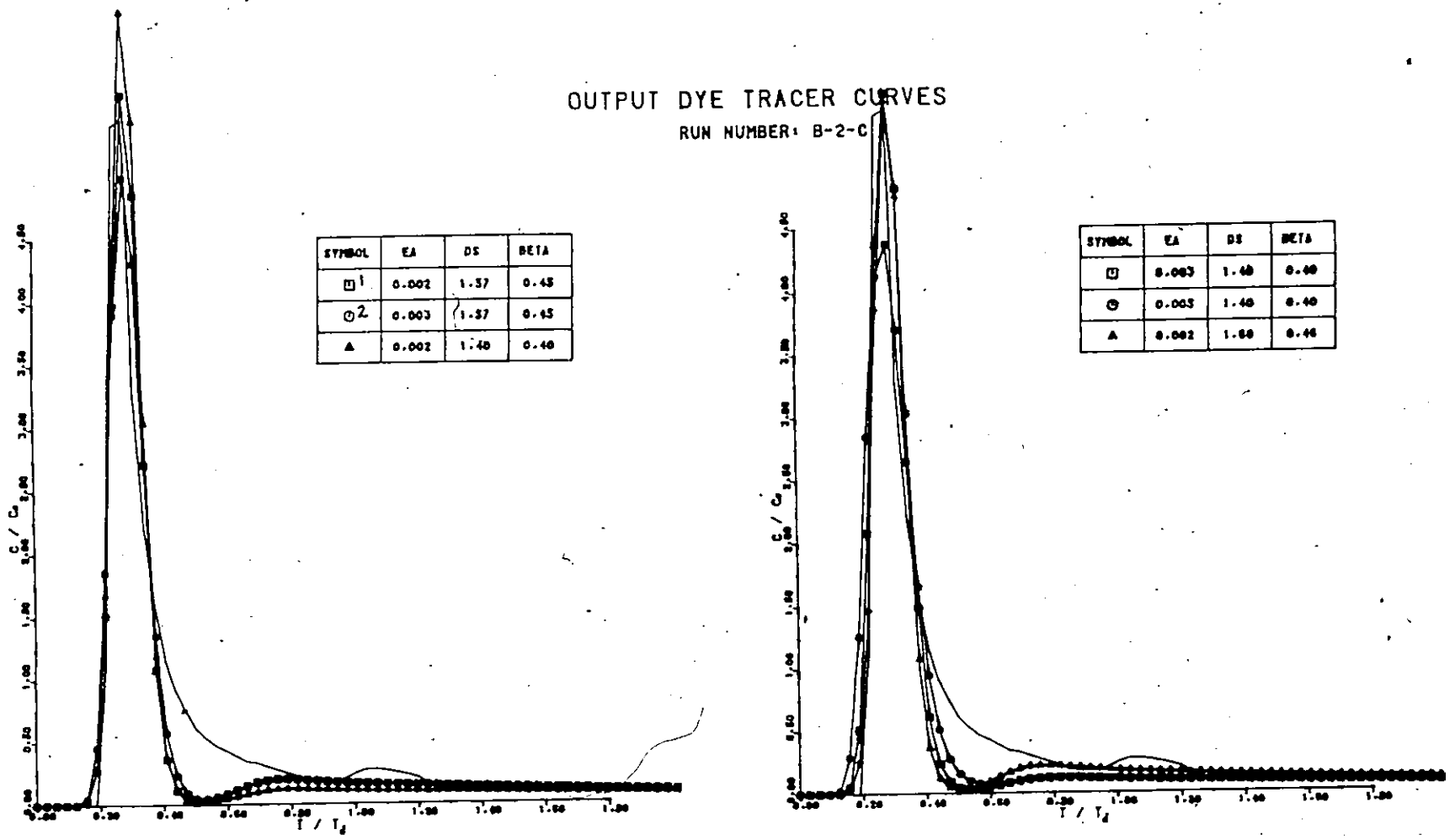

Figure 5.15

1 E_A, D_S and Beta calculated using Method II
2 E_A, D_S and Beta calculated using Method IV
Note: Experimental Curve has no symbol

OUTPUT DYE TRACER CURVES

RUN NUMBER: B-3-A

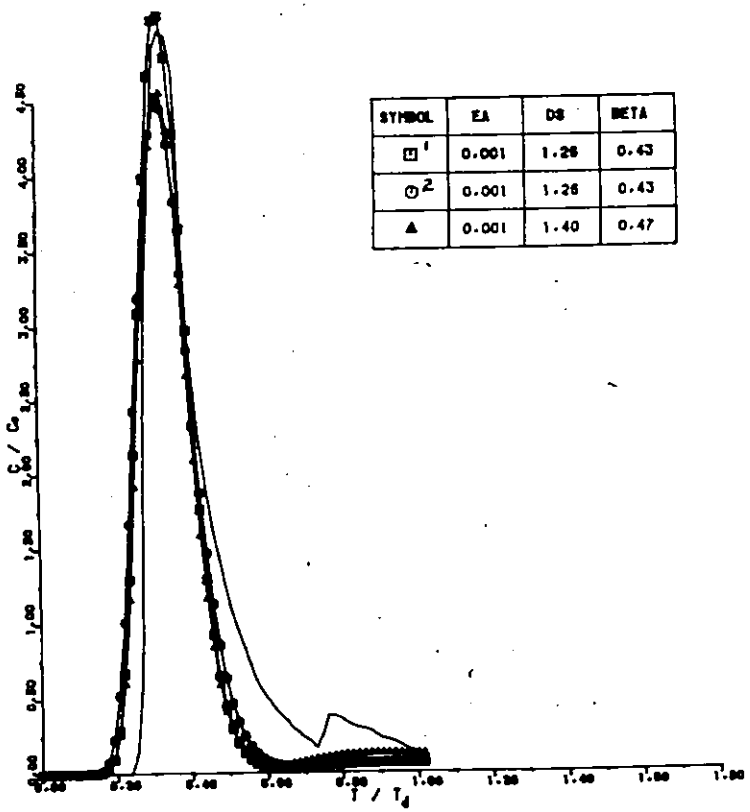

SYMBOL	EA	DS	BETA
□ [1]	0.001	1.26	0.43
⊙ [2]	0.001	1.26	0.43
▲	0.001	1.40	0.47

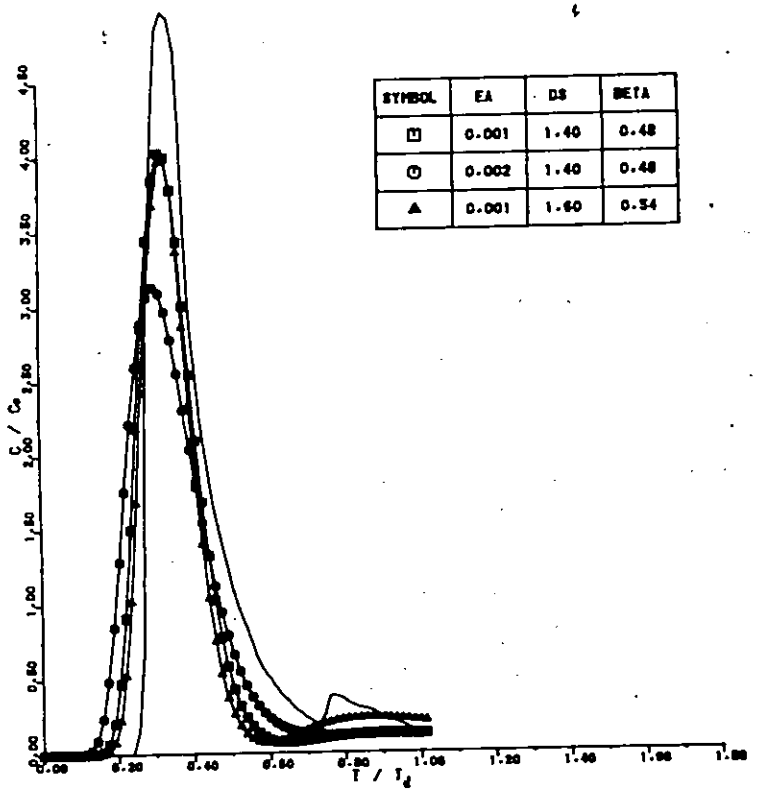

SYMBOL	EA	DS	BETA
□	0.001	1.40	0.48
⊙	0.002	1.40	0.48
▲	0.001	1.60	0.54

Figure 5.16

1 E_A, D_S and Beta calculated using Method II
2 E_A, D_S and Beta calculated using Method IV
Note: Experimental Curve has no symbol

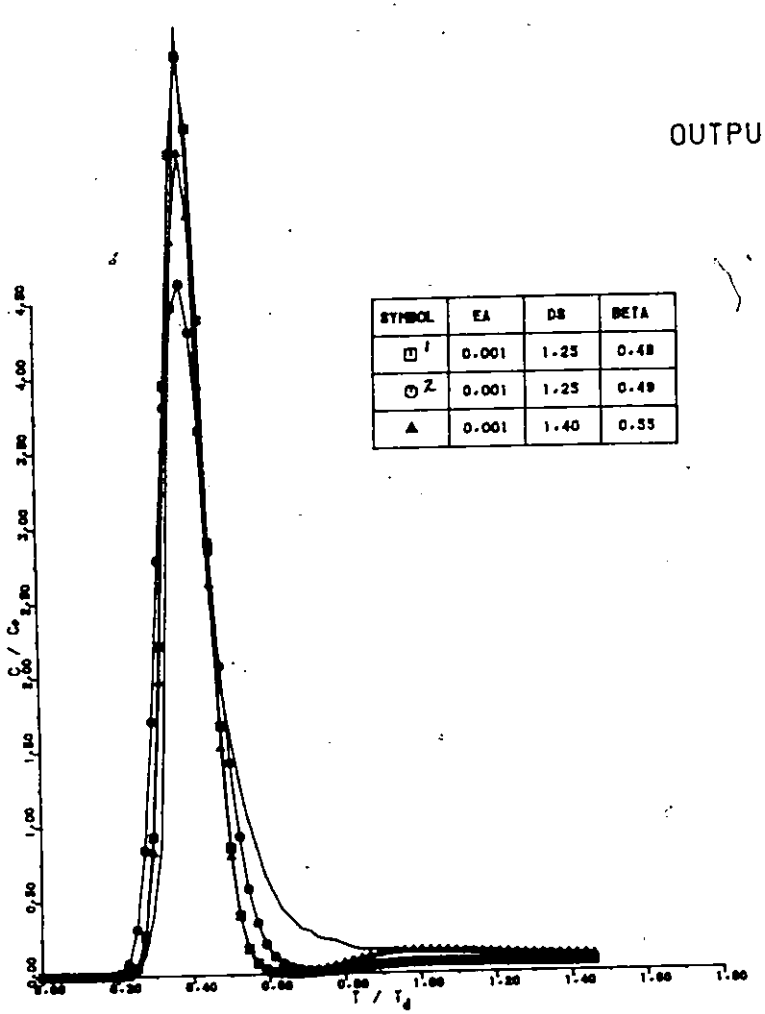

OUTPUT DYE TRACER CURVES

RUN NUMBER: B-3-B

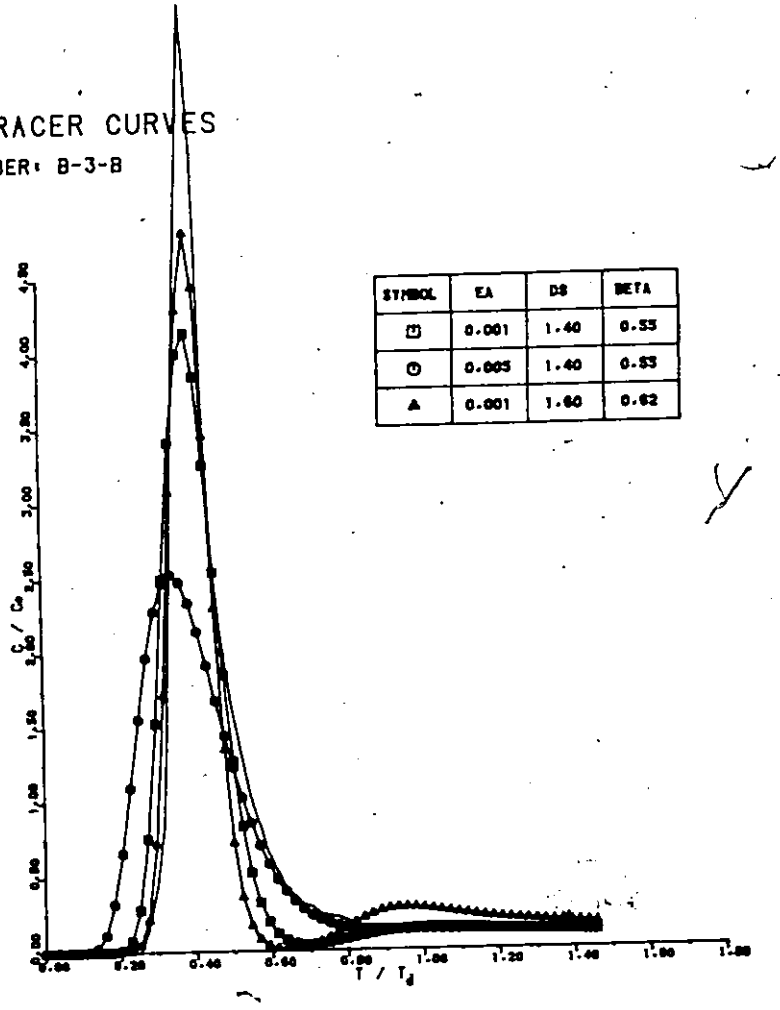

Figure 5.17

1 E_A, D_S and Beta calculated using Method II
2 E_A, D_S and Beta calculated using Method IV
Note: Experimental Curve has no symbol

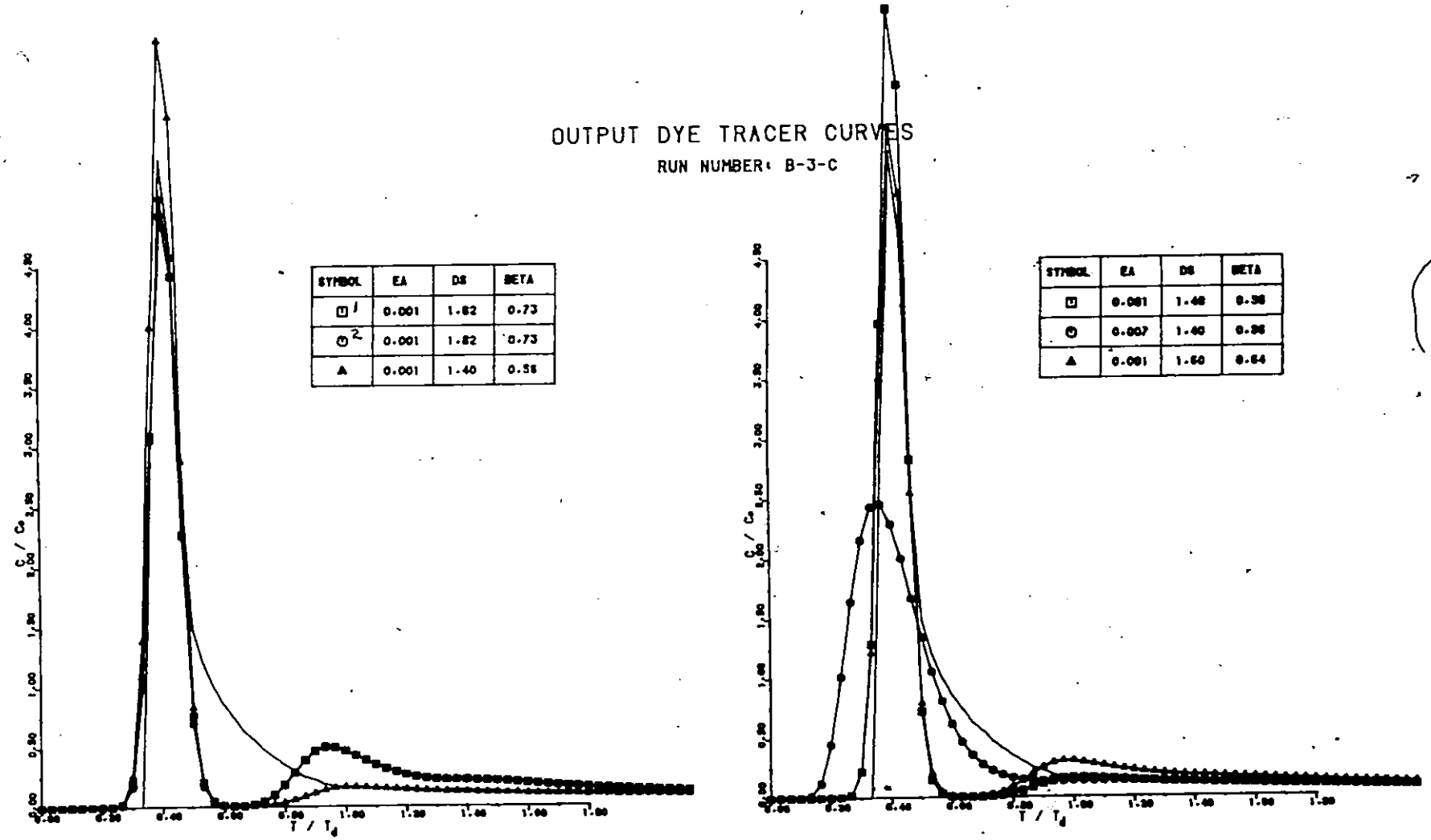

Figure 5.18

1 E_A, D_S and Beta calculated using Method II
2 E_A, D_S and Beta calculated using Method IV
Note: Experimental Curve has no symbol

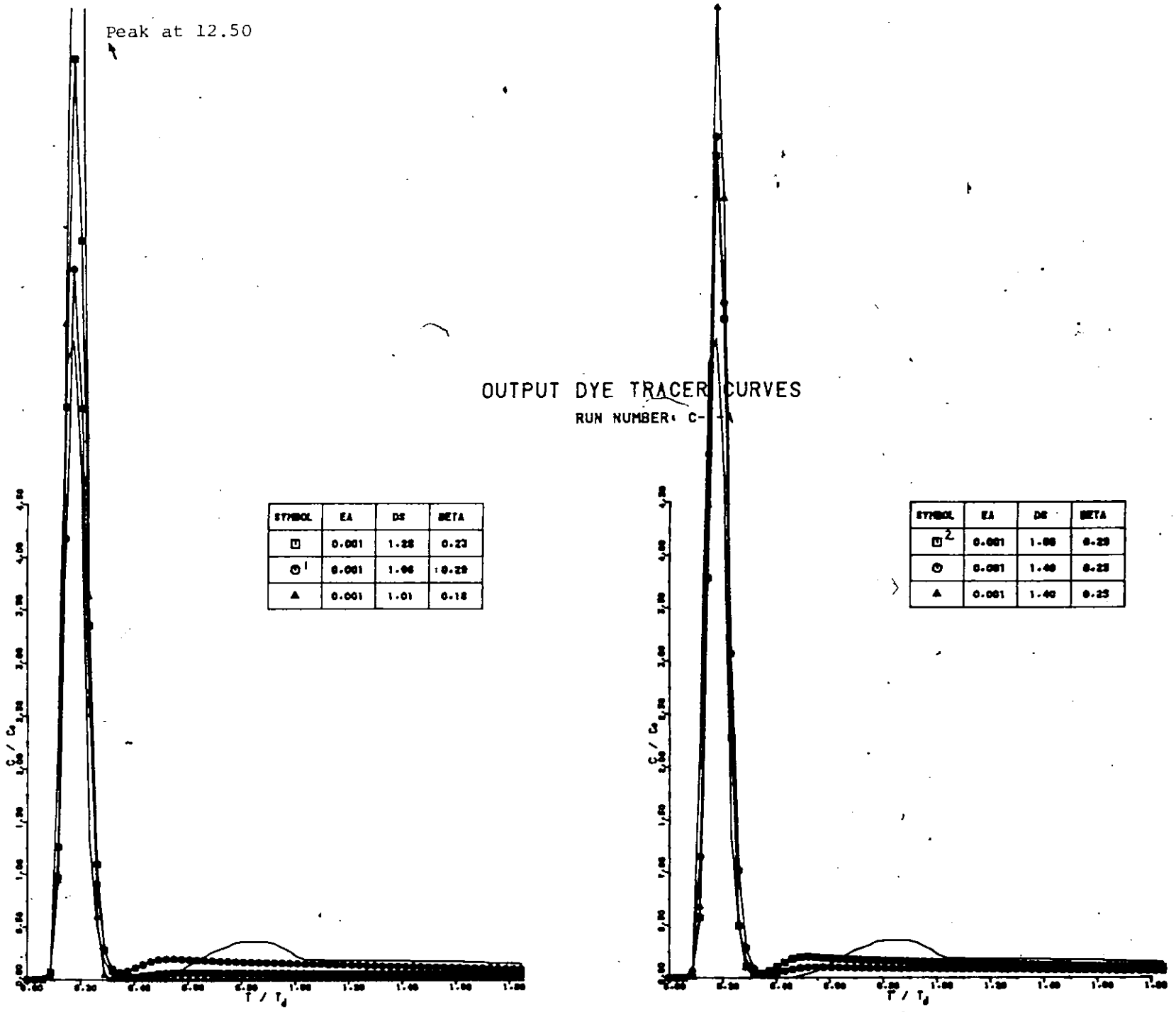

Figure 5.19

1 E_A, D_S and Beta calculated using Method II
2 E_A, D_S and Beta calculated using Method IV
Note: Experimental Curve has no symbol

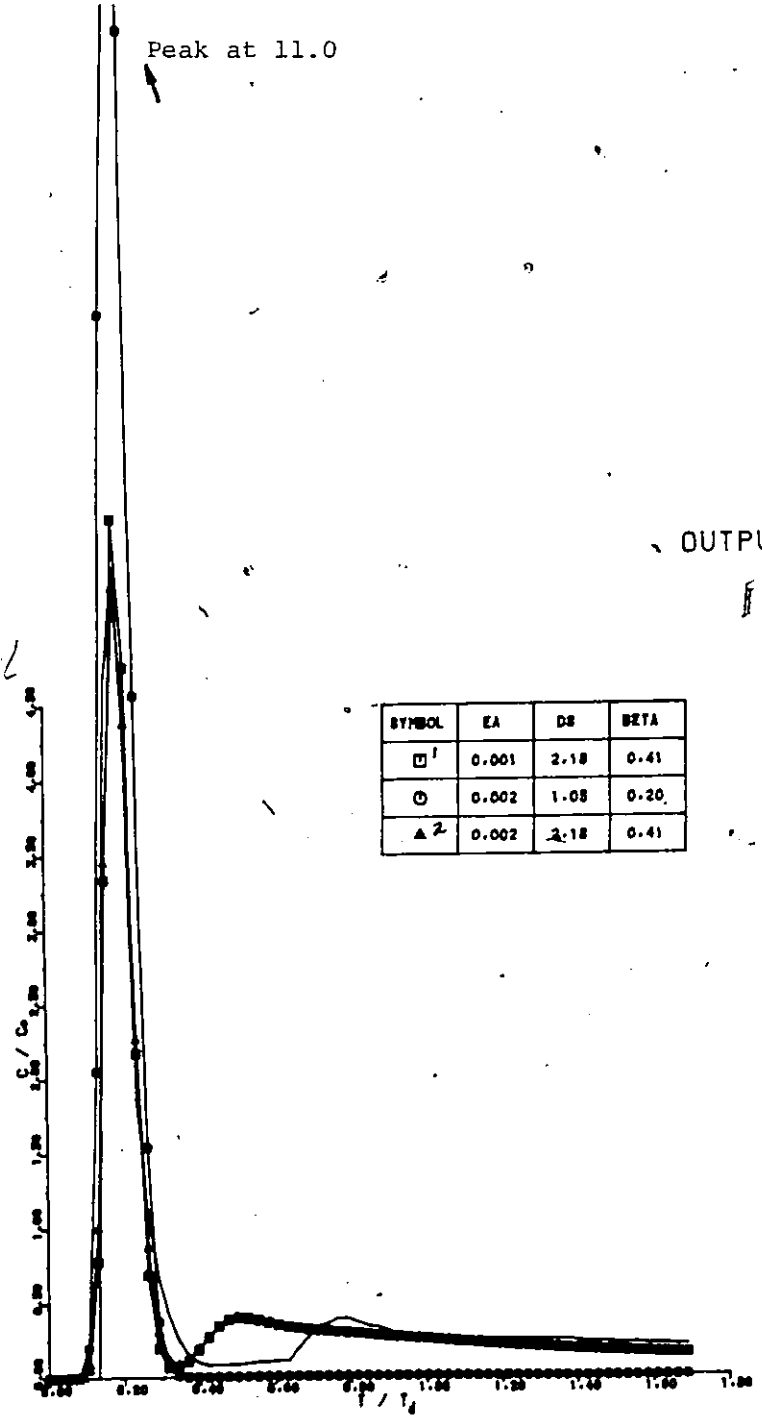

SYMBOL	EA	DS	BETA
□ [1]	0.001	2.18	0.41
○	0.002	1.08	0.20
△ [2]	0.002	2.18	0.41

OUTPUT DYE TRACER CURVES

RUN NUMBER: C-

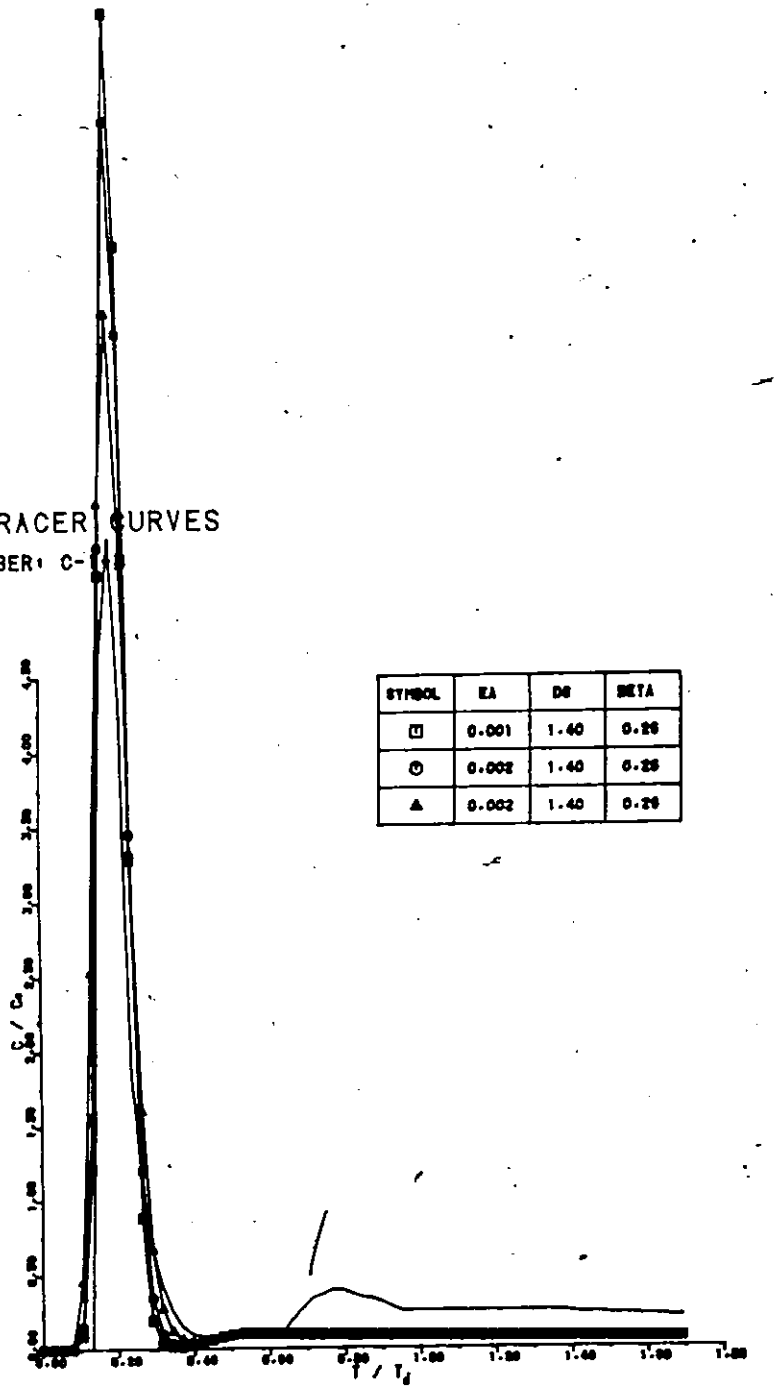

SYMBOL	EA	DS	BETA
□	0.001	1.40	0.26
○	0.002	1.40	0.26
△	0.002	1.40	0.26

Figure 5.20

1 E_A, D_S and Beta calculated using Method II
2 E_A, D_S and Beta calculated using Method IV
Note: Experimental Curve has no symbol

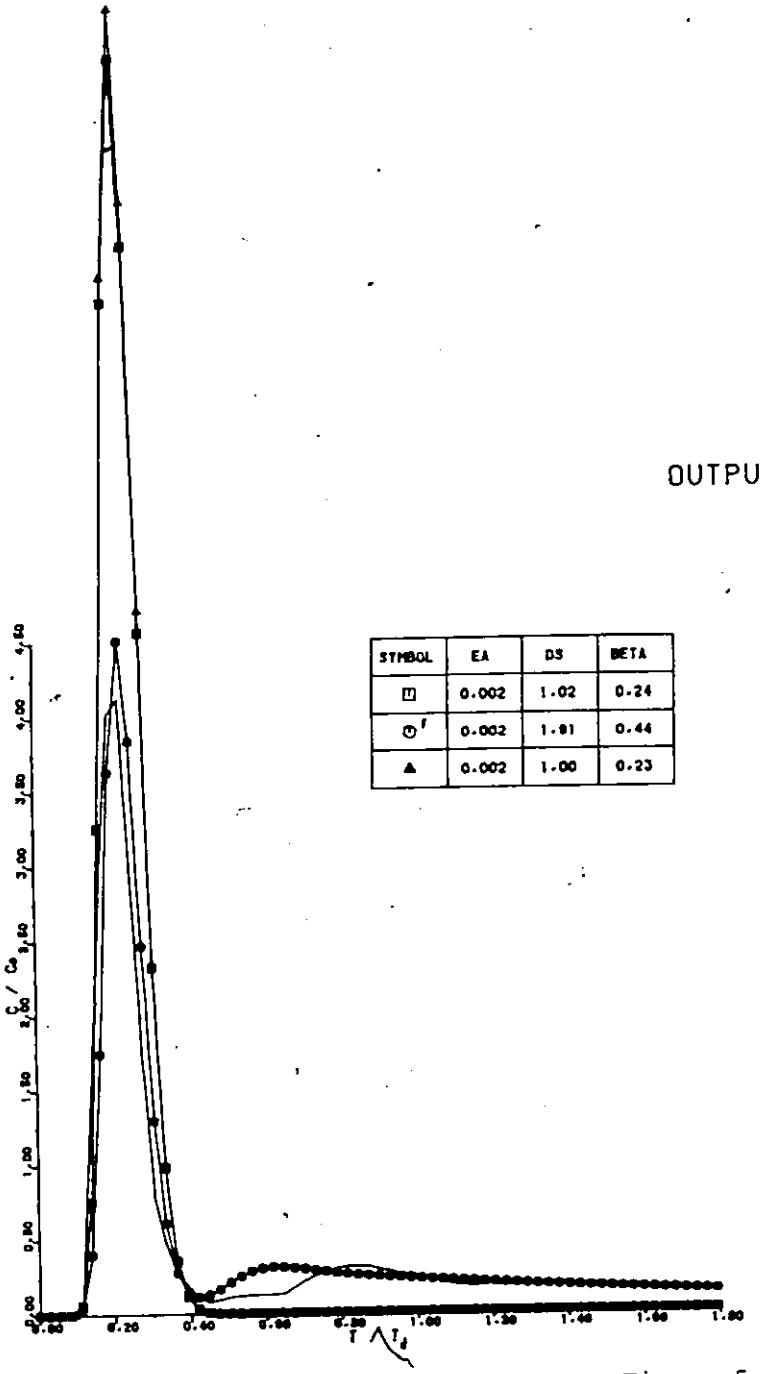

SYMBOL	EA	DS	BETA
□	0.002	1.02	0.24
⊙ [1]	0.002	1.81	0.44
▲	0.002	1.00	0.23

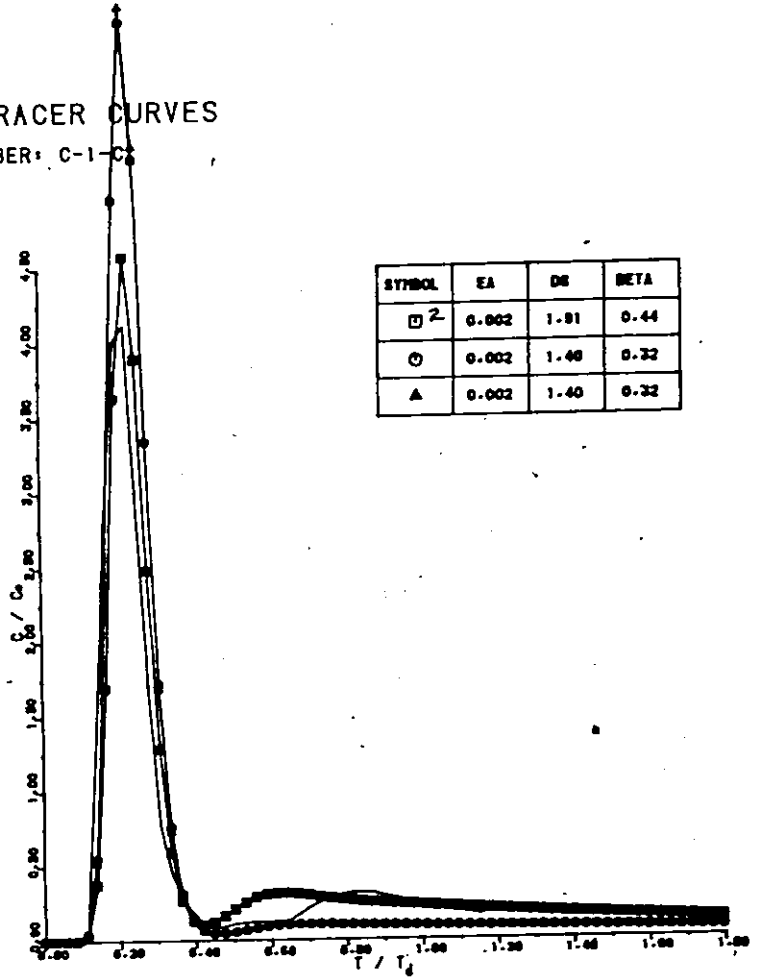

SYMBOL	EA	DS	BETA
□ [2]	0.002	1.81	0.44
⊙	0.002	1.40	0.32
▲	0.002	1.40	0.32

Figure 5.21

1 E_A, D_S and Beta calculated using Method II
2 E_A, D_S and Beta calculated using Method IV
Note: Experimental Curve has no symbol

OUTPUT DYE TRACER CURVES

RUN NUMBER: C-2-A

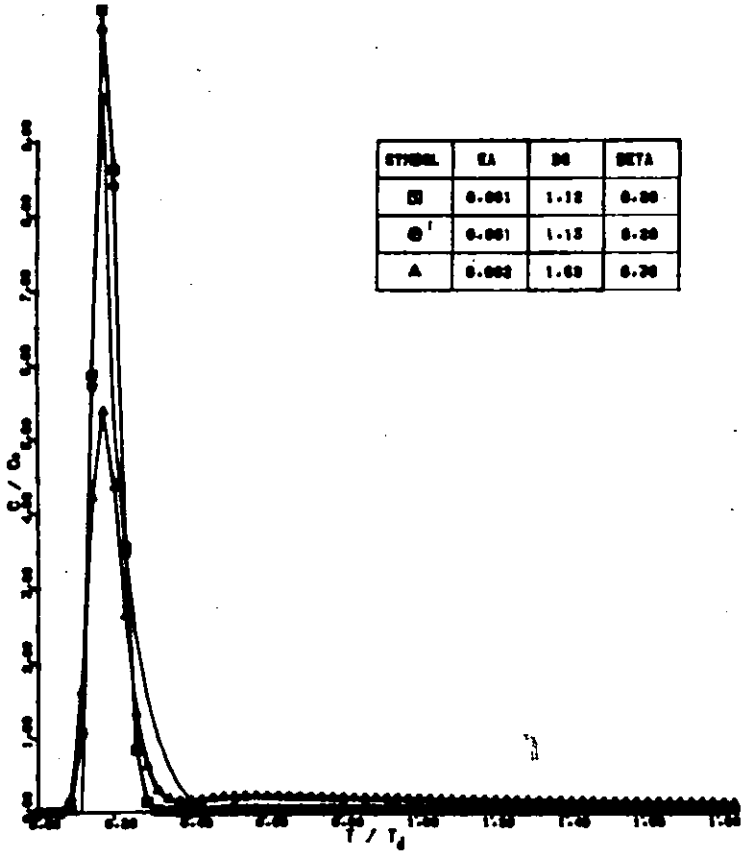

SYMBOL	EA	DS	BETA
□	0.001	1.12	0.00
◎ [1]	0.001	1.13	0.20
△	0.002	1.69	0.20

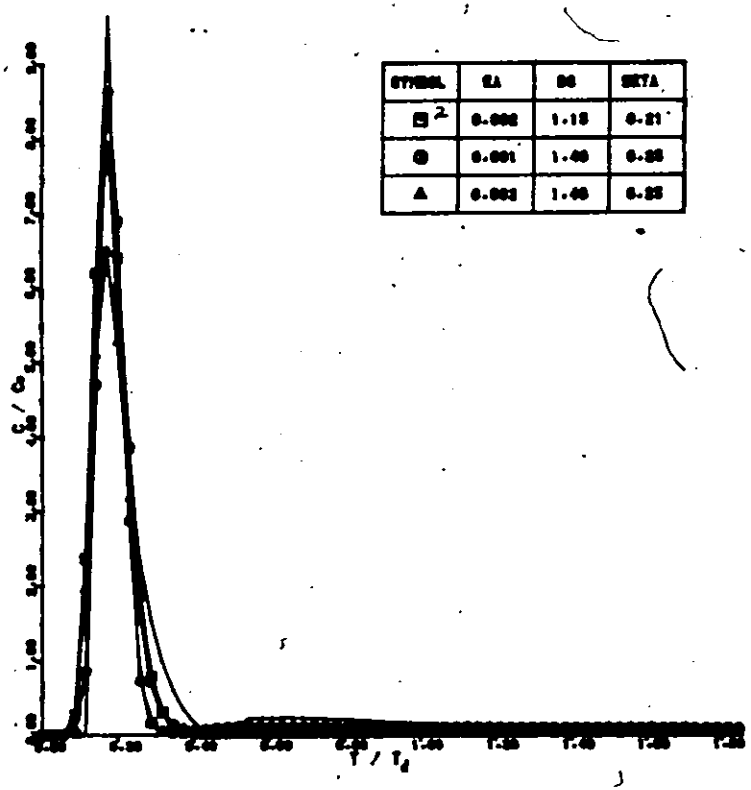

SYMBOL	EA	DS	BETA
□ [2]	0.002	1.15	0.21
◎	0.001	1.40	0.25
△	0.002	1.40	0.25

1 E_A, D_S and Beta calculated using Method II
2 E_A, D_S and Beta calculated using Method IV
Note: Experimental Curve has no symbol

Figure 5.22

OUTPUT DYE TRACER CURVES

RUN NUMBER: C-2-B

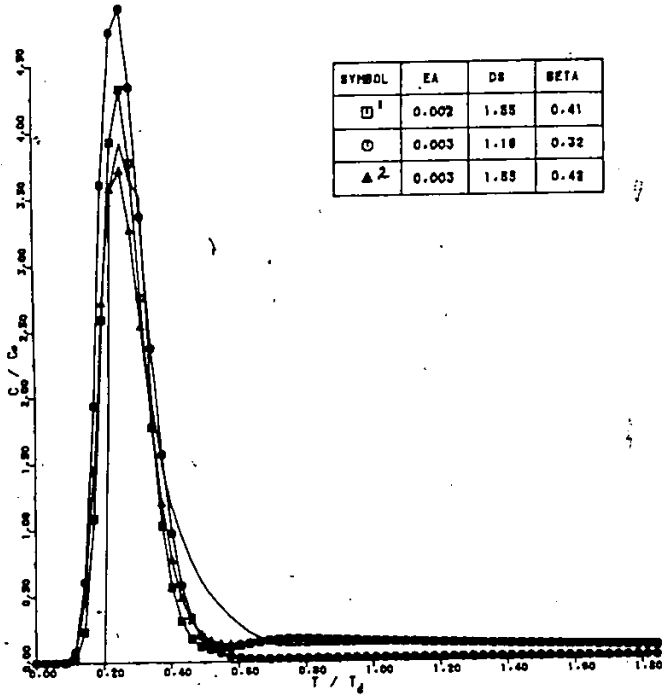

SYMBOL	EA	DS	BETA
□ [1]	0.002	1.55	0.41
○	0.003	1.18	0.32
△ [2]	0.003	1.55	0.42

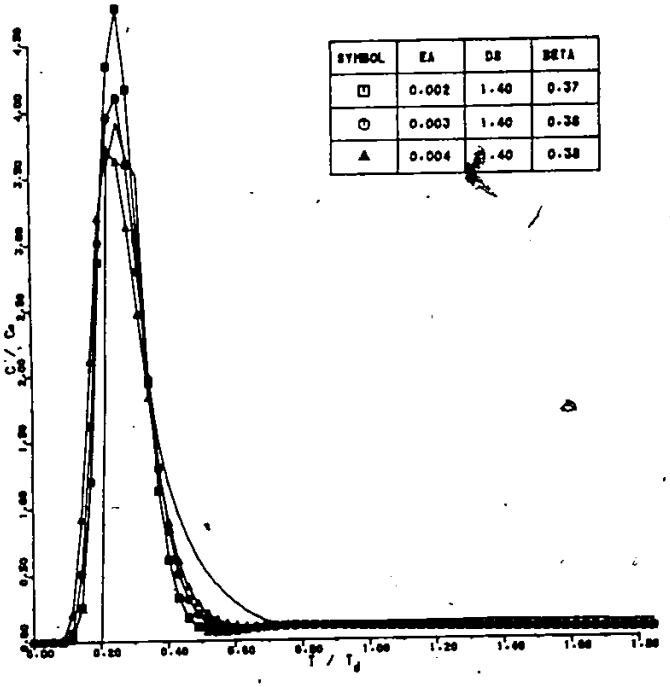

SYMBOL	EA	DS	BETA
□	0.002	1.40	0.37
○	0.003	1.40	0.38
△	0.004	1.40	0.38

1 E_A, D_S and Beta calculated using Method II
2 E_A, DS and Beta calculated using Method IV
Note: Experimental Curve has no symbol

Figure 5.23

OUTPUT DYE TRACER CURVES

RUN NUMBER: C-2-C

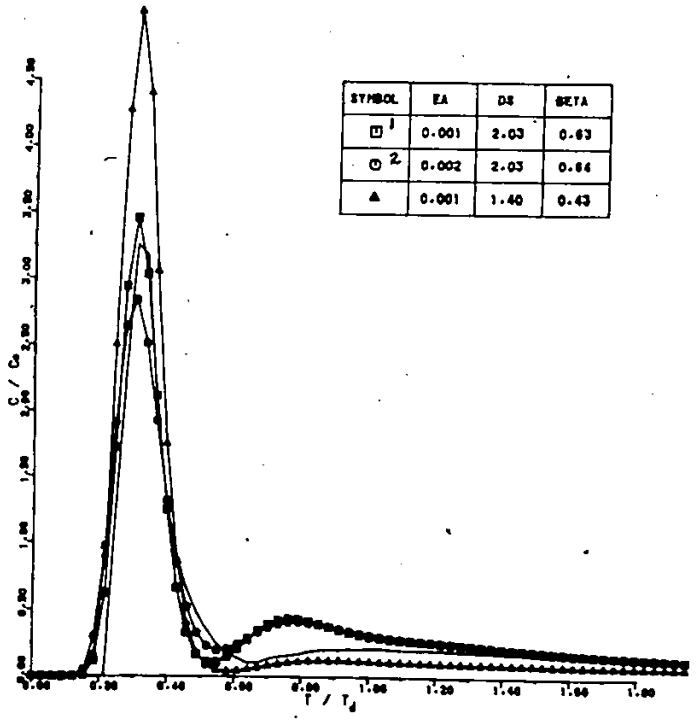

SYMBOL	EA	DS	BETA
□ 1	0.001	2.03	0.63
○ 2	0.002	2.03	0.64
△	0.001	1.40	0.43

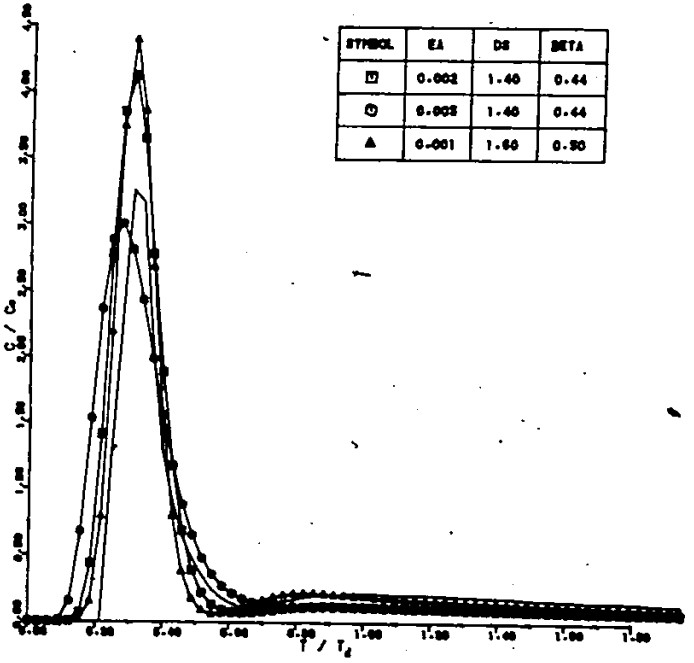

SYMBOL	EA	DS	BETA
□	0.002	1.40	0.44
○	0.002	1.40	0.44
△	0.001	1.60	0.50

1 E_A, D_S and Beta calculated using Method II
2 E_A, D_S and Beta calculated using Method IV
Note: Experimental Curve has no symbol

Figure 5.24

OUTPUT DYE TRACER CURVES

RUN NUMBER: C-3-A

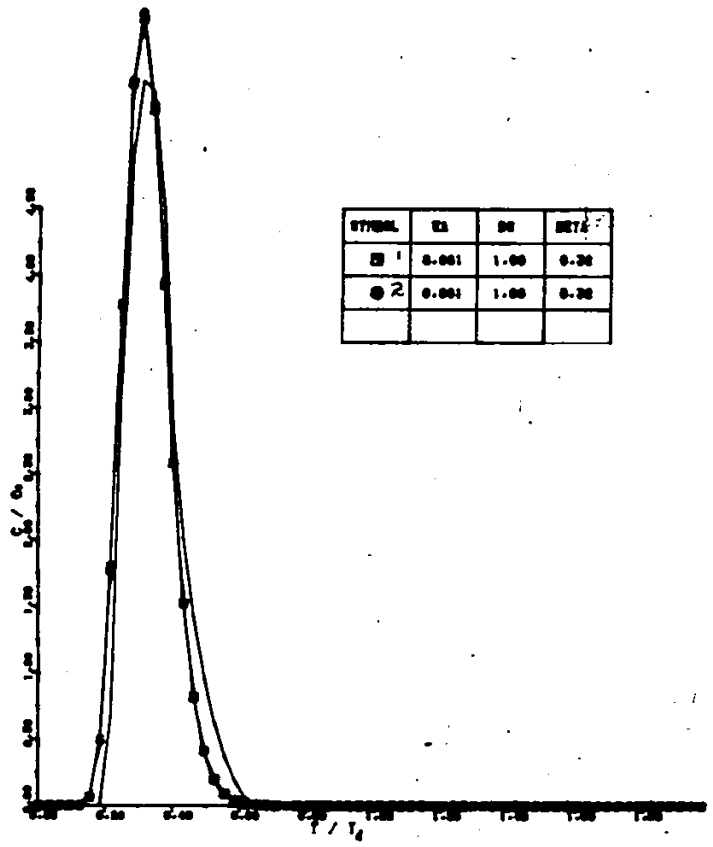

Figure 5.25

1 E_A, D_S and Beta calculated using Method II
2 E_A, D_S and Beta calculated using Method IV
Note: Experimental Curve has no symbol

OUTPUT DYE TRACER CURVES

RUN NUMBER: C-3-B

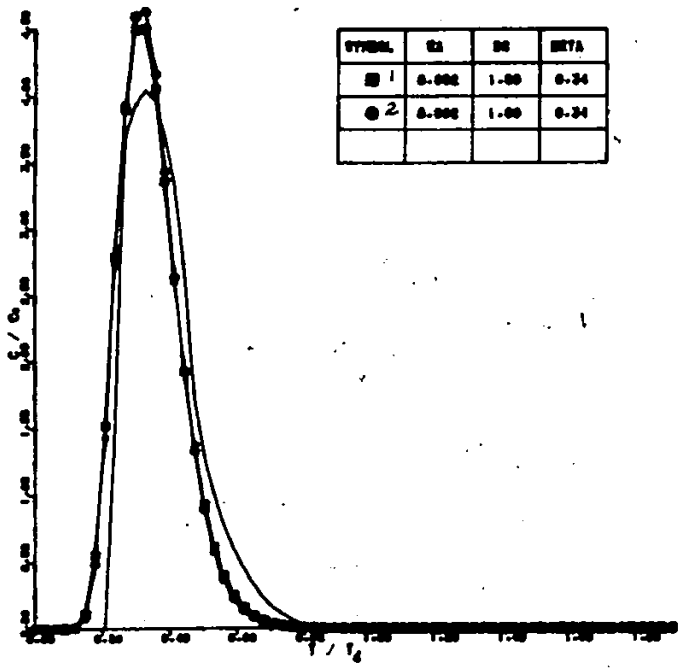

Figure 5.25

1 E_A, D_S and Beta calculated using Method II
2 E_A, D_S and Beta calculated using Method IV
Note: Experimental Curve has no symbol

OUTPUT DYE TRACER CURVES

RUN NUMBER: C-3-C

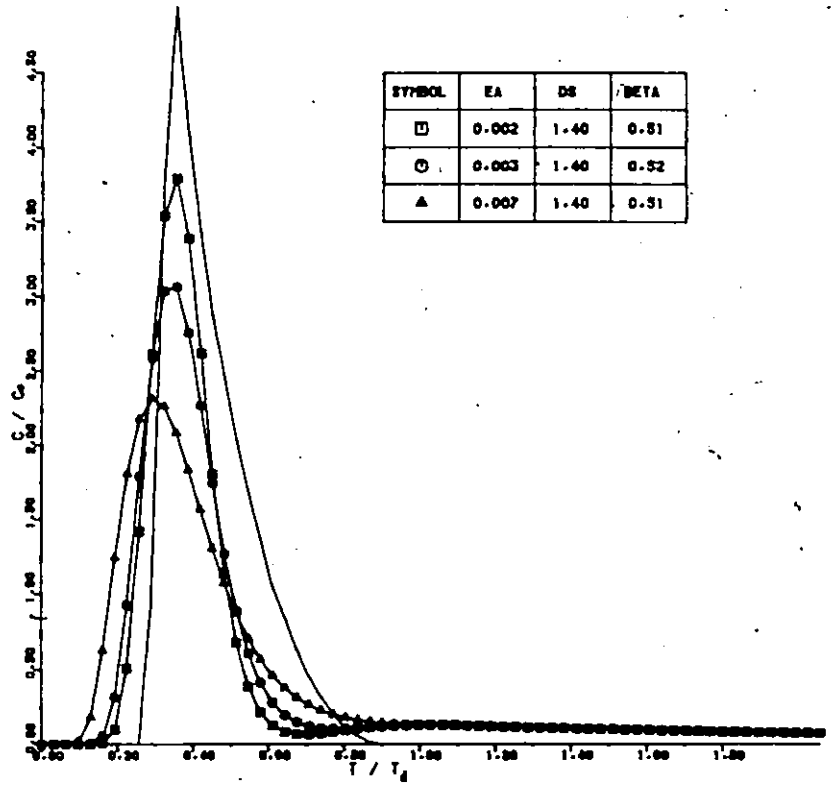

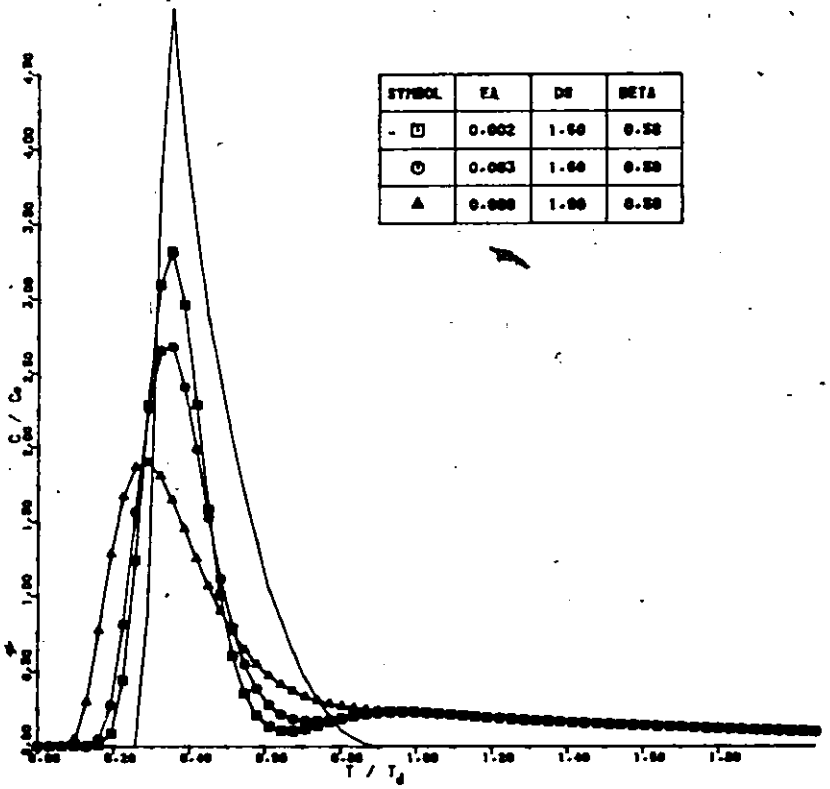

1 E_A, D_S and Beta calculated using Method II
2 E_A, D_S and Beta calculated using Method IV
Note: Experimental Curve has no symbol

Figure 5.27

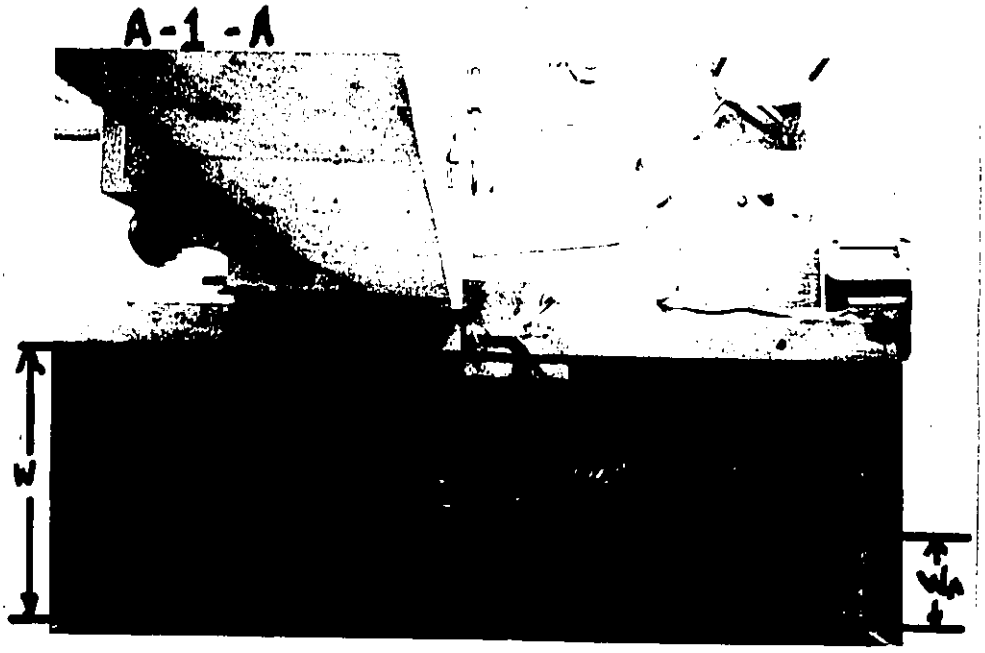

Figure 5.28

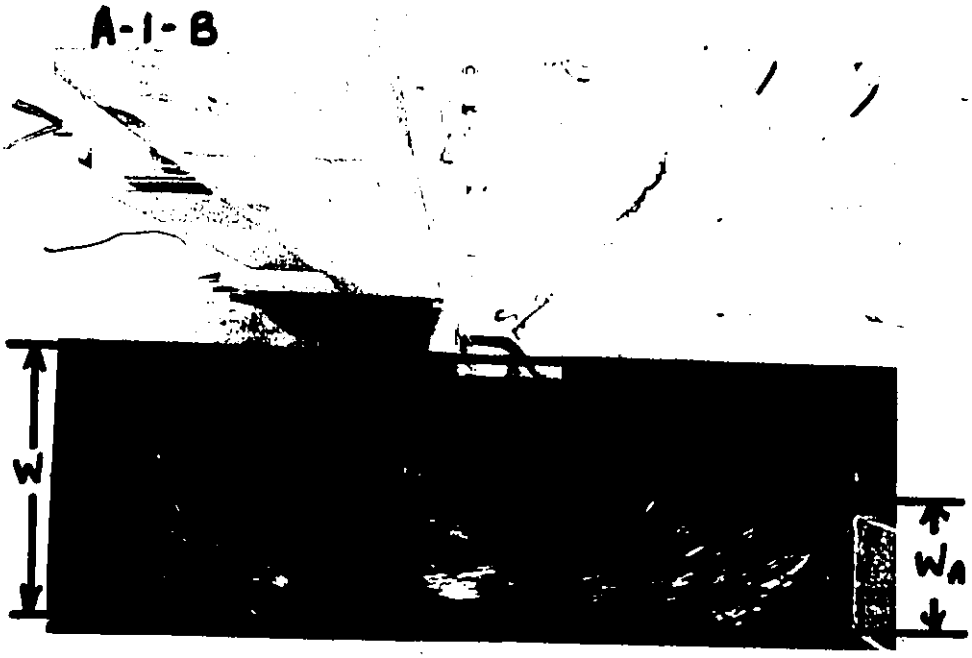

Figure 5.29

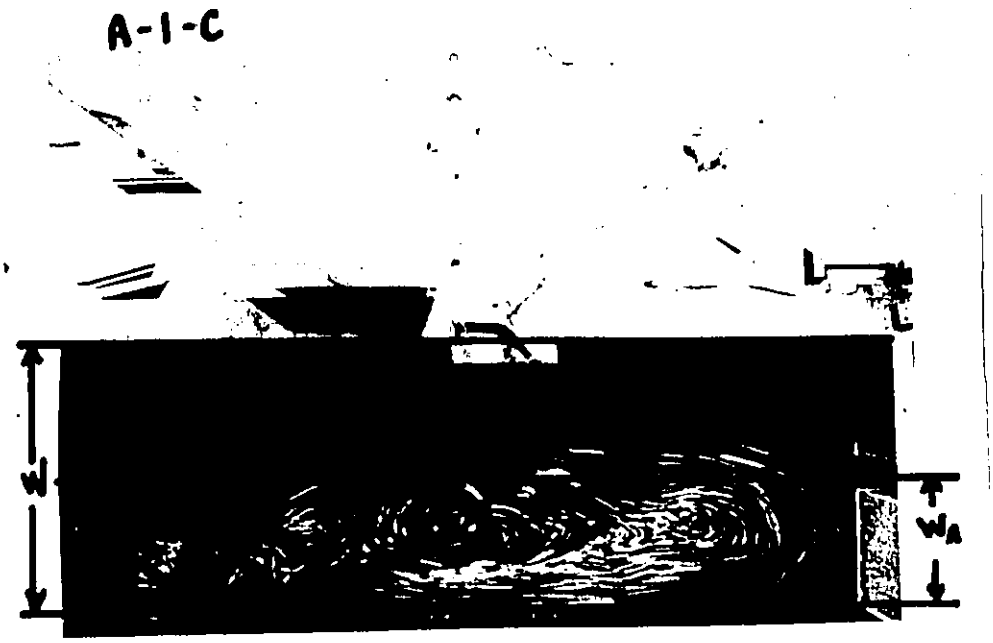

Figure 5.30

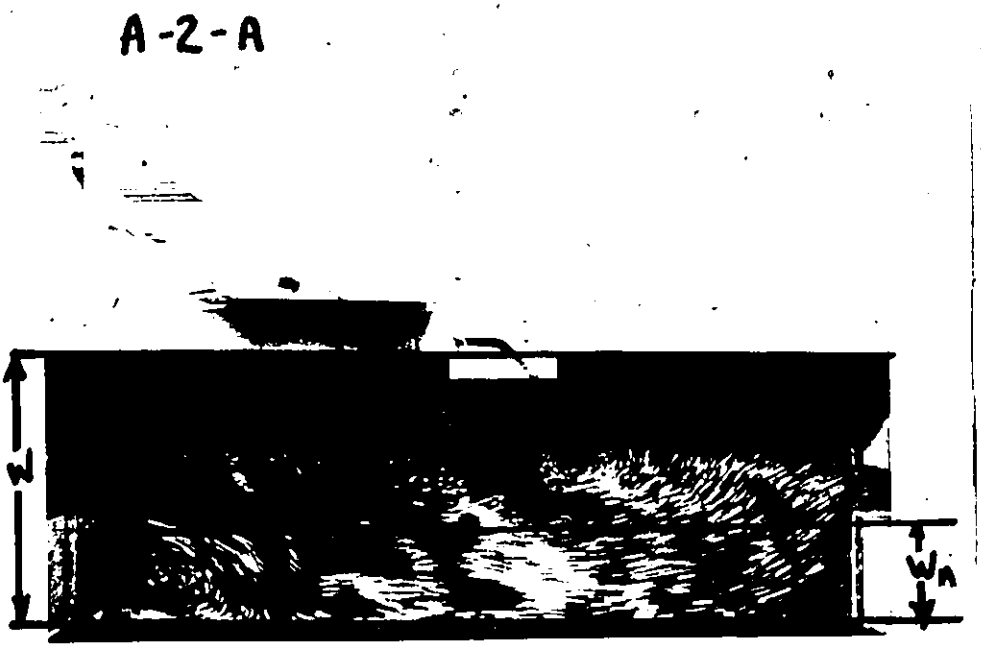

Figure 5.31

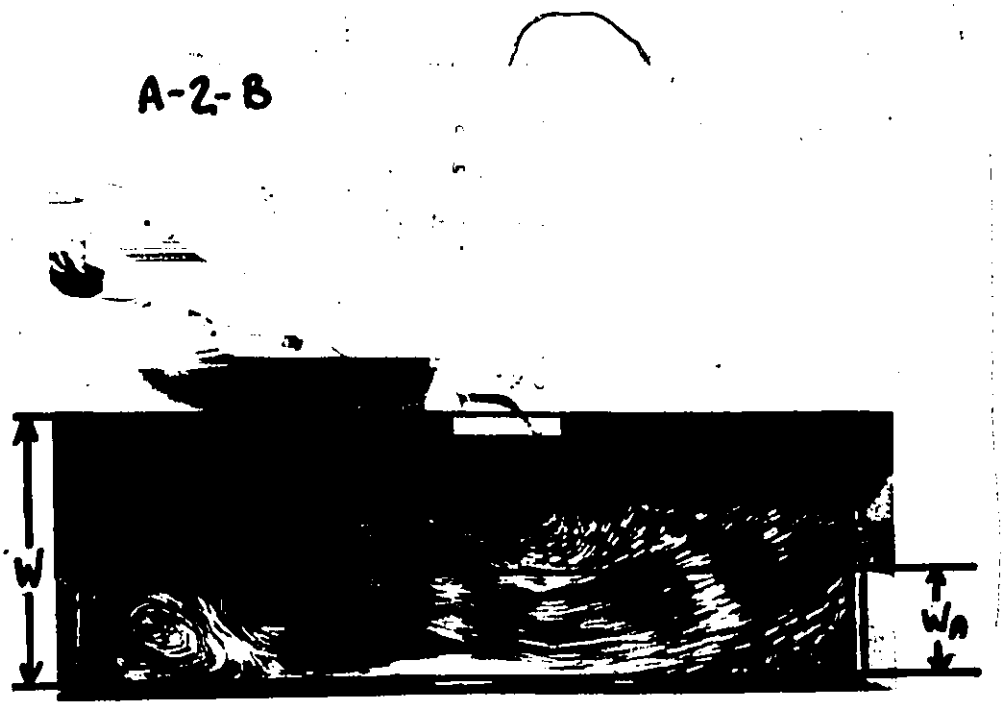

Figure 5.32

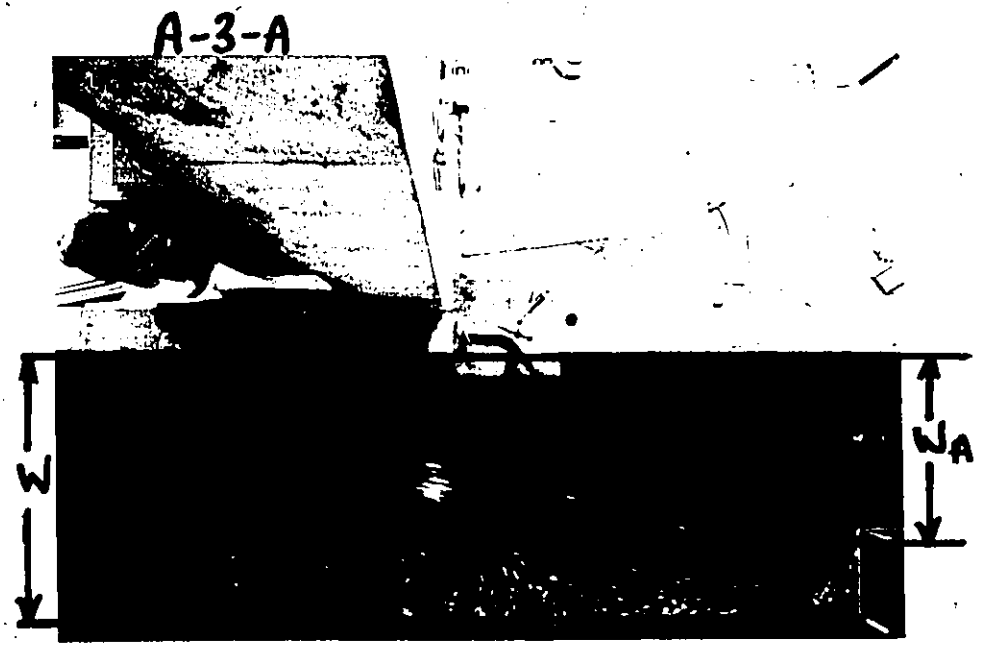

Figure 5.33

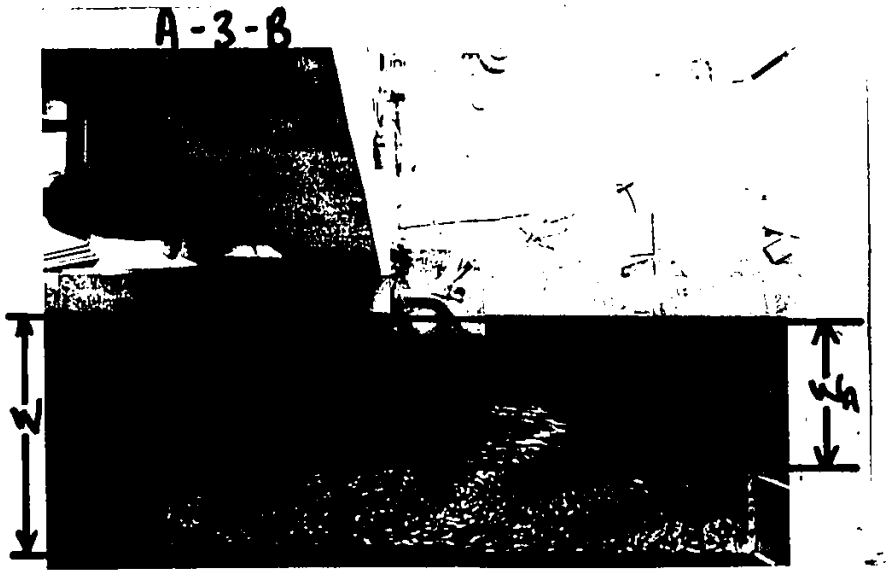

Figure 5.34

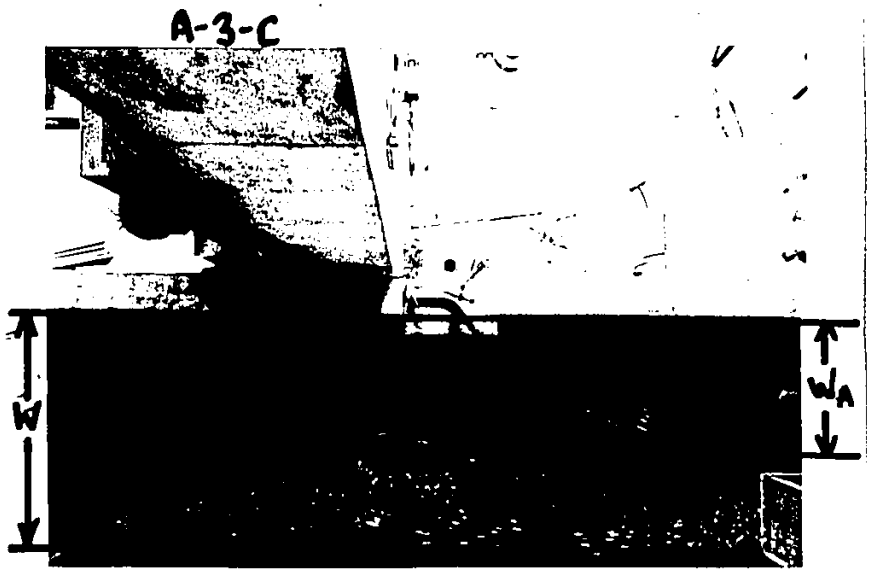

Figure 5.35

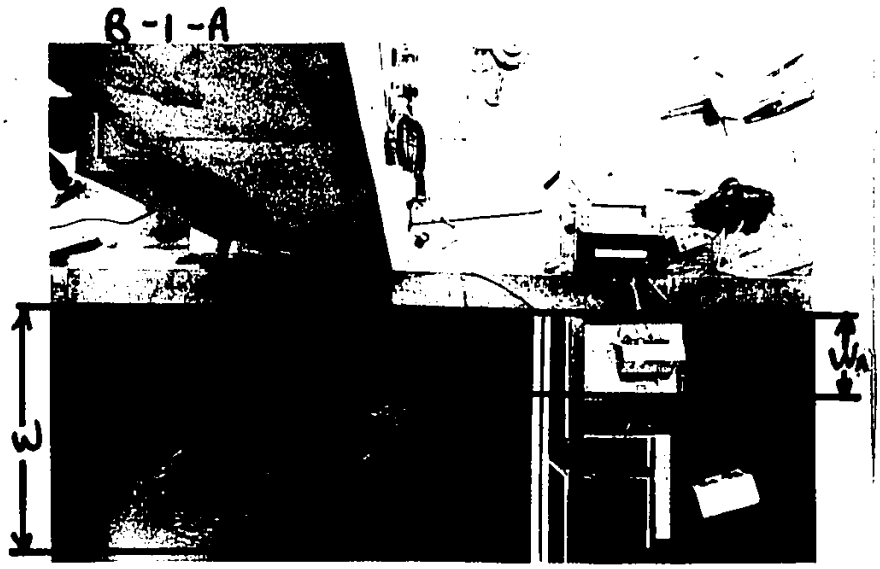

Figure 5.36

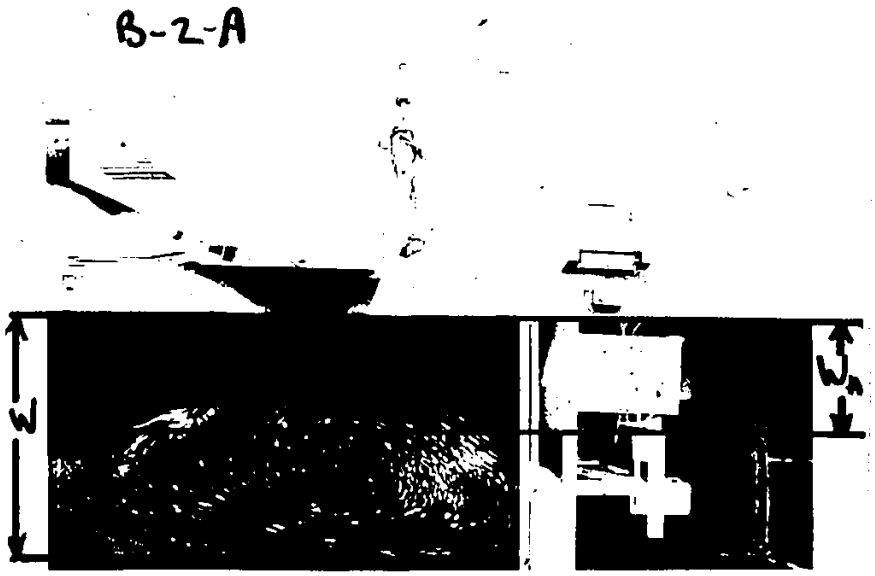

Figure 5.37

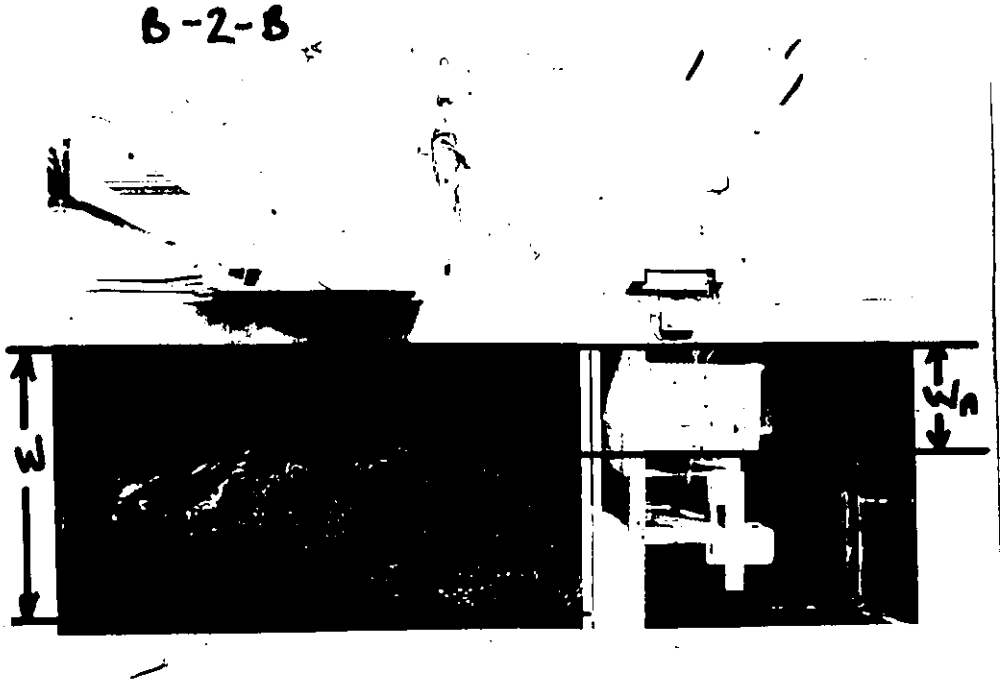

Figure 5.38

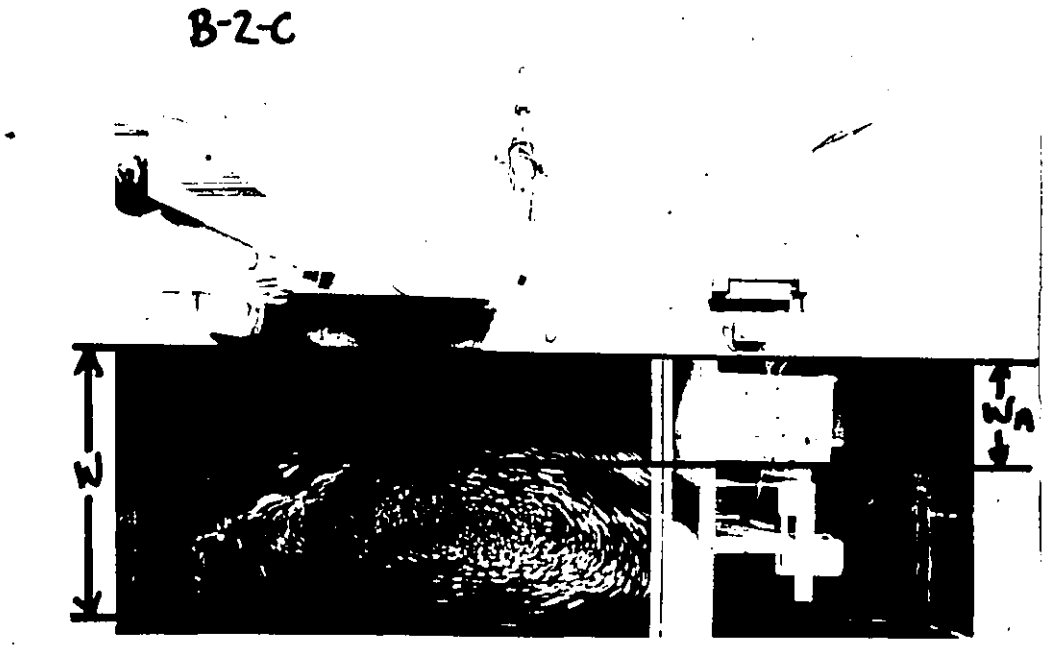

Figure 5.39

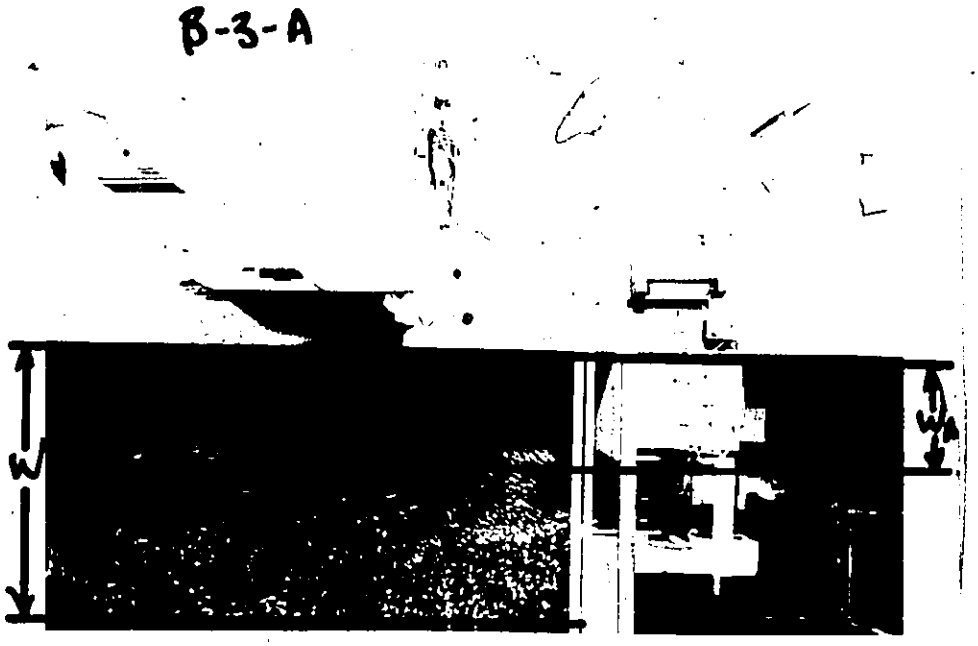

Figure 5.40

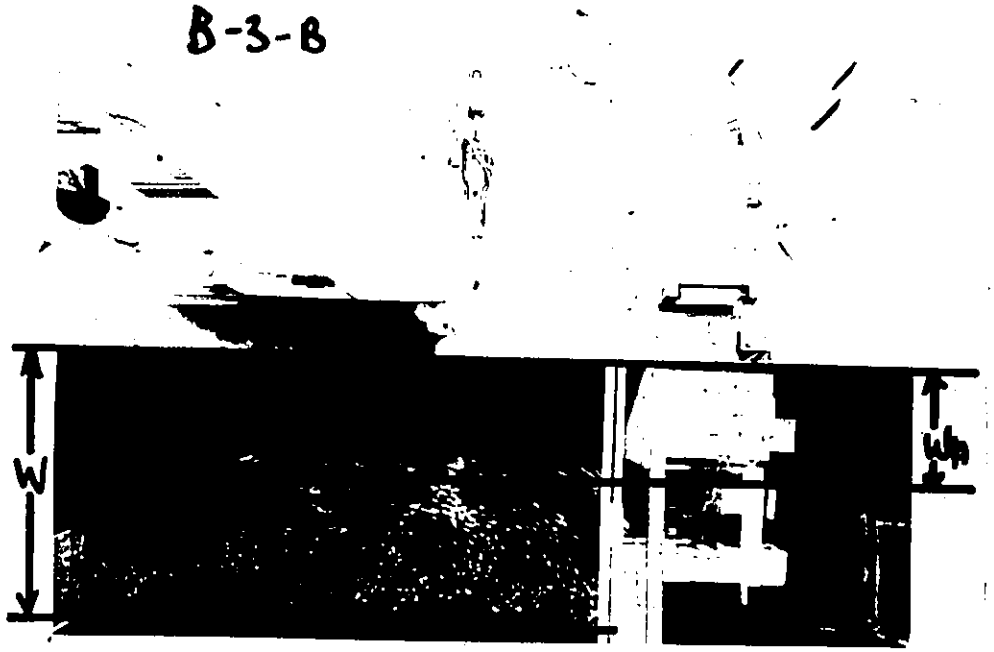

Figure 5.41

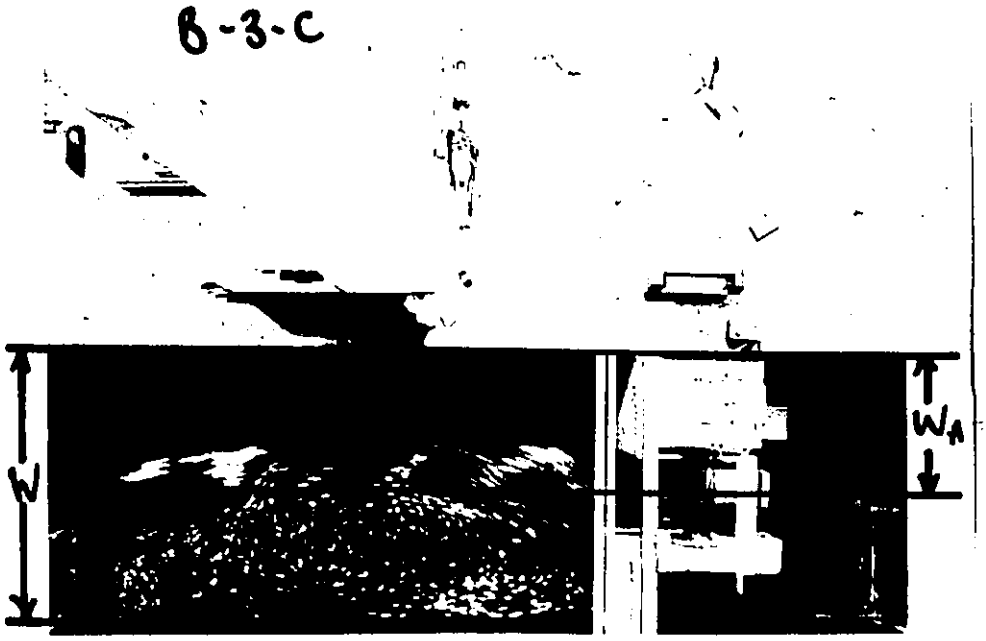

Figure 5.42

Figure 5.43

Figure 5.44

Figure 5.45

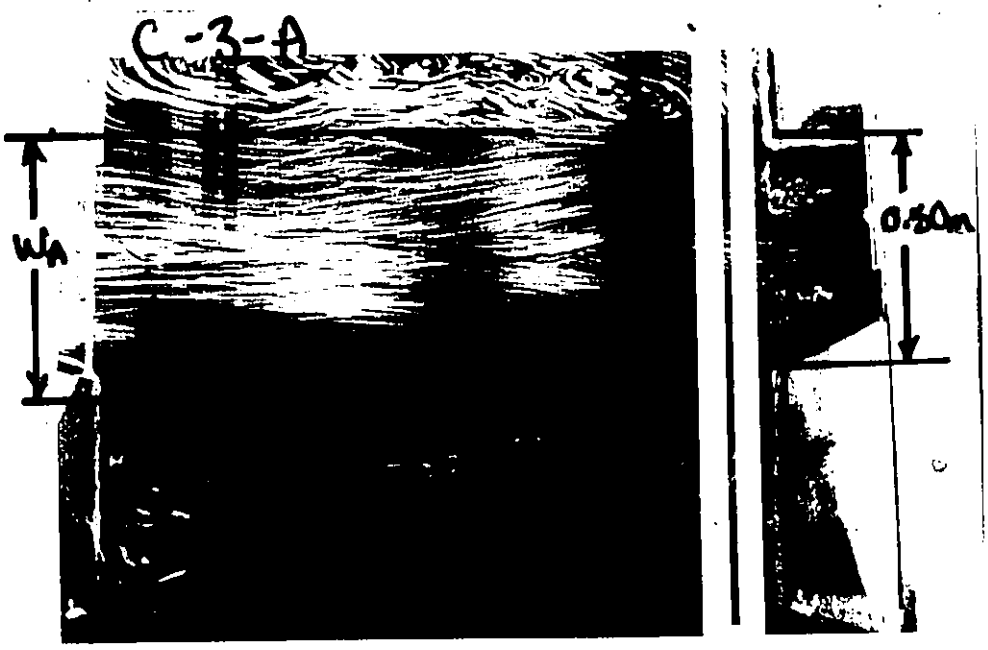

Figure 5.46

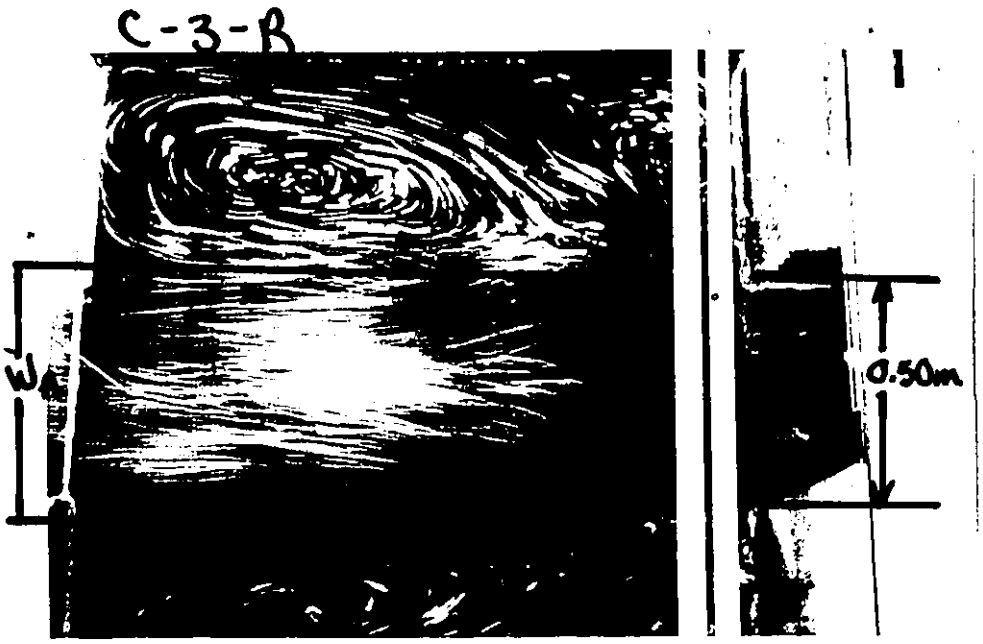

Figure 5.47

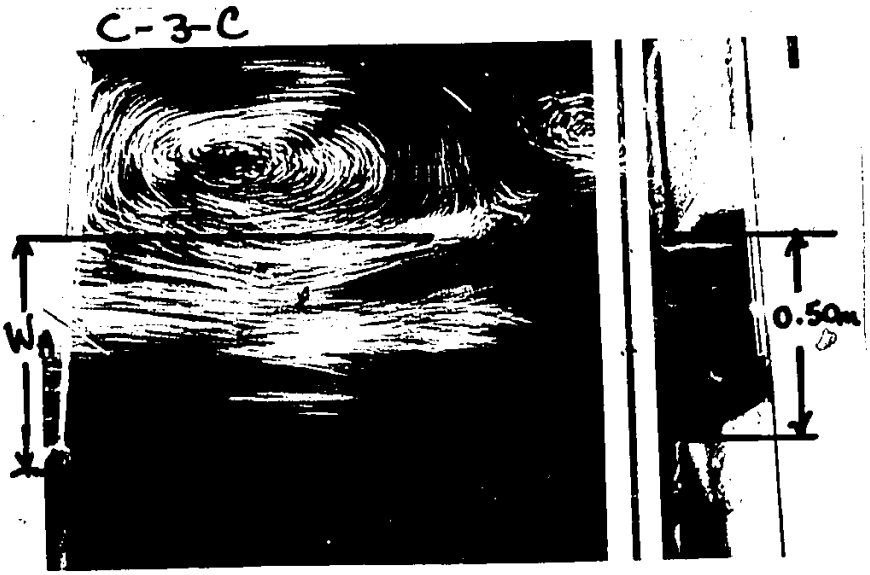

Figure 5.48

CHAPTER VI

ANALYSIS OF RESULTS AND DISCUSSION

6.1 Introduction

The model experimental runs were outlined in the previous chapter. A finite difference program of the mathematical model was developed to analyse experimental results. The Crank-Nicholson technique was used to the solve the partial differential equation because of its stability and convergence characteristics. The program's theoretical development and its listing can be found in the Appendix. This program allows for the reproduction of the experimental response dye output tracer curve to a slug input for the various experimental runs.

Four methods of estimating the model's parameters from the theory presented in Section 3.4.3 were investigated as well as the Ferrara and Harleman trial and error method. The methods used for estimating the parameters are defined below. The major differences in the methods center on the use of variance of the dye output curve or peak concentration on it to estimate E_A and on the use of Fischer's equation or Eq. (3.19a) to estimate the active volume.

Method	E_A Determination	β Determination	D_m Determination
I	From the peak concentration on the dye output curve (Eq. 3.22)	From Fischer's equation (Eq. 3.31a)	(Eq. 3.19b)
II	From the peak concentration on the dye output curve (Eq. 3.22)	(Eq. 3.19b)	From mass ratio of dye (Eq. 3.37)
III	From the variance of the dye output curve (Eq. 3.25)	From Fischer's equation (Eq. 3.31a)	(Eq. 3.19b)
IV	From the variance of the dye output curve (Eq. 3.25)	(Eq. 3.19b)	From mass ratio of dye (Eq. 3.37)

It was mentioned in Section 3.4.3 that the slope of the energy grade line could also be used to calculate the value of β. The slope of the energy grade line in the experimental model pond was so small that it was practically unmeasurable with a cathetometer and a point gauge (precision of one one-hundredth of a millimeter). Therefore, this method was not practical for model studies. It may, however, be practical for large scale studies of prototype ponds.

6.2 Optimum Number of Time Steps and Elemental Volumes

The finite difference program was checked for the minimum number of time steps (NT) and number of incremental

volumes (NV) required to obtain accurate results without unnecessarily extending the computational time. Table 6.1 lists the values of the peak relative concentration for the following values of the model's parameters.

The dispersion coefficient is 0.100E-02 m^2/s.
The dilution ratio is 3.00.
The ratio of the volume of the active zone to the total volume is 0.500.
The detention time in the active zone is 43.7 s.
The flow velocity in the active zone is 0.10427 m/s.
The Reynolds number in the active zone is 24797.
The Reynolds number for the entire basin is 4691.
The Froude number for the entire basin is 0.016222.

Also, in Fig.'s 6.1 and 6.2 the curves for the various number of time steps and number of incremental volumes are shown.

From the values in Table 6.1, it would appear that the minimum number of time steps and of elemental volumes should be 390. This was also the case for the following values for the model's parameters for which results are tabulated in Table 6.2 and shown in Fig.'s 6.3 and 6.4.

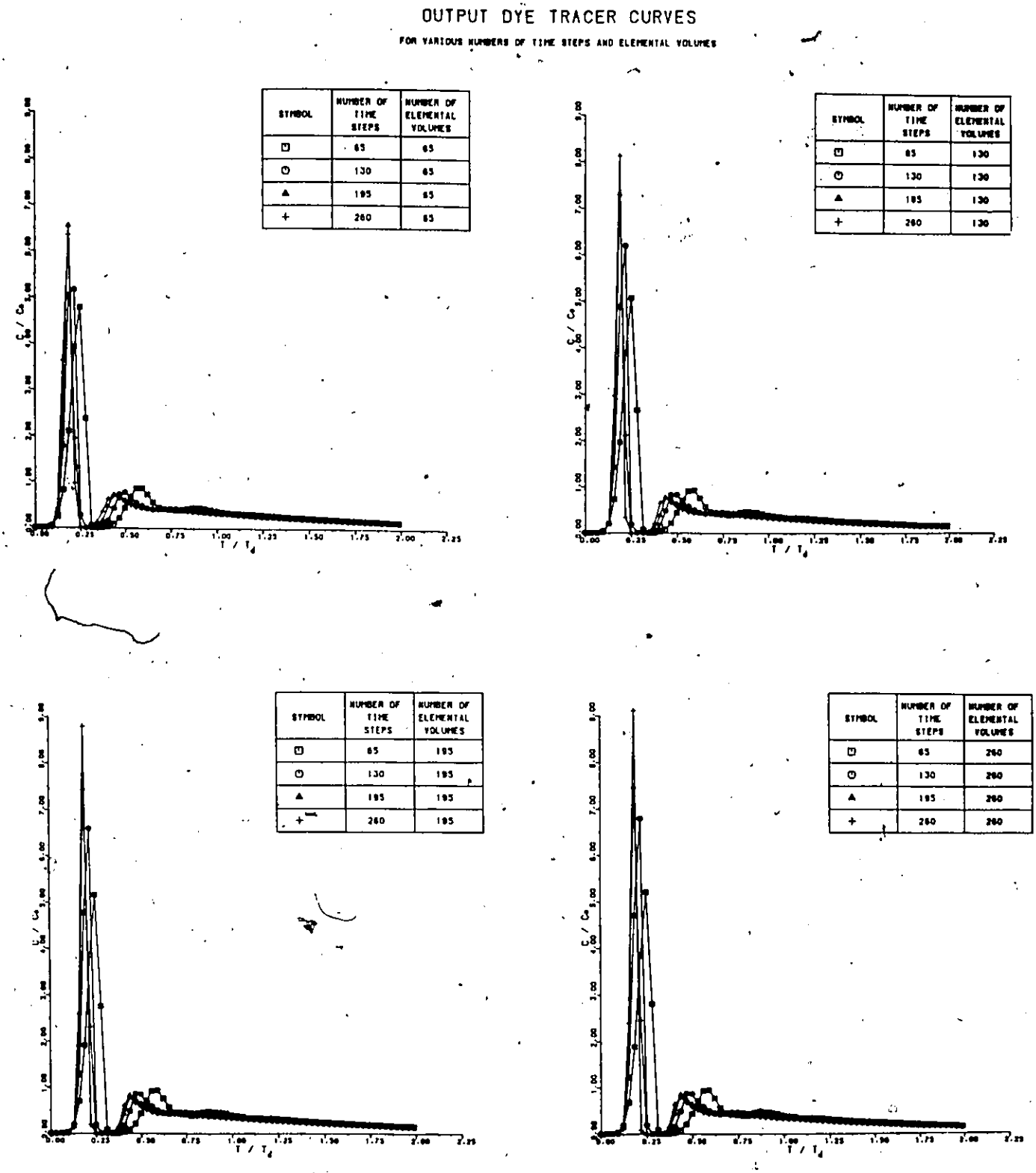

Figure 6.1 Output Dye Tracer Curves for Various Numbers of Time Steps and Elemental Volumes.

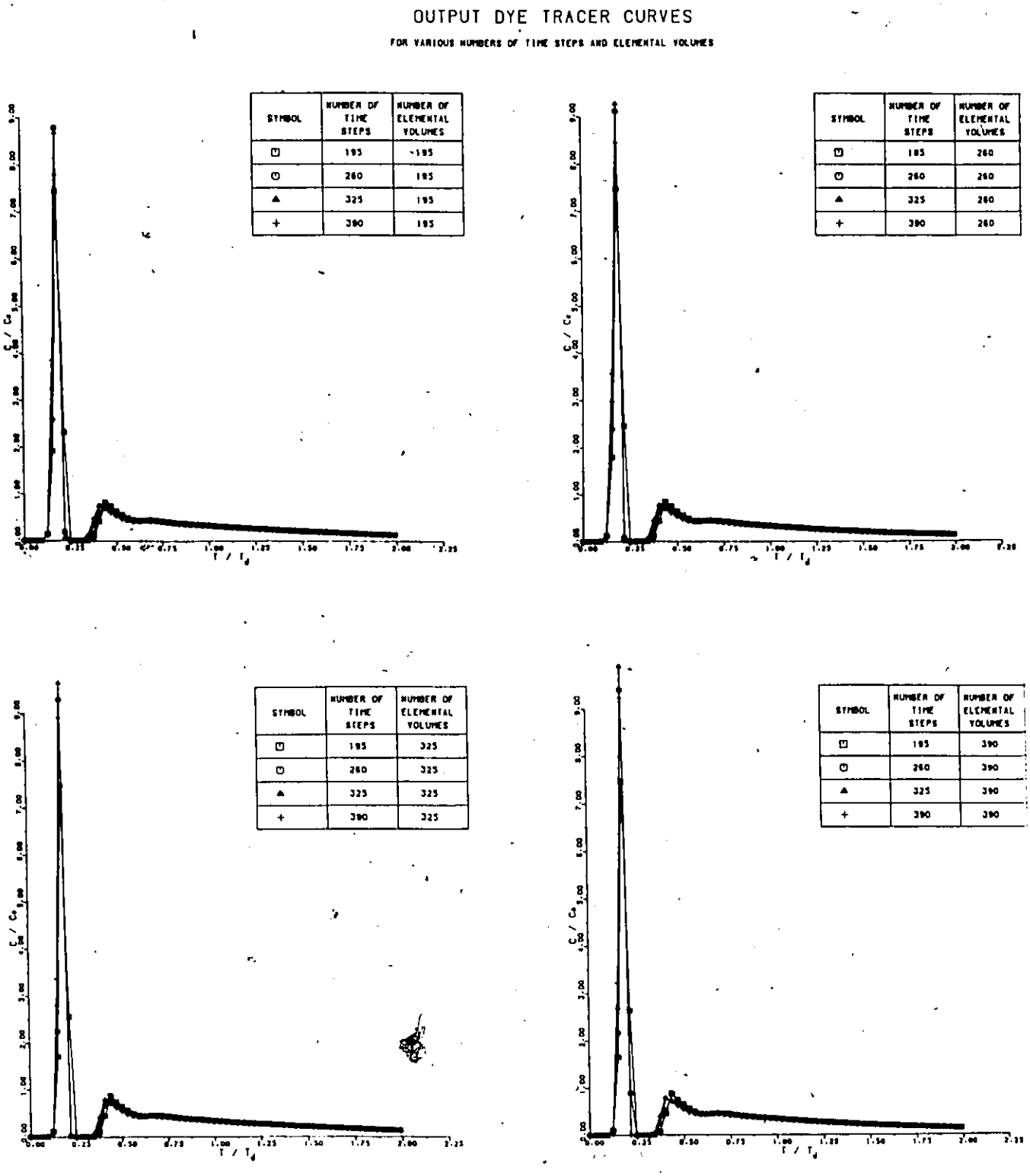

Figure 6.2 Output Dye Tracer Curves for Various Numbers of Time Steps and Elemental Volumes

Table 6.1: Values of the Peak Relative Concentration for Various Values of NT and NV

NT \ NV	65	130	195	260	325	390	455	520
65	4.78	5.07	5.16	5.21				
130	5.18	6.19	6.59	6.79				
195	6.55	7.30	7.44	7.47	7.48	7.47		
260	6.36	8.12	8.79	9.11	9.29	9.41		
325			8.68	9.27	9.65	9.91	9.92	9.92
390			7.80	8.45	8.90	9.24	9.24	9.24
455					8.90	9.24	9.24	9.24
520					8.90	9.23	9.24	9.24

Table 6.2: Values of the Peak Relative Concentration for Various Values of NT and NV.

NT \ NV	65	130	195	260	325	390
65	3.28	3.38	3.41	3.42		
130	3.04	3.14	3.18	3.19		
195	2.88	2.97	3.01	3.03	3.04	3.05
260	2.88	2.94	2.97	2.98	2.98	2.99
325			2.96	2.97	2.98	2.99
390			2.95	2.95	2.97	2.98

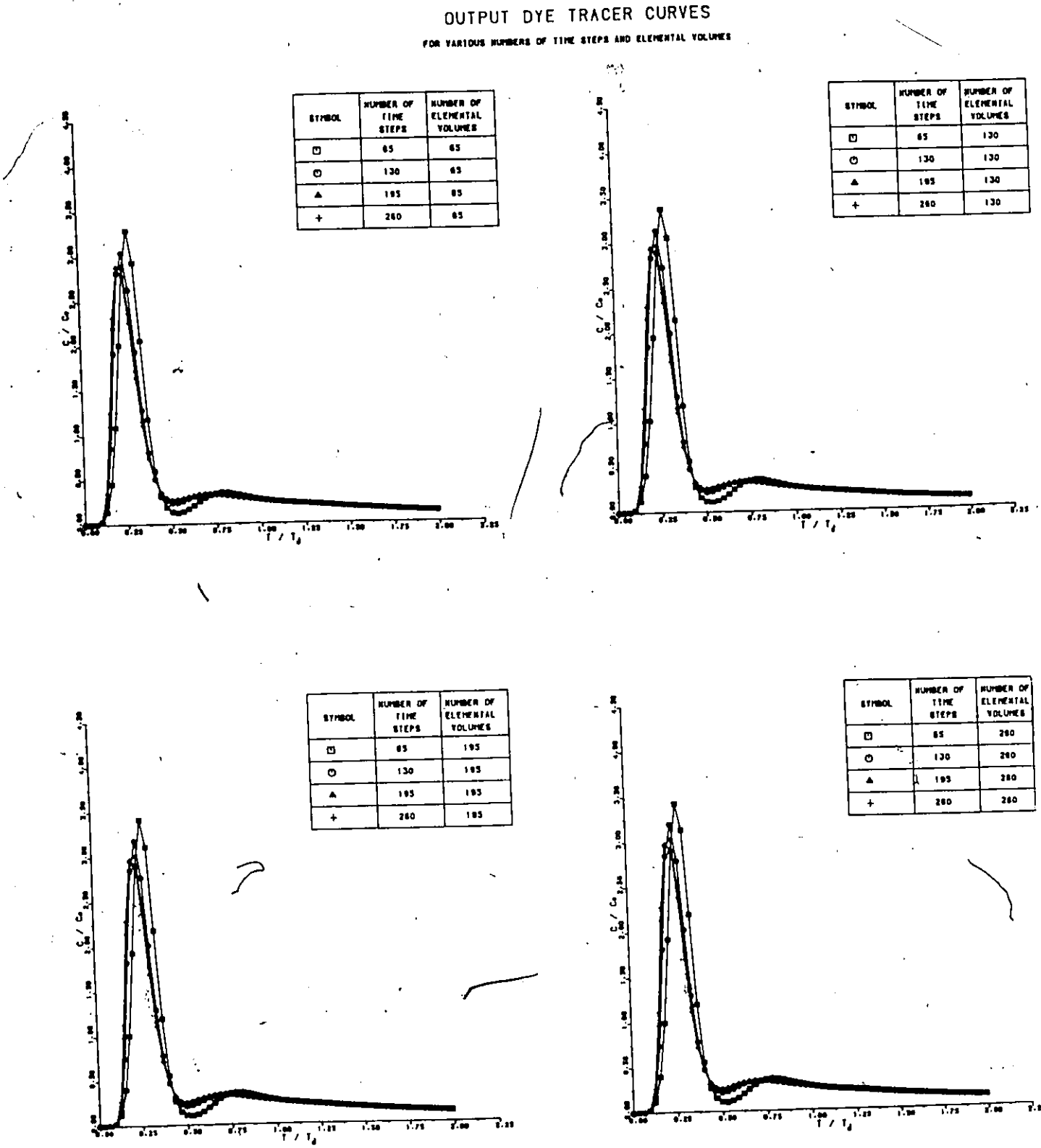

Figure 6.3 Output Dye Tracer Curves for Variόus Numbers of Time Steps and Elemental Volumes.

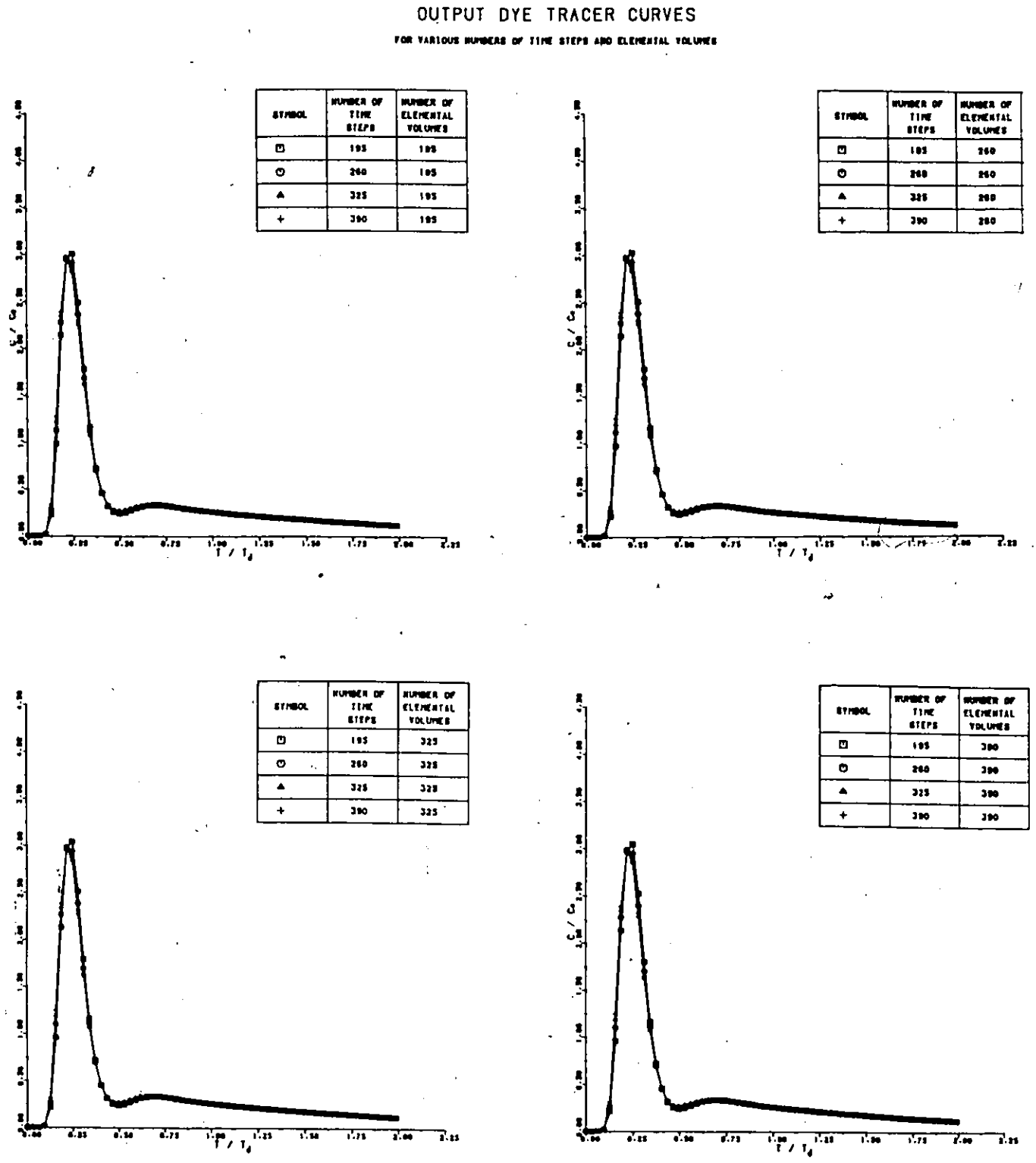

Figure 6.4 Output Dye Tracer Curves for Various Numbers of Time Steps and Elemental Volumes.

For Table 6.2 the following apply:

The dispersion coefficient is 0.0010 m^2/s.
The dilution ratio is 2.00.
The ratio of the volume of the active zone to the total volume is 0.500.
The detention time in the active zone is 65.6 s.
The flow velocity in the active zone is 0.06952 m/s.
The Reynolds number in the active zone is 16531.
The Reynolds number for the entire basin is 4691.
The Froude number for the entire basin is 0.016222.

6.3 Reproducibility of Results

The reproducibility of results was well demonstrated in Fig. 4.5. Checks on the reproducibility of the experimental dye output curves were also undertaken at other model setups and flow rates. The reproducibility of the results was maintained throughout these checks. Another typical comparison of the experimental output dye tracer curves is shown in Fig. 6.5.

6.4 Evaluation of the Methods for Estimating the Mixing Model's Parameters

In the third chapter, various methods of estimating the mixing model's parameters are presented. These methods, if successful, would enable a modeller to estimate the mixing model's parameters without having to resort to tedious and lengthy trial and error finite difference runs.

The analysis of the experimental results included an estimation of the model's parameters by the various proposed methods as well as Ferrara and Harleman's[14] trial and error

OUTPUT DYE TRACER CURVES

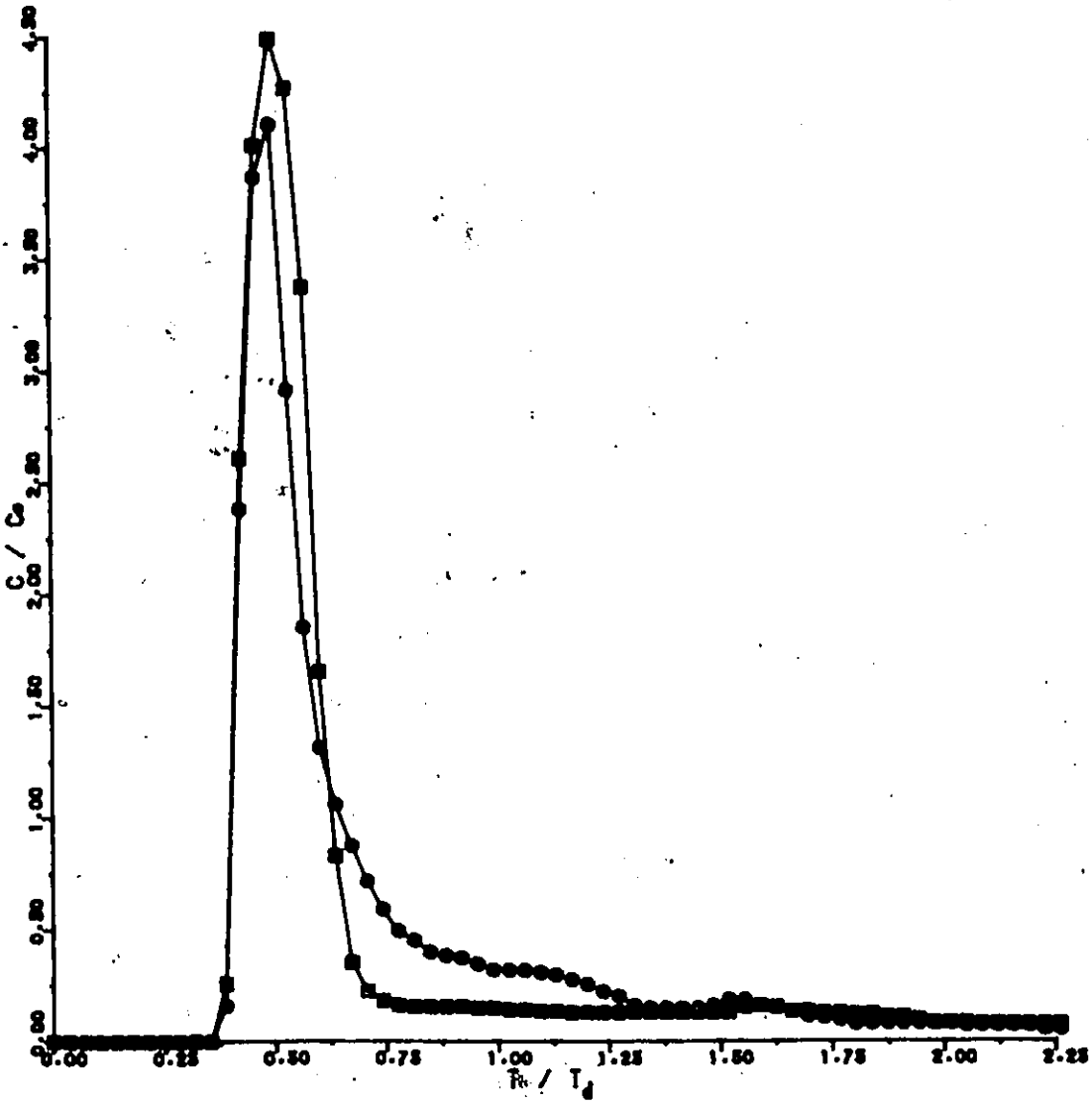

Figure 6.5: Output Dye Tracer Curves Demonstrating the Reproducibility of Results

solution. All of the estimated parameters from the various methods were run with the finite difference program. The standard error of the estimate (Eq. (6.1)) was calculated for each method and the results are listed in Table 6.3.

$$S_E = [(\sum_{i=1}^{i=m} (C_i - C_{ci})^2)/(m-1)]^{1/2} \qquad (6.1)$$

where S_E = standard error of estimate
C_i = concentration from output dye tracer curve at time i
C_{ci} = calculated concentration at time i
m = number of concentration values

From the table, it was evident that the best methods for estimating the parameters were Method II and Method IV (they had the lowest S_E values the most often). These two methods both calculated the dilution ratio, Ds, from the ratio of the mass of unrecycled dye to the total mass of dye. However, in Method II, the dispersion coefficient was estimated from the peak concentration on the reduced dye output curve, while in Method IV, the dispersion coefficient was estimated from the variance of the dye output curve.

It should be pointed out here that the accuracy of the two methods in evaluating the dispersion coefficient relied on the ability of the modeller to separate the unrecycled dye from the remainder of the output dye tracer curve. As discussed in the chapter on theory, the cutoff point is sometimes difficult to identify, and this will cause greater

Table 6.3: Summary of the Estimate of Error for the Various Methods Used to Calculate the Models' Parameters

Run ID	Method I	Method II	Method III	Method IV	Ferrara and Harleman
A1A	1.20	0.50	0.78	0.74	0.65
A1B	2.69	0.32	1.50	0.39	0.68
A1C	0.89	0.46	0.54	0.50	0.59
A2A	1.02	0.62	0.60	0.60	0.58
A2B	1.31	0.69	1.41	0.68	0.87
A2C	4.32	0.43	1.42	0.48	0.63
A3A	2.24	0.38	1.62	0.39	0.68
A3B	6.60	0.59	9.02	0.57	1.00
A3C	2.26	0.25	3.10	0.20	0.78
B1A	0.99	0.43	0.67	0.62	0.64
B1B	2.04	0.66	0.66	0.67	0.67
B1C	0.78	0.67	0.69	0.67	0.73
B2A	1.35	0.38	0.61	0.40	0.56
B2B	0.26	0.21	0.19	0.20	0.20
B2C	1.15	0.36	0.71	0.33	0.39
B3A	1.24	0.56	0.82	0.59	0.84
B3B	3.82	0.38	1.32	0.45	0.88
B3C	9.31	0.33	5.15	0.33	0.72
C1A	0.55	0.34	1.15	0.47	0.26
C1B	1.50	0.25	1.08	0.24	0.38
C1C	0.94	0.26	1.00	0.27	0.19
C2A	0.56	0.53	0.66	0.44	0.44
C2B	0.87	0.41	0.58	0.43	0.53
C2C	1.93	0.18	1.08	0.21	0.44
C3A	0.72	0.25	0.75	0.25	0.79
C3B	0.37	0.33	0.40	0.33	0.64
C3C	1.33	0.58	0.68	0.57	0.79

NOTE: Underlined values are minimum values for a particular run.

errors in the dispersion coefficient estimate when it is calculated from the variance. The results presented in Table 6.3 support this. Method II produced a better fit (*i.e.*, a lower S_E) (19 out of 27 cases) more often than Method IV (14 out of 27 cases). It was noted, however, that in most cases (18 out of 27) the S_E's found for both methods were very similar, indicating that, in most cases, the cut-off point was determined with a fair degree of accuracy.

The appropriateness of Methods II and IV in estimating the model's parameters can also be verified in Fig.'s 5.1 to 5.27, where, in practically every run, the dye tracer curves resulting from these two methods most nearly approximated the experimental curve.

Method I relied on the peak concentration to evaluate the dispersion coefficient whereas Method III used the variance. The width of the active zone, however, was obtained from a modified Fischer's equation (Eq. (3.34)). These methods did not produce very good results.

In Ferrara and Harleman's method, a trial and error approach was taken in which various trial values were assigned to Ds until a best fit (smallest S_E) was found. The dispersion coefficient in this method was obtained from Fischer's equation. In most cases, the method's results were not as accurate as those found from Methods II and IV. This will be discussed further in Section 6.5.1.

Another method of determining W_A was proposed in the theory section. This method again used a modification of

Fischer's equation in which the shear velocity term was replaced by S, the slope of the energy grade line (Eq. (3.31)). Unfortunately, in model studies of this size, no measurement of S was possible due to lack of a measurable differential elevation between the two ends of the basin. Therefore, it was impossible to check this method.

From the results presented in Table 6.3 and this discussion, Method II was chosen as the most reliable. Therefore, the remainder of the analysis of the results was based on the results from this method. It should be pointed out that the values of Ds and W_A obtained from this method were exactly the same as the values obtained from Method IV since they were calculated in the same way. The mixing model's parameters from Method II are tabulated in Table 6.4.

6.5 Analysis of the Dispersion Coefficient

6.5.1 Comparison with E_A Calculated from Fischer's Equation

In Method II, the dispersion coefficient was estimated from the peak concentration on the dye output curve (Eq. (3.22)). The values of E_A for the various runs are tabulated in Table 6.4. Included with these are the values calculated from Fischer's equation (E_A(FISCHER)) (Eq. (3.14)) with the same values of Ds and β as in Method II.

Table 6.4 : Parameters for the Model (Obtained from the peak concentration and the mass ratio)

Run ID	E_a x10^3	D_m	R_v	T_p/T_d	E_a(Fischer) x10^3	$\frac{E_a(Fischer)}{E_a}$	Nf
A1A	1.17	2.12	0.407	0.190	2.78	2.4	0.0049
A1B	1.08	2.43	0.690	0.283	8.01	7.4	0.0088
A1C	3.68	2.10	0.507	0.238	7.34	2.0	0.0119
A2A	1.19	1.58	0.364	0.229	2.17	1.8	0.0055
A2B	1.65	1.37	0.398	0.288	3.59	2.2	0.0100
A2C	1.00	2.56	0.690	0.344	13.2	13.2	0.0136
A3A	0.59	1.48	0.864	0.577	3.95	6.7	0.0055
A3B	0.53	2.08	0.819	0.393	9.75	18.4	0.0100
A3C	1.44	1.27	0.640	0.499	6.90	4.8	0.0148
B1A	1.19	1.66	0.348	0.207	2.02	1.7	0.0051
B1B	1.51	2.26	0.510	0.224	6.06	4.0	0.0089
B1C	3.97	1.57	0.432	0.268	5.07	1.3	0.0122
B2A	1.28	2.18	0.486	0.220	3.72	2.9	0.0055
B2B	3.37	1.29	0.474	0.355	3.87	1.1	0.0101
B2C	2.17	1.57	0.449	0.283	6.12	2.8	0.0139
B3A	0.93	1.26	0.425	0.333	1.99	2.1	0.0056
B3B	0.72	1.25	0.489	0.387	4.01	5.6	0.0105
B3C	0.63	1.82	0.729	0.399	11.3	17.9	0.0152
C1A	1.22	1.66	0.294	0.173	1.83	1.5	0.0051
C1B	1.34	2.18	0.409	0.185	5.04	3.8	0.0089
C1C	2.34	1.91	0.439	0.224	6.23	2.7	0.0122
C2A	1.00	1.15	0.203	0.173	1.04	1.0	0.0051
C2B	1.94	1.55	0.414	0.255	3.99	2.1	0.0101
C2C	1.47	2.03	0.629	0.304	9.93	6.8	0.0138
C3A	0.77	1.00	0.317	0.308	1.30	1.7	0.0056
C3B	2.20	1.00	0.339	0.325	2.51	1.1	0.0105
C3C	1.75	1.00	0.361	0.354	3.69	2.1	0.0150

On the average, E_A(FISCHER) is four times greater than E_A(PEAK). It is possible that the variations between E_A(FISCHER) and E_A may be due to the lower Reynolds numbers found in model studies. Results from Ferrara and Harleman[22] indicated that the dispersion coefficient was accurately modelled by Fischer's equation in their studies on large scale waste stabilization ponds.

6.5.2 Relationship of Reynolds Number to the Dispersion Coefficient

The values of the Reynolds number (Nr) for the active zone for each run were tabulated in Table 6.5. E_A was plotted against Nr in Fig. 6.6. As expected, E_A increased as Nr increased. A linear regression was performed to fit the data (correlation coefficient = 0.68).

6.5.3 Variation of E_A with $W_{CHANNEL}$ (Width of Inlet and Outlet Channels)

Table 6.6 lists the values of average E_A for the various $W_{CHANNEL}$. Fig. 6.7 demonstrates that the dispersion coefficient decreased with increasing $W_{CHANNEL}$. This phenomena was attributed to the fact that E_A values represent the longitudinal dispersion in the active zone as well as the dispersion occurring in the jet expansion of the influent stream. In the case of the narrower channels, the influent stream was entering at a higher velocity, thus undergoing a more extreme jet expansion and a higher degree

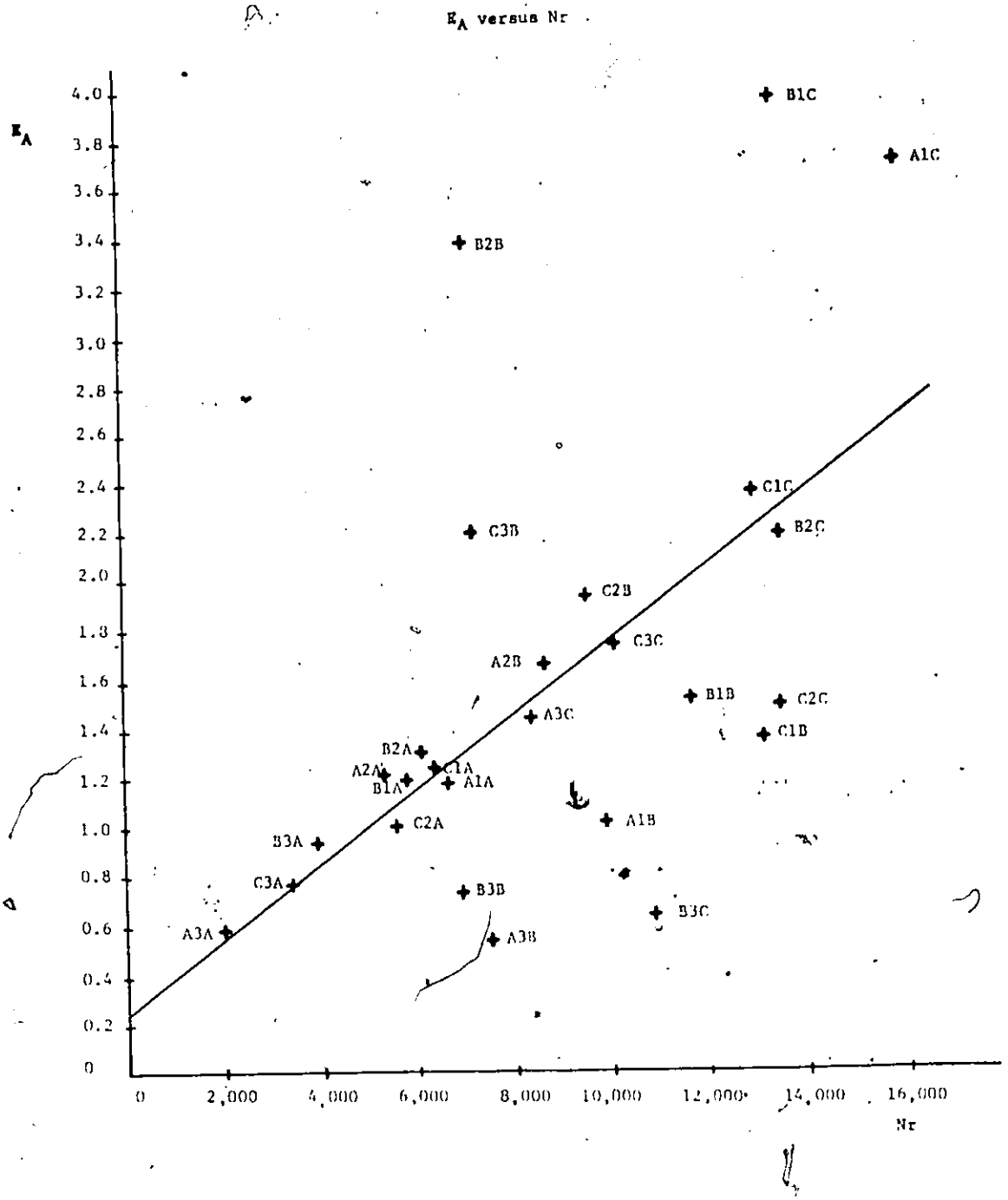

Figure 6.6: Plot of E_A versus Nr

Table 6.5: Dispersion Coefficient Data

Run ID	E_A (m2/s)x10^3	L (m)	U_A (m/s)	F	Nr Active	β	β Photo
A1A	1.17	4.56	0.0283	0.0091	6600	0.41	0.42
A1B	1.08	4.56	0.0353	0.0067	9900	0.69	0.53
A1C	3.68	4.56	0.0583	0.0138	16000	0.51	0.51
A2A	1.19	4.56	0.0251	0.0104	5400	0.36	0.36
A2B	1.65	4.56	0.0377	0.0096	8700	0.40	0.39
A2C	1.04	4.56	0.0445	0.0049	6800	0.89	
A3A	0.69	4.56	0.0100	0.0129	2000	0.86	0.71
A3B	0.53	4.56	0.0284	0.0041	7500	0.82	0.63
A3C	1.44	4.56	0.0323	0.0098	8400	0.64	0.59
B1A	1.19	2.98	0.0262	0.0152	5800	0.35	0.33
B1B	1.51	2.98	0.0477	0.0113	11700	0.31	
B1C	3.97	2.98	0.0519	0.0232	13500	0.43	
B2A	1.28	2.98	0.0262	0.0164	6100	0.49	0.47
B2B	3.37	2.98	0.0299	0.0378	7200	0.47	0.41
B2C	2.17	2.98	0.0545	0.0134	13500	0.45	0.43
B3A	0.93	2.98	0.0174	0.0179	3900	0.43	0.42
B3B	0.72	2.98	0.0290	0.0083	6900	0.49	0.44
B3C	0.63	2.98	0.0412	0.0051	10900	0.73	0.55
C1A	1.22	1.53	0.0311	0.0256	6500	0.29	
C1B	1.34	1.53	0.0538	0.0163	13200	0.41	
C1C	2.34	1.53	0.0622	0.0246	13000	0.43	
C2A	1.00	1.53	0.0311	0.0256	6500	0.29	0.33
C2B	1.94	1.53	0.0412	0.0308	9600	0.41	0.31
C2C	1.47	1.53	0.0500	0.0192	13500	0.63	0.30
C3A	0.77	1.53	0.0186	0.0271	3400	0.32	0.39
C3B	2.20	1.53	0.0333	0.0432	7200	0.34	0.39
C3C	1.75	1.53	0.0452	0.0253	10100	0.36	0.39

of dispersion. The three points on Fig. 6.7 formed, surprisingly, a straight line.

Table 6.6: Average Value of E_A for Various $W_{CHANNEL}$

Average E_A ($\times 10^{-3} m^2/s$)	$W_{CHANNEL}$ (m)
1.94	0.20
1.67	0.30
1.06	0.50

6.5.4 Variation of E_A with Q (Flow Rate)

In Table 6.7, the average values of E_A for the three different flow rates are listed. These results, which are plotted in Fig. 6.8, show that E_A increased with the flow rate. This was expected since a higher flow rate produces a higher the Reynolds number and the degree of turbulence, and therefore, a higher dispersion coefficient. The results in this case were again linear.

Table 6.7: Average Value of E_A for Various Flow Rates

Average E_A ($\times 10^{-3} m^2/s$)	Q (l/s)
1.04	1.0
1.59	2.0
2.05	3.0

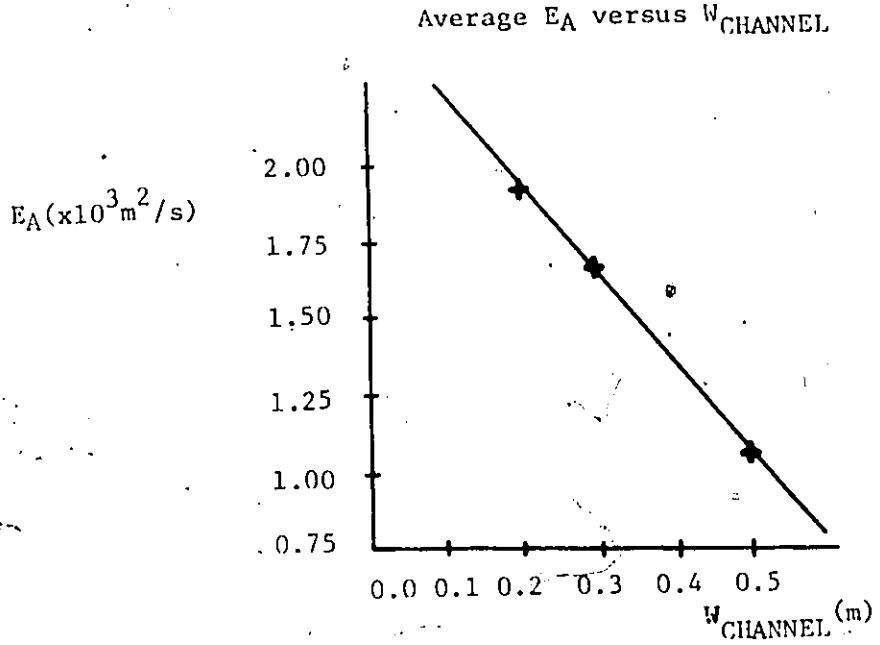

Figure 6.7: Plot of Average E_A versus $W_{CHANNEL}$

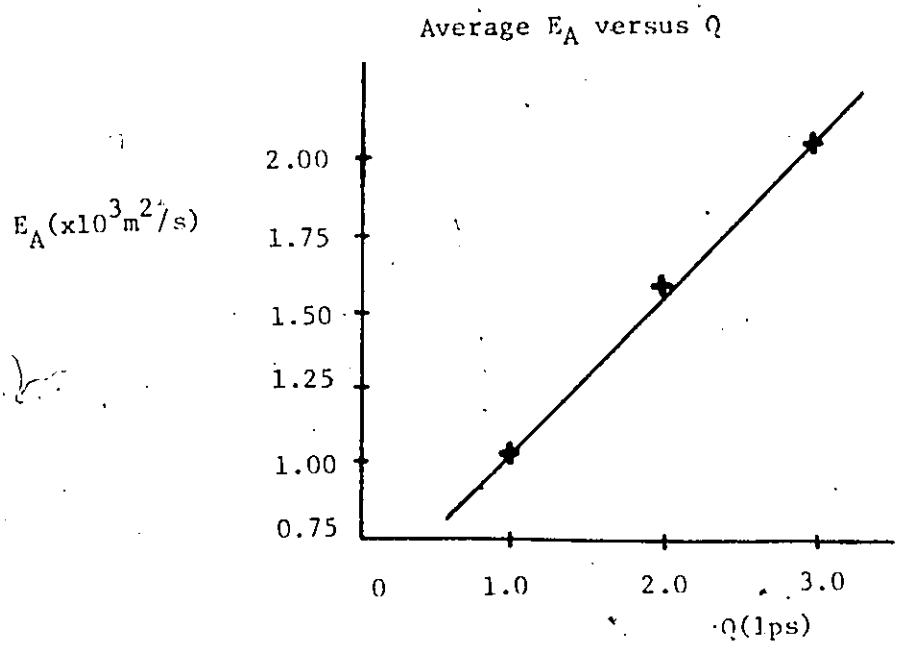

Figure 6.8: Plot of Average E_A versus Q

6.5.5 Variation of E_A with Length to Width Ratio

In Table 6.5, an extra column was added in which the value of the reduced dispersion coefficient (F) was entered. In Table 6.8, the various values for average E_A and average F were tabled for the three different L:W ratios. The relationship between E_A and L:W is shown in Fig. 6.9 and for F and L:W in Fig. 6.10. In Fig. 6.9, E_A was seen to increase as the L:W ratio was decreased from 3:1 to 2:1, and then to decrease when L:W was decreased to 1:1. Thus, it can be said that E_A appears to be independent of the L:W ratio.

Table 6.8: Average Values of E_A and F for the Various L:W Ratios

L:W	E_A	F
3:1	1.39×10^3	0.0090
2:1	1.75×10^3	0.0165
1:1	1.56×10^3	0.0264

The graph of F versus L:W (Fig. 6.10) behaved in a more predictable manner in that F decreased as the L:W ratio increased. This was expected since F is obtained by dividing E_A by L and U_A. Thus, if U_A remains constant, F at a L:W ratio of 1:1 should be three times greater than F at a L:W ratio of 3:1.

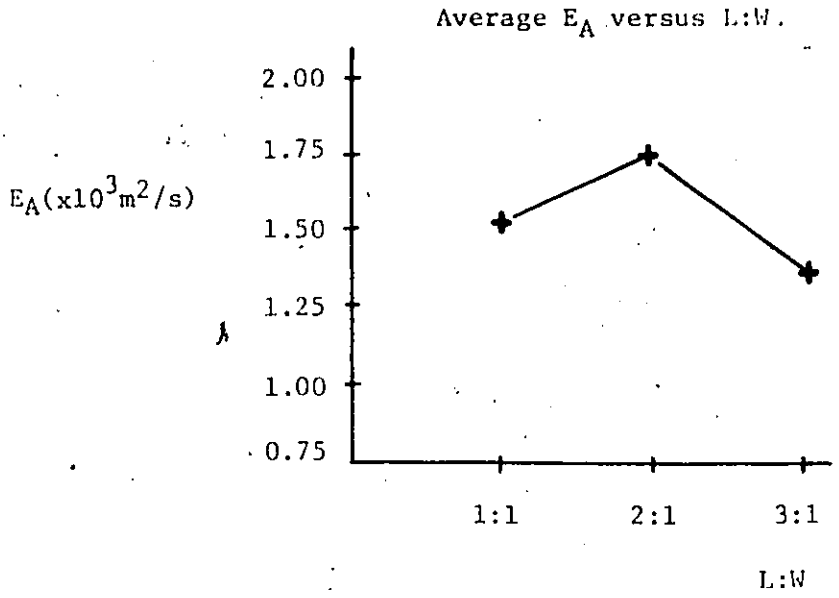

Figure 6.9: Plot of Average E_A versus L:W

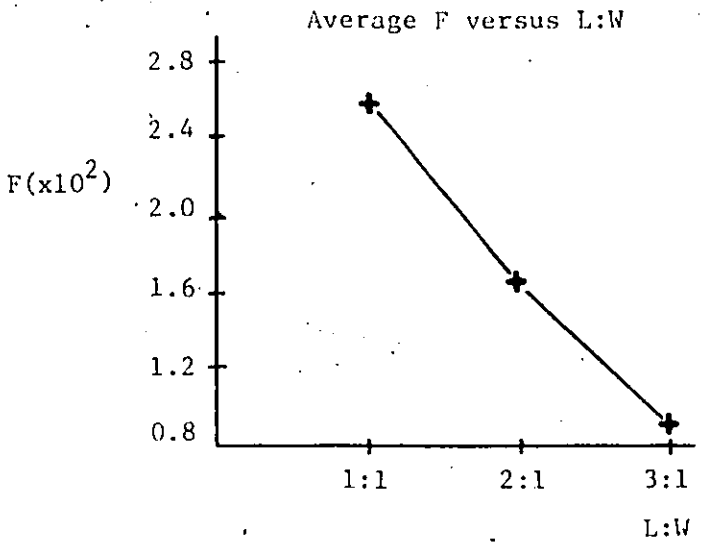

Figure 6.10: Plot of Average F versus L:W

6.6 Analysis of the Dilution Factor

The values of Ds estimated from Method II are listed in Table 6.4 for all runs. Plots of Ds versus Froude number are presented in Fig. 6.11 for the length to width ratios.

6.6.1 Variation of Ds with $W_{CHANNEL}$

In Table 6.9, average values of Ds for the L:W ratios and $W_{CHANNEL}$ are presented along with their respective overall averages. Plots of Ds versus $W_{CHANNEL}$ are shown in Fig. 6.12. Ds decreased as $W_{CHANNEL}$ increased. This was attributed to a decrease in velocity of the incoming stream as $W_{CHANNEL}$ increases, therefore, less momentum transfer occurred which reduced the amount of induced recirculation flow.

6.6.2 Variation of Ds with L:W Ratio

The average values of Ds for the various $W_{CHANNEL}$ were also tabulated in Table 6.9. In Fig. 6.13, it was shown that curves of Ds versus L:W ratio varied from concave upward when $W_{CHANNEL}$ was 0.20 to nearly a vertical down sloped line when $W_{CHANNEL}$ was 0.30 to a concave downward curve when $W_{CHANNEL}$ was 0.50. These tendencies may be due to experimental error. In general, Ds decreased as L:W decreased. Considering that the amount of circulation should increase as the length of contact, momentum transfer between recycle and active zones should also increase. Thus, more flow in the active zone was required to compensate for increased circulation.

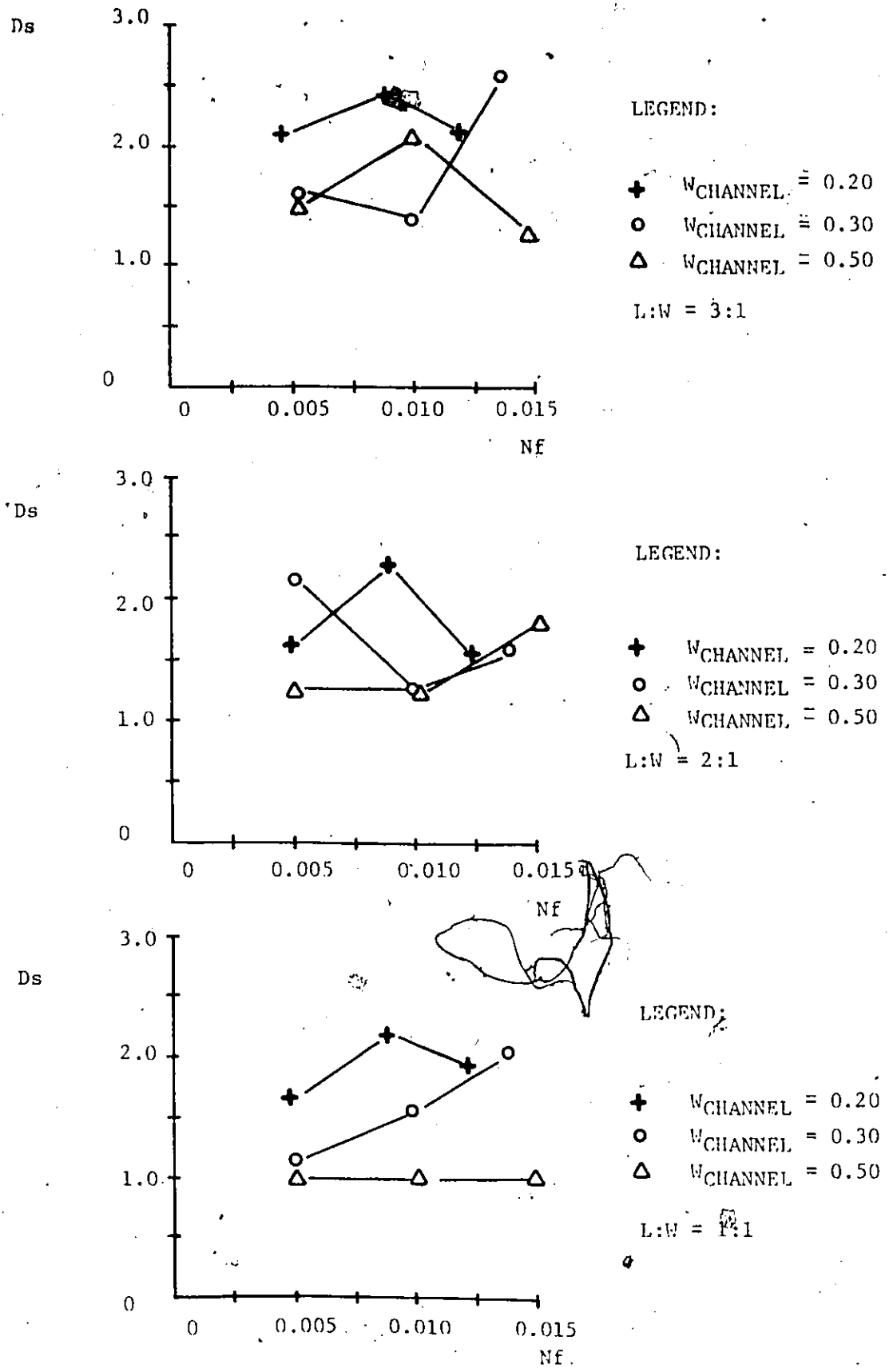

Figure 6.11: Variation of Ds with Froude Number (Nf)

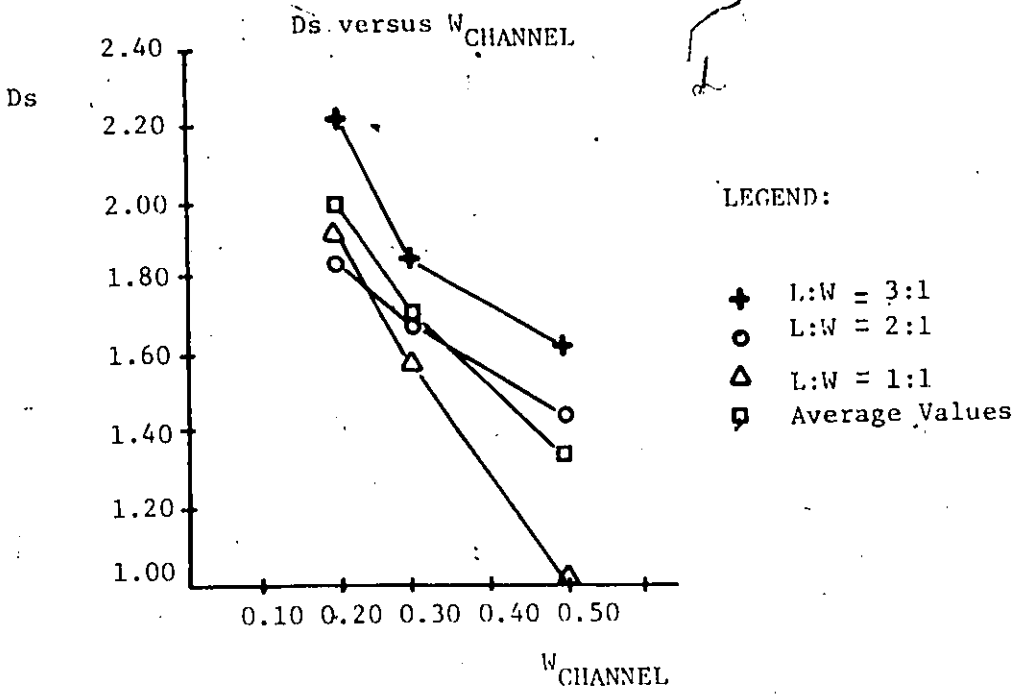

Figure 6.12: Plot of Ds versus $W_{CHANNEL}$

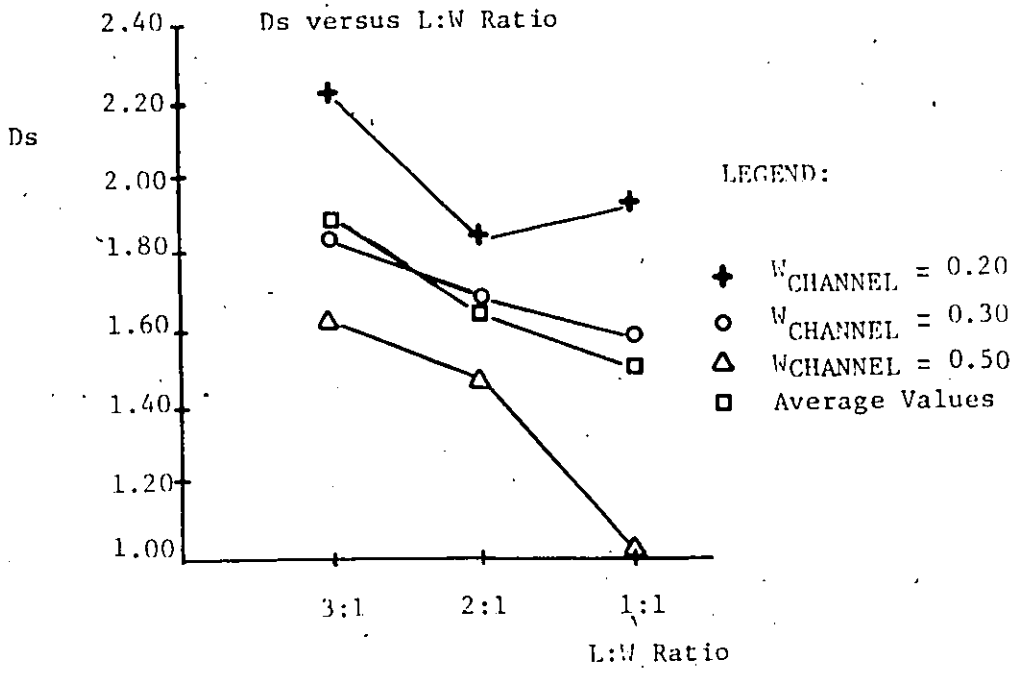

Figure 6.13: Plot of Ds versus L:W Ratio

Table 6.9: Average Values of Ds for the Various L:W Ratios and $W_{CHANNEL}$'s

$W_{CHANNEL}$ L:W	3:1	2:1	1:1	Average
0.20	2.22	1.83	1.92	1.99
0.30	1.84	1.68	1.58	1.70
0.50	1.61	1.44	1.00	1.35
Average	1.89	1.65	1.50	

6.6.3 Variation of Ds with Froude Number

The average values of Ds for the three flow rates are tabulated in Table 6.10. For simplicity, the flow rates were used instead of Froude number since the depth was maintained nearly constant in all the runs, and therefore, Nf was nearly constant for all runs with the same Q. From the values in Table 6.10, Ds was assumed to be independent of flow rate.

Table 6.10: Average Values of Ds for the Various Q's

Ds	Q (l/s)
1.57	1.0
1.71	2.0
1.76	3.0

6.6.4 Ds for Runs C3A, C3B and C3C

In these three runs, Ds was equal to one. This occurred because all of the dye appeared in the effluent before the cut-off point. No detectable dye entered the recycle zones of the basin. In these three situations, the mixing model was the same as a dispersed model with a reduced volume equal to the volume of the active zone.

6.7 Analysis of the Volume Ratio (β)

The values of β for the various runs as estimated from Method II were tabulated in Table 6.4. Figures 5.28 to 5.48 are time exposure photographs of the mixing patterns in the laboratory model during some of the experiments. From these photographs, values of β referred to as $\beta_{(PHOTO)}$ were measured. These values are tabulated in Table 6.5. Figure 6.14 is a plot of β versus $\beta_{(PHOTO)}$. The closeness of the data to the 45 degree line on this graph supports the fact that the chosen mixing model's parameters had physically meaningful results.

6.7.1 Variation of β with L:W Ratio

The values of β in Table 6.4 were averaged with the L:W ratios, tabulated in Table 6.11 and plotted in Fig. 6.15. As expected, β increased as L:W increased. This is analogous to saying that as the L:W ratio of a vessel is increased, the recirculation zones become more insignificant and, thus, the basin behaves more closely to a

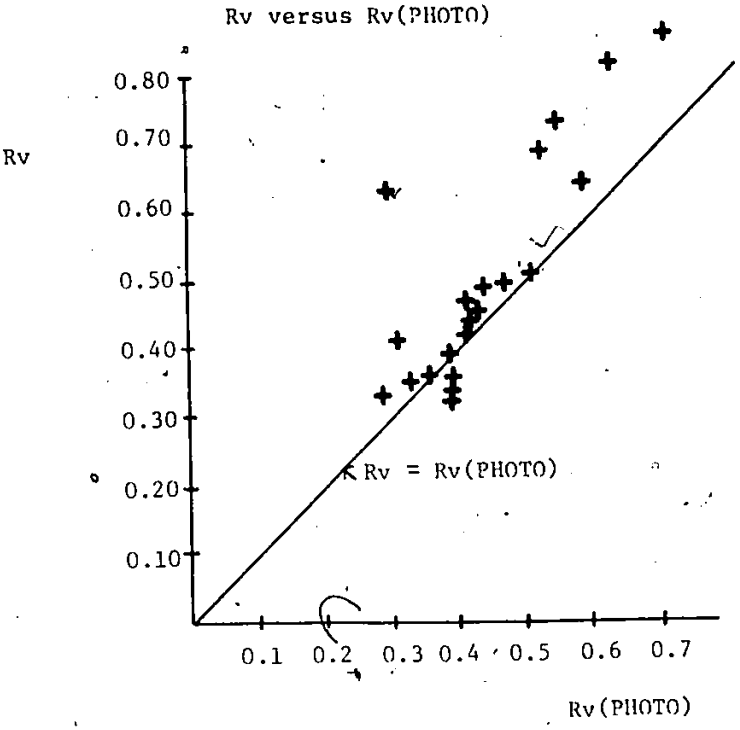

Figure 6.14: Plot of Rv versus Rv(PHOTO)

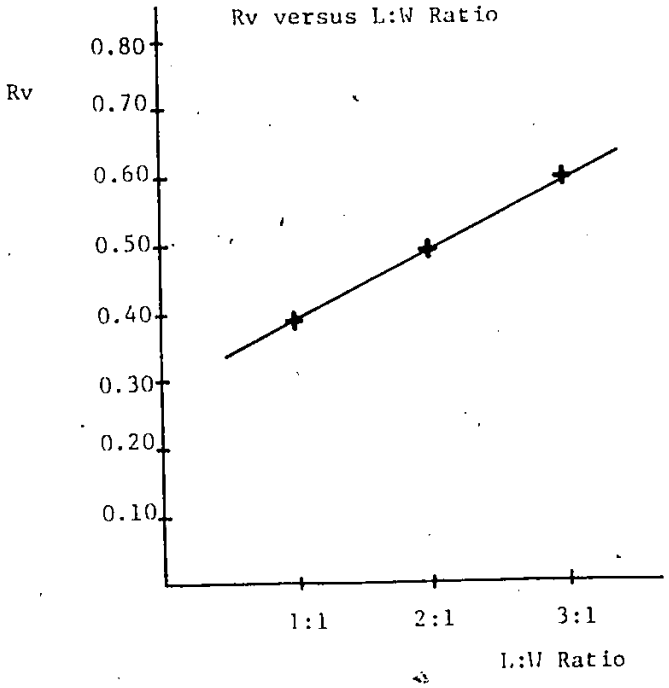

Figure 6.15: Plot of Average Rv versus L:W Ratio

dispersed flow or CM tanks in series model. The relationship between β and L:W appeared linear in Fig. 6.15 although the line must ultimately curve to reach β equal to one asymptotically. If the line was linearly extended (which must necessarily somewhat underestimate the ratio), a L:W ratio of 6.7:1 was required to have had a β equal to one. At that point, the entire volume of the basin would have been the volume of the active zone. It should be noted that the value of 6.7:1 for L:W was an average value for all flow rates and width of inlet and outlet channels.

The characteristic relationship between β and L:W ratio was explainable by the jet expansion of the influent stream. It stands to reason that a jet stream would continue to expand as distance increased, therefore, the fact that the width of the active zone increased as L:W increased was expected.

Table 6.11: Average values of β for the Various L:W Ratios

L:W	Average β
3:1	0.598
2:1	0.482
1:1	0.378

6.7.2 Variation of β with $W_{CHANNEL}$

Figure 6.16 is a plot of the averaged values of β for the three different values of $W_{CHANNEL}$ which are tabulated

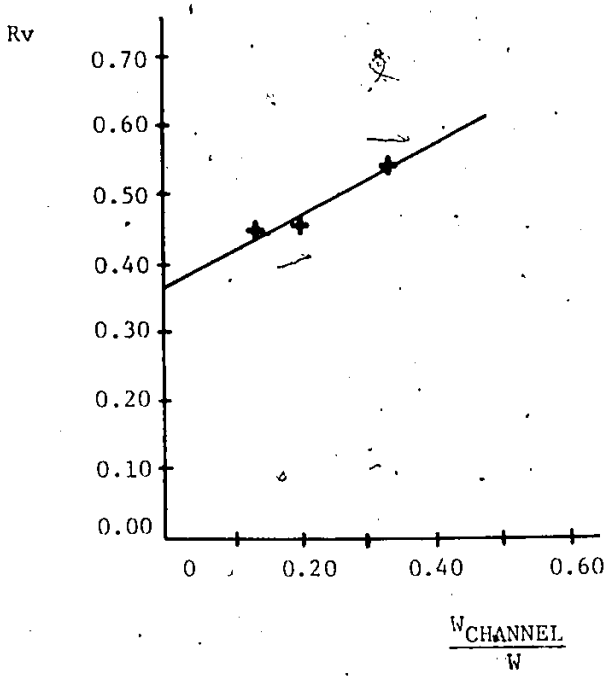

Figure 6.16: Plot of Rv versus $W_{CHANNEL}/W$

in Table 6.12. Again, this line should curve to reach β equal to one asymptotically when $W_{CHANNEL}/W$ reaches one.

Table 6.12: Average Values of β for the Various $W_{CHANNEL}/W$

$W_{CHANNEL}$ / W	Average β
0.133	0.448
0.200	0.456
0.333	0.554

6.7.3 Variation of β with Froude Number

The averaged values of β for the different flow rates are tabulated in Table 6.13. The volumetric flow rate, Q, was utilized instead of Nf because, as discussed previously, the depth was maintained constant, thus Nf is proportional to Q. The values in Table 6.13 indicated that β increased as the flow rate increased. This phenomenon was predicted by the theory on corner circulation by Abbott and Rasmussen[1] which was stated in Section 3.1: the higher the incoming stream velocity the greater is its ability to spread laterally across the flow field to reduce resistance.

Table 6.13: Average Values of β for the Various Q

Q (l/s)	Average β
1.0	0.412
2.0	0.505
3.0	0.542

6.8 Analysis of the Time to Peak

The time required to reach the maximum dye concentration on the experimental output dye tracer curves was termed the time to peak (Tp). When Tp is divided by T_d, the value thus obtained (Tp/T_d) gives an indication of the degree of short-circuiting in the basin. A value of 1.0 indicates PF whereas a value of 0.0 indicates a CM situation. The values of Tp/T_d are tabulated in Table 6.4.

Figure 6.17 is a series of plots of Tp/T_d versus Nf for all the laboratory experiments. From these plots, the following general statements can be made:

1) Tp/T_d increases as L:W increases

2) Tp/T_d increases as Nf increases

3) Tp/T_d increases as $W_{CHANNEL}$ increases.

The implications of point (2) above should be carefully studied. It is true that as Nf is increased, Tp/T_d is increased. It must be remembered, however, that as Nf is increased, T_d is decreased. For instance, if Nf is doubled (*i.e.*, Q is doubled), two basins of the same volume would be required to achieve the same T_d and a higher Tp/T_d.

The above analysis of Tp/T_d indicated that to achieve better treatment efficiency (higher Tp/T_d), one should increase the L:W ratio of the basin, increase the number of compartments in the basin, and/or use wider channels (diffusers or baffles) in the inlet and outlet channels.

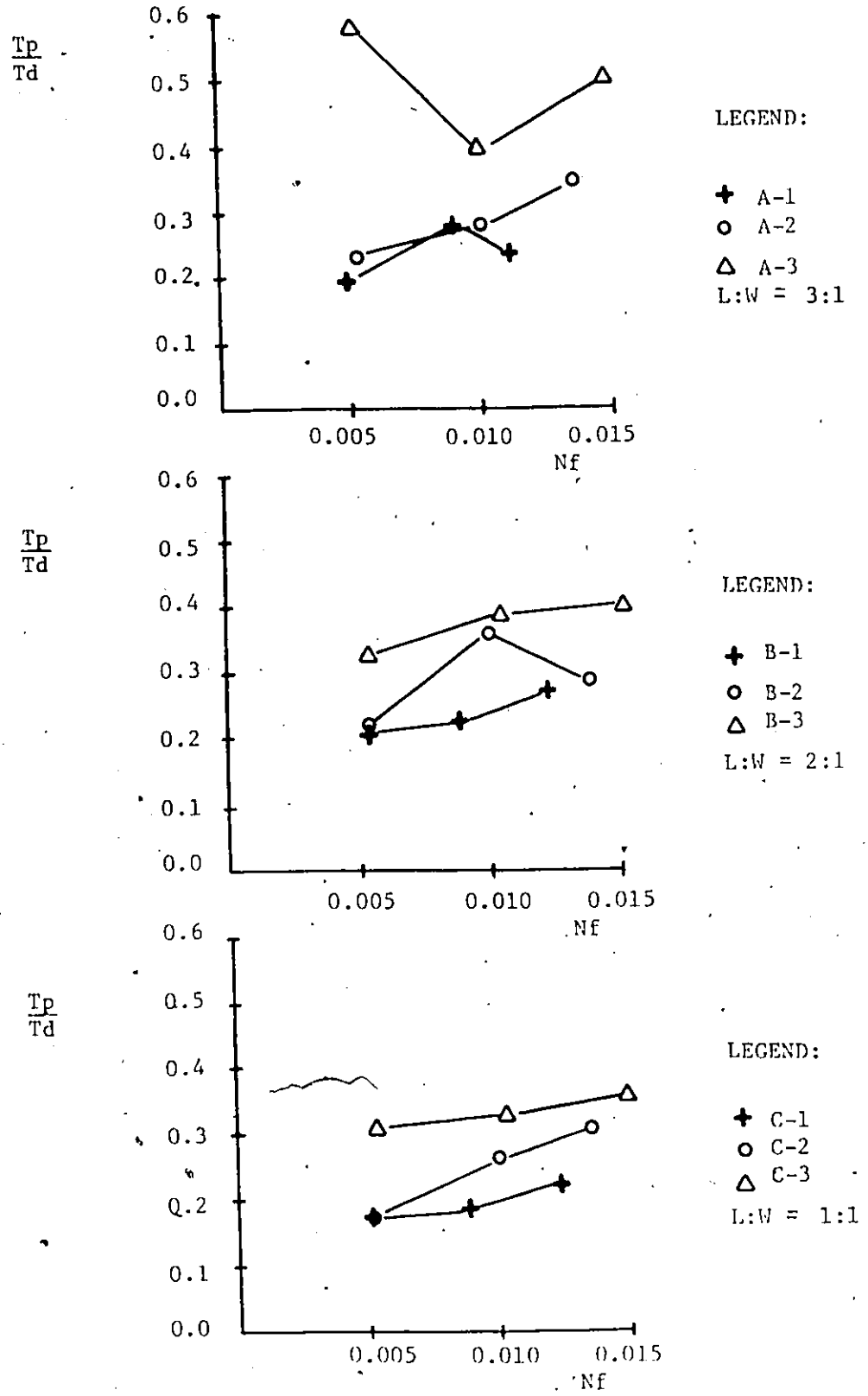

Figure 6.17: Variation of Tp/Td with Froude Number (Nf)

CHAPTER VII

CONCLUSIONS

The Ferrara and Harleman model was chosen for representing the mixing properties of a SWTP. The model is characterized by a central fast flowing zone in which longitudinal dispersion occurs in connection with CM recycle zones along the sides of the central zone.

A Crank-Nicholson finite difference solution to the governing partial differential equation was developed into a computer program which took into consideration the dye being recirculated through the recycle zones at each time increment. It was found that the number of time steps as well as the number of incremental volumes should be kept at a minimum of 390 each.

The mixing model closely reproduced the dye output tracer curves from the laboratory model study. The choice of mixing model depended on this criterion as well as ease of application. Methods of estimating the mixing model's parameters were evaluated. It was found that the dispersion coefficient was best evaluated by Levenspiel and Smith's equation (Eq. (3.22)) relating the peak concentration on the dye tracer curve to the reduced dispersion coefficient.

The dilution ratio was found to be accurately represented by the ratio of recycled dye to total dye. The mixing model's parameters were, therefore, easily obtained from an analysis of the output dye tracer curve, thereby not requiring a series of trial and error runs on the computer to identify the model's parameters.

The Ferrara and Harleman mixing model was also found to yield physically meaningful results. The estimated values of the ratio of the volume of the active zone to the total volume were found to be very similar to the values measured off the photographs from the model runs.

The following conclusions apply only to ponds of the same geometric shape and Froude number range as that of the laboratory model.

1. The dispersion coefficient increased as the flow rate and the Reynolds number increased. The dispersion coefficients in the model were found to be four times smaller than those predicted by Fischer's equation (Eq. (3.14)) on the average. The dispersion coefficient decreased as the width of the inlet and outlet channels increased.

2. The dilution ratio was found to decrease as $W_{CHANNEL}$ increased and as L:W ratio decreased. It was also found to be independent of flow rate. Thus, Ds was solely a function of the pond's geometry.

3. β was a function of pond geometry and flow rate. It was found to increase with (1) L:W ratio, with (2) $W_{CHANNEL}$, and with (3) Nf.

4. Tp/T_d was found to increase as the L:W ratio was increased, the $W_{CHANNEL}$ was increased and the flow rate was increased.

5. Results should be scaled up according to Froude's Law. In some instances, because of the small depth of flow in the prototypes, a distorted model may be necessary. The values of Ds found in the model studies could be applied to prototypes of the same L:W ratio and $W_{CHANNEL}$ as the models. The values of β could also be extended to prototypes of the same L:W ratio and $W_{CHANNEL}$ as the models, but only at the same Froude number. More work is required for the dispersion coefficient since it appears to be a function of Reynolds number and the model studies were not operated at Reynolds numbers in the range of the prototypes. However, as an alternative, one may assume that Fischer's equation applies in large prototype ponds.

CHAPTER VIII

RECOMMENDATIONS FOR FUTURE RESEARCH

1. The validity of Fischer's equation for calculating the dispersion coefficient should be checked in larger basins.

2. More tests with higher length to width ratios should be performed to find the ratio at which the entire basin volume becomes active ($\beta = 1.0$). This ratio is expected to change as the width of the inlet and outlet channels is varied.

3. To better estimate experimental errors, more tracer curves (three to five) under the same conditions should be obtained and averaged.

4. The influence of the jet expansion on the value of the dispersion coefficient should be quantified.

5. A larger pump should be tested with the five-tube sampler to see if it eliminates the dispersion problem that existed with this sampler.

6. A convolution of the dye tracer curve under unsteady conditions to find flow conditions could be attempted. This

would include changes in influent concentrations, as well as changes in the model's parameters as flow rate changed.

7. With a larger data bank of results, one may be able to define Ds as a function of L:W ratio and $W_{CHANNEL}$ and also, ß as a function of L:W ratio, $W_{CHANNEL}$ and Froude number.

REFERENCES

1. Abbott, M. B., Rasmussen, C. H., "On the Numerical Modelling of Rapid Expansions and Contractions in Models that are Two-Dimensional in Plan," *Proceedings, 17th Congress of the International Association for Hydraulic Research*, Baden-Baden, Germany, Vol. 2, Proc. Paper A104, 1977, pp. 229-237.

2. Alder, R.J., Long, W.M., Rooze, J. and Weinstein, H. "The Use of Finite Stage Models for Analysis and Design of Continuous Chemical Reactors." *Proceedings of the World Petroleum Congress*, pp. 103-20.

3. Allen, J., *Scale Models in Hydraulic Engineering*, Longmans, Greens and Co., London, England, 1977.

4. Barfield, B. J., Wells, L. G., Tapp, J. S., Uhl, R. A., Wilson, B., "Design Model for Sediment Control on Mined Lands," *Proceedings, Symposium on Watershed Management*, Boise, Idaho, Vol. 2, Published by ASCE, New York, N.Y., July, 1980, pp. 628-642.

5. Beer, T., Young, P.C., "Longitudinal Dispersion in Natural Streams", *Journal of the Environmental Engineering Division*, ASCE, Vol. 109, No. 5., Proc. Paper 18269, October, 1983, pp. 1049-1067.

6. Camp, T.R., "Sedimentation and the Design of Settling Tanks", *Transactions of the American Society of Civil Engineers*, 111, 1946, pp. 895-936.

7. Carnahan, B., Luther, H.A. and Wilkes, J.O., "Applied Numerical Methods", *John Wiley and Sons*, New York, New York, 1969.

8. Chen, C. N., "Design of Sediment Retention Basins," *National Symposium of Urban Hydrology and Sediment Control - Mini Course No. 2*, University of Kentucky, Lexington, Kentucky, July 28-31, 1975, pp. 285-293.

9. Cholette, A., Cloutier, L., "Mixing Efficiency Determinations for Continuous Flow Systems," *Canadian Journal of Chemical Engineering*, Vol. 37, 1959, pp. 105-112.

10. Chow, V. T., *Open Channel Hydraulics*, McGraw-Hill Book Company, New York, N.Y., 1959.

11. de Vries, M., *Solving River Problems by Hydraulic and Mathematical Models*, Delft Hydraulic Laboratory, Report No. 76-II, September, 1971.

12. Elder, J. W., "The Dispersion of Marked Fluid in Turbulent Shear Flow," *Journal of Fluid Mechanics*, Vol. 5, 1959, pp. 544-560.

13. Ferrara, R.A., Harleman, D.R.F., "A Dynamic Nutrient Cycle Model for Waste Stabilization Ponds", Report No. 237, R.M. Parsons Laboratory, Massachusetts Institute of Technology, December, 1978.

14. Ferrara, R. A., Harleman, D. R. F., "Hydraulic Modelling for Waste Stabilization Ponds," *Journal of the Environmental Engineering Division*, ASCE, Vol. 107, No. EE4, Proc. Paper 16470, August, 1981, pp. 817-830.

15. Fischer, H.B., "The Mechanics of Dispersion in Natura Streams", *Journal of the Hydraulics Division*, ASCE, Vol. 93, No. HY6, Proc. Paper 5392, November, 1957, pp. 187-216.

16. Grady, C.P.L., Lim, H.C., *Biological Wastewater Treatment - Theory and Applications*, Marcel Dekker, Inc., New York, New York, 1980.

17. Haan, C. T., Ward, A. D., *Evaluation of Detention Basins for Controlling Urban Runoff and Sedimentation*, Office of Water Research and Technology, U.S. Department of Commerce, Research Report No. 112, August, 1978, 20 pages.

18. Harleman, D. R. F., "Pollution in Estuaries," *Estuary and Coastline Hydrodynamics*, Ippen, et al, authors, McGraw-Hill Book Company, New York, N.Y., 1966.

19. Hawley, M. E., Bondelid, T. R., McCuen, R. H., "A Planning Method for Evaluating Downstream Effects of Detention Basins," *Water Resources Bulletin*, American Water Resources Association, Vol. 17, No. 5, October, 1981, pp. 806-813.

20. Heinemann, H. G., "A New Sediment Trap Efficiency Curve for Small Reservoirs," *Water Resources Bulletin*, American Water Resources Association, Vol. 17, No. 5, October, 1981, pp. 825-830.

21. Henderson, F. M., *Open Channel Flow*, The MacMillan Co., New York, N.Y., 1966.

22. Hovorka, R.B., *An Asymmetric Residence-Time Distribution Model for Flow Systems*, Ph.D. Dissertation, Case Institute of Technology, 1961.

23. Imam, E., McCorquodale, J. A., "Simulation of Flow in Rectangular Clarifiers," *Journal of the Environmental Engineering Division*, ASCE, Vol. 109, No. 3, Proc. Paper 18006, June, 1983, pp. 713-730.

24. Ivicsics, L., *Hydraulic Models*, Water Resources Publications, U.S.A., 1980.

25. Kamedulski, G. E., McCuen, R. H., "The Effects of Maintenance on Stormwater Detention Basin Efficiency," *Water Resources Bulletin*, American Water Resources Bulletin, Vol. 15, No. 4, August, 1979, pp.

26. Levenspiel, O., *Chemical Reaction Engineering*, John Wiley and Sons, Inc., New York, N.Y., 1972, pp. 253-314.

27. Levenspiel, O., Bischoff, K. B., "Patterns of Flow in Chemical Process Vessels," *Advances in Chemical Engineering*, Vol. 4, Academic Press, New York, N.Y., 1963, pp. 95-198.

28. Levenspiel, O., Smith, W. K., "Notes on the Diffusion-Type Model for the Longitudinal Mixing of Fluids in Flow," *Chemical Engineering Science*, Vol. 6, 1957, pp. 227-233.

29. Medina, M. A. Jr., Huber, W. C., Heany, J. P., "Modelling Stormwater Storage/Treatment Transients: Theory," *Journal of the Environmental Engineering Division*,

ASCE, Vol. 104, No. EE4, Proc. Paper 16467, August, 1981, pp. 781-797.

30. Medina, M. A. Jr., Huber, W. C., Heany,J. P., "Modelling Stormwater Storage/Treatment Transients: Applications," *Journal of the Environmental Engineering Division*, ASCE, Vol. 104, No. EE4, Proc. Paper 16471, August, 1981, pp. 791-816.

31. Novak, P., Cabelka, J., *Models in Hydraulic Engineering*, Pitman Publishing Inc., Massachusetts, 1981.

32. Oliver, L. J., Grigoropoulos, S. J., "Control of Storm-Generated Pollution Using a Small Urban Lake," *Journal of the Water Pollution Control Federation*, Vol. 53, No. 5, May, 1981, pp. 594-603.

33. Ploeg, J., Prandle, D., *Note on a Model Study to Reduce Local Pollution Levels in Swimming Areas*, National Research Council of Canada, Division of Mechanical Engineering, Report No. 3654882, Ottawa, 1971, 26 pages.

34. Pratte, Dr. B. D., personal conversation, February, 1984.

35. Rideau River Stormwater Management Study, *Urban Runoff Treatment in the Kennedy-Burnett Settling Pond*, Ottawa, 1983.

36. Russel, R. C. H., *Methods of Choosing Scales for Models in Use at the Hydraulics Research Station*, Hydraulics Research Station, Wallingford, Report No. INT. 40, November, 1964.

37. Ryan, P.J., Harleman, D.R.F., "An Analytical and Experimental Study of Transient Cooling Pond Behaviour", T.R. 161, R.M. Parsons Laboratory, Massachusetts Institute of Technology, January, 1973.

38. Schamber, D. R., Larock, B. E., "A Finite Element Model of Turbulent Flow in Primary Sedimentation Basins," *Proceedings, Second International Conference on Finite Elements in Water Resources*, C. A. Brebbia et al, eds., Pentech Press, London, England, 1978, pp. 3.3-3.21.

39. Sharp, J. J., *Hydraulic Modelling*, Butterworths, Toronto, Canada, 1981.

40. Simmons, H. B., "Tidal and Salinity Model Practice," *Estuary and Coastline Hydrodynamics*, Ippen et al., authors, McGraw-Hill Book Company, New York, N.Y., 1966.

41. Small, M. J., Di Toro, D. M., "Stormwater Treatment Systems," *Journal of the Environmental Engineering Division*, ASCE, Vol. 105, No. EE3, Proc. Paper 14647, June, 1979, pp. 557-569.

42. Smith, D. P. Jr., Bedient, P. B., "Detention Storage for Urban Flood Control," *Journal of the Water Resources Planning and Management Division*, ASCE, Vol. 106, No. WR2, Proc. Paper 15555, July, 1980, pp. 413-425.

43. Taylor, G.I., "The Dispersion of Matter in Turbulent Flow Through a Pipe", *Proceedings of the Royal Society of London*, Vol. 223, Series A, 1954.

44. Townsend, Dr. D., personal conversation, February, 1984.

45. Whipple, W. Jr., McIntosh, A. W., *Dual Purpose Detention Basins and Surveillance Procedures in Urbanizing Watersheds*, Office of Water Research and Technology, Department of the Interior, Project No. A-048-N.J., January, 1979.

46. Wehner, J.F., Wilhelm, R.H., "Boundary Conditions of Flow Reactor", *Chemical Engineering Science*, Vol. 6, 1956, pp. 89-93.

47. Wolf, D., Resnick, W., "Residence Time Distribution in Real Systems," *Industrial and Engineering Chemistry*, Vol. 2, No. 4, November, 1963, pp. 287-293.

48. Yalin, M. S., *Theory of Hydraulic Models*, MacMillan Press, London, England, 1971.

APPENDIX

A.1 Finite Difference Operators

The governing partial differential equation (PDE) is:

$$\frac{\partial C}{\partial t} = E \frac{\partial^2 C}{\partial x^2} - U \frac{\partial C}{\partial x}$$

When using a finite difference technique to solve a PDE, a network of grid points is set up throughout the region of interest occupied by the independent variables. The partial derivatives of the original PDE are approximated by suitable finite difference expressions.

A space-time grid representation of elements is set up. The procedure leads to a set of algebraic equations in terms of the estimates of the dependent variable, $u_{i,j}$, whose values may then be determined. By making the grid spacing sufficiently small, it is hoped that $u_{i,j}$ will become a sufficiently close approximation to the true value at any grid point (i,j).

The grid can be set up as follows:

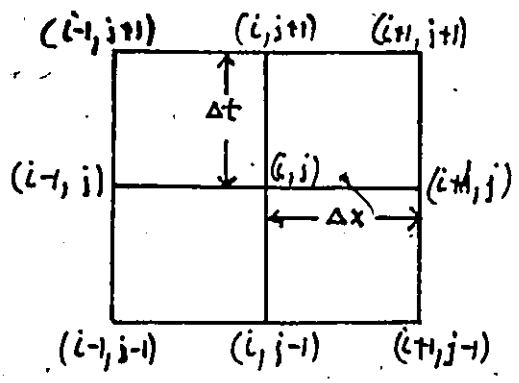

The following operators may be used to estimate the derivatives[7].

(a). Forward difference:

$$\frac{dU}{dx} = \frac{U_{i+1,j}-U_{i,j}}{\Delta x} + O(\Delta x)$$

(b). Backward difference:

$$\frac{dU}{dx} = \frac{U_{i,j}-U_{i-1,j}}{\Delta x} + O(\Delta x)$$

(c). Central difference:

$$\frac{dU}{dx} = \frac{U_{i+1,j}-U_{i-1,j}}{2\Delta x} + O[(\Delta x)^2]$$

(d). For the second derivative:

$$\frac{d^2U}{dx^2} = \frac{U_{i-1,j}-2U_{i,j}+U_{i+1,j}}{(\Delta x)^2} + O[(\Delta x)^2]$$

A.2 The Crank-Nicholson Equations for Solution of the Model

The model of Ferrara and Harleman[14] is shown in Fig. 3.11. This model assumes that the central active zone behaves as dictated by the rules of the dispersed flow model, while the outside recirculating zones closely approximate the behaviour of the completely-mixed flow model.

In the formulation of their model, Ferrara and Harleman have assumed that the active zone does not intermix with the recirculation zones for simplicity and ease of mathematical representation. These zones only interact with the inflow and outflow of the active zone.

The PDE for the dispersed flow zone is the equation given above. The recycle zones are CM and no intermixing between

the zones is considered except at the ends of the vessel. The recycle zones are fed water at the far end of the vessel and return water to the active (dispersed) zone at the entrance to the vessel. Equations for the CM zone are presented after a discussion of the dispersed zone solution. The Crank-Nicholson formulations were chosen because of their stability.

The partial derivatives may be expressed as follows:

$$\frac{\partial C}{\partial t} = \frac{C_{i,n+1} - C_{i,n}}{\Delta t}$$

$$E \frac{\partial^2 C}{\partial x^2} = \frac{1}{2\,\Delta x^2} \{ E_i (C_{i+1,n} - C_{i,n}) - E_{i-1} (C_{i,n} - C_{i-1,n}) + E_i (C_{i+1,n+1} - C_{i,n+1}) - E_{i-1} (C_{i,n+1} - C_{i-1,n+1}) \}$$

$$U \frac{\partial C}{\partial x} = \frac{1}{2\Delta x} (U_i C_{i,n} - U_{i-1} C_{i-1,n} + U_i C_{i,n+1} - U_{i-1} C_{i-1,n+1})$$

In finite difference form, the partial differential equation can be expressed as follows:

$$\frac{C_{i,n+1} - C_{i,n}}{\Delta t} = \frac{1}{2\Delta x^2} \{E_i (C_{i+1,n} - C_{i,n}) - E_{i-1} (C_{i,n} - C_{i-1,n}) + E_i (C_{i+1,n+1} - C_{i,n+1}) - E_{i-1} (C_{i,n+1} - C_{i-1,n+1})\} + \frac{1}{2\Delta x} (U_{i-1} C_{i-1,n} - U_i C_{i,n} + U_{i-1} C_{i-1,n+1} - U_i C_{i,n+1})$$

For element 1, the equation is:

$$\frac{C_{1,n+1} - C_{1,n}}{\Delta t} = \frac{1}{2\Delta x^2} \{E_1 (C_{2,n} - C_{1,n}) - E_0 (C_{1,n} - C_{0,n}) + E_1 (C_{2,n+1} - C_{1,n+1}) - E_0 (C_{1,n+1} - C_{0,n+1})\} + \frac{1}{2\Delta x} \{U_0 C_{0,n} - U_1 C_{1,n} + U_0 C_{0,n+1} - U_1 C_{1,n+1}\}$$

For element N, the last elemental volume (N is the total number of elemental volumes), the equation is:

$$\frac{C_{N,n+1}-C_{N,n}}{\Delta t} = \frac{1}{2\Delta x^2}\{E_N(C_{N+1,n}-C_{N,n})-E_{N-1}(C_{N,n}-C_{N-1,n}) + E_N(C_{N+1,n+1}-C_{N,n+1})-E_{N-1}(C_{N,n+1}-C_{N-1,n+1})\} + \frac{1}{2\Delta x}(U_{N-1}C_{N-1,n}-U_NC_{N,n}+U_{N-1}C_{N-1,n+1}-U_NC_{N,n+1})$$

For element 1, rearranging, the equation is:

$$(2+\frac{E_1\Delta t}{\Delta x^2}+\frac{U_1\Delta t}{\Delta x})C_{1,n+1}-\frac{E_1\Delta t}{\Delta x^2}C_{2,n+1}=(2-\frac{E_1\Delta t}{\Delta x^2}-\frac{U_1\Delta t}{\Delta x})C_{1,n}+\frac{E_1\Delta t}{\Delta x^2}C_{2,n} + \frac{U_o\Delta t}{\Delta x}(C_{o,n}+C_{o,n+1})$$

For element N, rearranging, the equation is:

$$(2+\frac{E_{N-1}\Delta t}{\Delta x^2}+\frac{U_N\Delta t}{\Delta x})C_{N,n+1}-(\frac{E_{N-1}\Delta t}{\Delta x^2}+\frac{U_{N-1}\Delta t}{\Delta x})C_{N-1,n+1}$$

$$=(\frac{E_{N-1}\Delta t}{\Delta x^2}+\frac{U_{N-1}\Delta t}{\Delta x})C_{N-1,n}+(2-\frac{E_{N-1}\Delta t}{\Delta x^2}-\frac{U_N\Delta t}{\Delta x})C_{N,n}$$

The following simplifications can be made:

$E_1 = E_2 \ldots = E_{i-1} = E$, where $i = N$.

$E_o = E_N = 0$ (boundary conditions)

$U_o = U_1 = U_2 = \ldots = U_{x-1} = U_x = U$

let $\frac{D\Delta t}{\Delta x^2} = p$ $\qquad C_1' = C_{1,n+1}$

$\frac{U\Delta t}{\Delta x} = q$ $\qquad C_1 = C_{1,n}$

The solution for the set of n equations in matrix form is:

$$\begin{bmatrix} 2+p+q & -p & 0 & 0 & 0 & \dots & 0 & 0 \\ -p-q & 2+2p+q & -p & 0 & 0 & \dots & 0 & 0 \\ 0 & -p-q & 2+2p+q & -p & & \dots & 0 & 0 \\ 0 & 0 & -p-q & 2+2p+q & -p & \dots & 0 & 0 \\ \cdot & \cdot & \cdot & \cdot & \cdot & & \cdot & \cdot \\ \cdot & \cdot & \cdot & \cdot & \cdot & & \cdot & \cdot \\ \cdot & \cdot & \cdot & \cdot & \cdot & & \cdot & \cdot \\ 0 & 0 & 0 & \dots & -p-q & & 2+2p+q & -p \\ 0 & 0 & 0 & \dots & 0 & & -p-q & 2+p+q \end{bmatrix} \times$$

$$\begin{bmatrix} C_1' \\ C_2' \\ C_3' \\ C_4' \\ \cdot \\ \cdot \\ \cdot \\ C'_{x-1} \\ C'_x \end{bmatrix} = \begin{bmatrix} (2-p-q)C_1 + C_2 + q(C_0+C'_0) \\ (p+q)C_1 + (2-2p-q)C_2 + pC_3 \\ (p+q)C_2 + (2-2p-q)C_3 + pC_4 \\ (p+q)C_3 + (2-2p-q)C_4 + pC_5 \\ \cdot \\ (p+q)C_{i-1} + (2-2p-q)C_i + pC_{i+1} \\ \cdot \\ (p+q)C_{x-2} + (2-2p-q)C_{x-1} + pC_x \\ (p+q)C_{x-1} + (2-p-q)C_x \end{bmatrix}$$

A simpler matrix can be obtained with the following substitutions:

let $-a = -p-q$ $\quad b = 2+2p+q$ $\quad -c = -p$

$p+q = a$ $\quad e = 2-2p-q$ $\quad p = c$

$$\begin{bmatrix} b-c & -c & 0 & 0 & 0 & \dots & 0 & 0 & 0 & 0 & 0 \\ -a & b & -c & 0 & 0 & \dots & 0 & 0 & 0 & 0 & 0 \\ 0 & -a & b & -c & 0 & \dots & 0 & 0 & 0 & 0 & 0 \\ 0 & 0 & -a & b & -c & \dots & 0 & 0 & 0 & 0 & 0 \\ \cdot & \cdot & \cdot & \cdot & \cdot & & \cdot & \cdot & \cdot & \cdot & \cdot \\ \cdot & \cdot & \cdot & \cdot & \cdot & & \cdot & \cdot & \cdot & \cdot & \cdot \\ \cdot & \cdot & \cdot & \cdot & \cdot & & \cdot & \cdot & \cdot & \cdot & \cdot \\ 0 & 0 & 0 & 0 & 0 & \dots & -a & b & -c & 0 & 0 \\ 0 & 0 & 0 & 0 & 0 & \dots & 0 & -a & b & -c & 0 \\ 0 & 0 & 0 & 0 & 0 & \dots & 0 & 0 & -a & b & -c \\ 0 & 0 & 0 & 0 & 0 & \dots & 0 & 0 & 0 & -a & b \end{bmatrix} \times$$

$$\begin{bmatrix} C_1' \\ C_2' \\ C_3' \\ C_4' \\ \cdot \\ \cdot \\ \cdot \\ C_{x-3} \\ C'_{x-2} \\ C'_{x-1} \\ C'_x \end{bmatrix} = \begin{bmatrix} q(C_0+C_0') + (e+c)C_1 & +cC_2 \\ aC_1 + eC_2 & +cC_3 \\ aC_2 + eC_3 & +cC_4 \\ aC_3 + eC_4 & +cC_5 \\ \cdot & \cdot \\ \cdot & \cdot \\ \cdot & \cdot \\ aC_{x-4} & +eC_{x-3} \quad +cC_{x-2} \\ aC_{x-3} & +eC_{x-2} \quad +cC_{x-1} \\ aC_{x-2} & +eC_{x-1} \quad +cC_x \\ aC_{x-1} & +(e+c)C_x \quad 0 \end{bmatrix}$$

A.2.1 Solution of the Crank-Nicholson Equations by Gauss's Elimination Method (Without Pivoting)

First Step:

$$r_1 = b_1 = b-c$$

$$r_i = b_i - \frac{a_i}{r_{i-1}} C_{i-1}$$

$$r_2 = b_2 - \frac{a_2 C_1}{r_1} = b - \frac{ac}{b-c} = b - \frac{ac}{r_1}$$

$$r_3 = b_3 - \frac{a_3 C_2}{r_2} = b - \frac{ac}{r_2}$$

and, in general, $r_i = b - \frac{ac}{r_{i-1}}$ $\qquad (i=2,3,4,\ldots,I)$

Second Step:

$$S_1 = d_1 = -q(C_o+C_o') + (e+c)C_1 + cC_2 = d_1$$

$$S_i = d_i + \frac{a_i S_{i-1}}{r_{i-1}}$$

$$= d_i + \frac{a S_{i-1}}{r_{i-1}} \qquad (i=2,3,4,\ldots,I)$$

Third Step:

$$C'_N = S_N$$

$$C'_{N-1} = \frac{1}{r_{N-1}} (S_{N-1} + C_{I-1} C'_I)$$

$$C_i = \frac{1}{r_i} (S_i + cC'_{i+1}) \qquad (i=I-1, I-2, I-3, \ldots, 1)$$

A.2.2 Concentration, C_1 in First Elemental Volume at t=0:

M_{in} has a value such that $C_o = \frac{M_{in}}{V} = 1.0$.

Therefore,

$$M_{in} = V.$$

Also the mass in the first elemental volume must satisfy

$$M_{in} = V$$

$$C \cdot \Delta V = M_{in} = V$$

Rearranging, $C = \frac{V}{\Delta V} = \frac{L \times W_T \times D}{\Delta x \times W_a \times D} = \frac{L}{\Delta x} \times \frac{W_T}{W_a}$

$$C = N \cdot \beta$$

where: $N = L/\Delta x$ (number of elemental volumes)

$$\beta = \frac{W_a}{W_T} = \frac{V_a}{V_T}$$

or,

$$C_{in} = \frac{V}{\Delta V} = \frac{V}{Q\Delta t} = \frac{T_d}{\Delta t}$$

A.2.3 Mass Correction (at each time step)

A time t

i) $\text{Mass}(t) = \Sigma C_i(t) V_i$

where Mass (t) = mass of dye in the basin calculated from the sum of the elements at time t
$C_i(t)$ = dye concentration in element i at time t
V_i = volume of element i

ii) M(t) = Initial mass − mass that has been removed through the effluent

$$= V - \Sigma C_{out}(t)\, \Delta t \cdot Q$$

where V = initial mass of dye
$C_{out}(t)$ = concentration of dye in effluent at time t
Δt = time step
Q = flow rate

iii) $\text{Mass}_c(t) = \Sigma C_{ic}(t) V_i$

where $\text{Mass}_c(t)$ = corrected mass of dye in basin calculated from the sum of the elements at time t

$$C_{ic}(t) = C_i(t) \times \frac{M(t)}{\text{Mass}(t)}$$

= corrected dye concentration in element i at time t

A.3 Equations for a CM Reactor

The following equation applies to a CM reactor and was used in the program.

$$C_{out(n+1)} = \frac{C_{out(n)}\ V + C_{in(n+1)} Q\ t}{V + Q\Delta t}$$

Where $C_{out(n+1)}$ = concentration leaving CM reactor at time t + Δt (n+1)
$C_{in(n+1)}$ = concentration entering CM reactor at time t + Δt (n+1)
$C_{out(n)}$ = concentration in the reactor at time t (n)
V = volume of CM reactor
Δt = time step
Q = flow rate

This is obtained from a mass balance around the CM reactor.

A.4 Standard Error Formula

The formula below was used to estimate the standard error of the various methods used.

$$Se = \frac{\Sigma[y_i-(b_0+b_1x_i)]^2}{n-1}$$

Estimate of the population correlation coefficient is given by

$$R = \frac{\Sigma(x_i-x)(y_i-y)}{[\Sigma(x_i-x)^2][(y_i-y)^2]}$$

$$Se = \frac{\Sigma(y_i-y_{ei})^2}{n-1}$$

A.5 The Computer Program

The following pages list the computer program that was used to solve the equations above.

```
C     ****************************************************************
C     *                                                              *
C     ****************************************************************
      DIMENSION C(67),T(7,7),XT(67),COUT(67),FINAL(30,4),XC(67)
      REAL L,MANING
      REAL*8 IDENT
      INTEGER PLOTOP
      DATA PI/3.14159/,IAXIS/0/,IPLOT/4/,ITER/4/
      COMMON L,ND,DT,TD,W,D,Q,MANING,V,MCOUNT,PLOTOP
      READ (5,5) IDENT
      READ (5,1) ND,DT,Q,D,W,L
      READ (5,2) (XC(I),I=1,ND)
      READ (5,9) TZERO
      READ (5,7) IACT
      READ (5,201) METOPT
      READ (5,4) LOPT,MANING,SLOPE
      MCOUNT = 0
C
C     >>>>>>>>>>>>>>>>>>>>>>>>>>>>>>>>>>>>>>>>>>>>>>>>>>>>>>>> PLOT COMMANDS
C
      READ (5,6) PLOTOP
      IF (PLOTOP .NE. 1) GO TO 67
      IGRAPH = 0
      CALL PLOTS (100.0,27.5)
      CALL FACTOR (0.50)
      CALL SYMBOL (20.0,25.0,0.5,24HOUTPUT DYE TRACER CURVES,0.0,24)
      CALL SYMBOL (23.5,24.0,0.35,11HRUN NUMBER:,0.0,11)
      CALL SYMBOL (27.7,24.0,0.35,IDENT,0.0,8)
      XT(ND+1) = 0.0
      XT(ND+2) = 0.100
      C(ND+2) = 0.0
      C(ND+2) = 0.25
      COUT(ND+1) = 0.0
      COUT(ND+2) = 0.25
C
C     >>>>>>>>>>>>>>>>>>>>>>>>>>>>>>>>>>>>>>>>>>>>>>>>>>>>>>>> WRITE COMMANDS
C
   67 WRITE (6,18) IDENT
      WRITE (6,10) ND,DT,Q,D,W,L
      WRITE (6,34) MANING,SLOPE
      V = W * L * D
      WRITE (6,29) V
      TD = V / Q
      WRITE (6,28) TD
      WRITE (6,32) TZERO
      WRITE (6,11) (XC(I),I=1,ND)
C
C     >>>>>>>>>>>>>>>>>>>>>>>>>>> SET UP OF THE NORMALIZED TIME MATRIX
C
      DO 68 I = 1,ND
   68 XT(I) = FLOAT(I-1) * DT / TD
C
C     >>>>>>>>>>>>>>>>>>>>>>> NORMALIZATION OF THE CONCENTRATION MATRIX
C
      CALL TROMB(6,1,65,XC,T,7,DT)
```

```
      WRITE (6,12)
      DO 51 I = 1,7
      JX = 8 - I
   51 WRITE (6,13) (T(I,J),J=1,JX)
      FACTER = (T(1,7) + XC(ND) / 2.0 * (TZERO - FLOAT(ND - 1) * DT))
     C/ TD
      DO 50 I = 1,ND
   50 C(I) = XC(I) / FACTER
      WRITE (6,23)(C(I),I=1,ND)
C
C     >>>>>>>>>>>>>>>>>>>>>>>>> TIME LOCATION OF MAXIMUM CONCENTRATION
C
      CALL CMAX(ND,C,JMAX,SCMAX)
      TP = XT(JMAX)
      WRITE (6,14) SCMAX,TP
C
C     >>>>>>>>>>>>>>>>>>>>>>>>>>>>>>>>>>>>>>>>>>>>>>>>>>> METOPT CONTROL
C
      GO TO (90,90,90,60),METOPT
   90 CALL SIMP(IACT,XC,DT,CTOT)
      TPEAK = FLOAT(JMAX-1) * DT
C
C     >>>>>>>>>>>>>>>>>>>>>>>>>>>>>>> INITIAL ESTIMATE OF THE DETENTION
C     >>>>>>>>>>>>>>>>>>>>>>>>>>>>>>>>>>>>>>>>>>>>>> TIME OF THE ACTIVE ZONE
C
      TDA = 1.05 * TPEAK
C
C     >>>>>>>>>>>>>>>>>>>>>>>>>>>>>>>>>>>>>>>>>>>>>>>>>>> METOPT CONTROL
C
      GO TO (70,73,70,60),METOPT
C
C     >>>>>>>>>>>>>> SOLUTION OF LEVENSPIEL'S AND SMITH'S EQUATION FOR
C     >>>>>>>>>>>>>>> D/UL USING NEWTON'S ROOT SOLVING METHOD TO SOLVE
C     >>>>>>>>>>>>>>>>>>>>> THE EQUATION THE FOR MAXIMUM CONCENTRATION
C
C
C     >>>>>>>>>>>>>>>>>>>>>>>>>>>>>>>>>>>> CALCULATION OF THE LARGEST DYE
C     >>>>>>>>>>>>>>>>>>>>>>>>>>>>>>> CONCENTRATION IN THE ACTIVE ZONE
C
   70 METOP = 1
   71 XCMAX = XC(JMAX) * TDA / CTOT
      F = 0.001
   52 G = (F**2.0 + 1.0)**0.5
      FEXP = -1.0 * (G - 1.0) / 2.0 / F
      FF = EXP(FEXP) / 2.0 / ( PI * F)**0.5 / (G - F)**0.5
      FFP = FF * (G - F - 1.0) / 2.0 / F**2.0
      FP1 = F - (FF - XCMAX) / FFP
      IF (ABS(FP1 - F) / FP1 .LE. 0.001) GO TO 54
      F = FP1
      GO TO 52
   54 FP11 = FP1
C
C     >>>>>>>>>>>>>>>>>> CALCULATION OF THE TIME TO PEAK IN THE ACTIVE
C     >>>>>>>>>>>>>> ZONE AS A FUNCTION OF THE D/UL VALUE IN THAT ZONE
C     >>>>>>>>>>>>>>> (ACCORDING TO LEVENSPIEL'S AND SMITH'S EQUATION)
```

```
C
      TPA = G - FP1
C
C     >>>>>>>>>>>> NEXT GUESS OF THE DETENTION TIME OF THE ACTIVE ZONE
C
      TDA1 = TPEAK / TPA
      IF (ABS(TDA1 - TDA) / TDA1 .LE. 0.001) GO TO 76
      TDA = TDA1
      GO TO 71
C
C     >>>>>>>>>>>>>>>>>>>>>>>> CALCULATION OF THE VALUE OF D/UL FOR THE
C     >>>>>>>>>>>>>>>>>>>>>>>> ACTIVE ZONE BY USING THE VARIANCE OF THE
C      >>>>>>>>>>>>>>>>>>>> EXPERIMENTAL CONCENTRATION VERSUS TIME CURVE
   73 IF (METOPT.EQ.3) METOPT = 1
      METOP = 2
      SUMF = 0.0
      SUMXF = 0.0
      SUMXXF = 0.0
      DO 75 I = 1,IACT
      SUMF = SUMF + XC(I)
      SUMXF = SUMXF + XC(I) * XT(I)
   75 SUMXXF = SUMXXF + XC(I) * XT(I)**2.0
      SUMXF = SUMXF * TD
      SUMXXF = SUMXXF * TD**2.0
      VARIA2 = SUMXXF / SUMF - (SUMXF / SUMF)**2.0
   80 VAR2 = VARIA2 / TDA**2.0
      FP1 = ((VAR2 * 8.0 + 1.0)**0.5 - 1.0) / 8.0
      FP12 = FP1
      G = (FP1**2.0 + 1.0)**0.5
C
C     >>>>>>>>>>>>>>>>>>> CALCULATION OF THE TIME TO PEAK IN THE ACTIVE
C     >>>>>>>>>>>>>>>> ZONE AS A FUNCTION OF THE D/UL VALUE IN THAT ZONE
C     >>>>>>>>>>>>>>>> (ACCORDING TO LEVENSPIEL'S AND SMITH'S EQUATION)
C
      TPA = G - FP1
C
C     >>>>>>>>>>>> NEXT GUESS OF THE DETENTION TIME OF THE ACTIVE ZONE
C
      TDA2 = TPEAK / TPA
      IF (ABS(TDA2 - TDA) / TDA2 .LE. 0.001) GO TO 76
      TDA = TDA2
      GO TO 80
C
C     >>>>>>>>>>>>>>>>>>>>>>>>>>>>>>>>>>>>>>>>>>>>>>>>>>>>>>>>>>>> LOPT CONTROL
C
   76 GO TO (62,62,79,61,78),LOPT
C
C     >>>>>>>>>>>> SOLVING FISCHER'S DISPERSION COEFFICIENT EQUATION BY
C     >>>>>>>>>> NEWTON'S METHOD TO OBTAIN THE WIDTH OF THE ACTIVE ZONE
C     >>>>>>>>>>>>>>>>>>>>>>>>>>> (SLOPE IS DEFINED BY MANNING'S EQUATION)
C
   61 GO TO (99,91),METOP
   99 WRITE(6,15)
      GO TO 92
```

```
 91 WRITE(6,16)
 92 WRITE(6,21)
    CONSTA = 1.101126 * MANING / L
    WA = 0.7 * W
 55 RHA = WA * D / (WA + 2.0 * D)
    FWA = WA**2.0 * CONSTA / RHA**(7.0/6.0)
    FWAP = FWA / WA / 6.0 * (5.0 + 7.0 * RHA / D)
    WA1 = WA - (FWA - FP1) / FWAP
    IF (ABS(WA1 - WA) / WA1 .LE. 0.001) GO TO 57
    WA = WA1
    GO TO 55
 57 CALL DSBETA(TDA,EA,FP1,WA1,BETA,DS)
C
C >>>>>>>>>>>>>>>>>>>>>>>>>>>>>>>>>>>>>>>>>>>>>>>>>> PLOT COMMANDS
C
    CALL FINITE(BETA,DS,EA,FINAL,260,65,COUT,XT,C,IAXIS,IPLOT,ITER)
    IGRAPH = IGRAPH + 1
    IGRD2 = IGRAPH / 2
    IF ( IGRD2*2.NE.IGRAPH ) WRITE(6,20)
C
C   >>>>>>>>>>>>>>>>>>>>>>>>>>>>>>>>>>>>>>>>>>>>>>>>>> LOPT CONTROL
C
    GO TO (78,62,79,79,78),LOPT
C
C   >>>>>>>>>>>[illegible] SOLVING FISCHER'S DIPERSION COEFFICIENT EQUATION BY
C   >>>>>>>>> [illegible]WTON'S METHOD TO OBTAIN THE WIDTH OF THE ACTIVE ZONE
C   >>>>>>>>>>[illegible]>>>>>>>> (THE SLOPE IS OBTAINED FROM THE INPUT FILE).
C
 62 GO TO (93,[illegible]),METOP
 93 WRITE(6,15)
    GO TO 95
 94 WRITE(6,16)
 95 WRITE(6,22)
    WA = 0.7 * W
    CONSTA = 1.101126 * SLOPE**0.5 * TDA / L**2.0
 58 RHA = WA * D / (WA + 2.0 * D)
    FWA = CONSTA * WA**2.0 / RHA**0.5
    FWAP = CONSTA * WA**0.5 * (2.0*WA+D) / D**0.5 / (WA+2.0*D)**0.5
    WA1 = WA - (FWA - FP1) / FWAP
    IF (ABS(WA1 - WA) / WA1 .LE. 0.001) GO TO 63
    WA = WA1
    GO TO 58
 63 CALL DSBETA(TDA,EA,FP1,WA1,BETA,DS)
C
C >>>>>>>>>>>>>>>>>>>>>>>>>>>>>>>>>>>>>>>>>>>>>>>>>> PLOT COMMANDS
C
    CALL FINITE(BETA,DS,EA,FINAL,260,65,COUT,XT,C,IAXIS,IPLOT,ITER)
    IGRAPH = IGRAPH + 1
    IGRD2 = IGRAPH / 2
    IF ( IGRD2*2.NE.IGRAPH ) WRITE(6,20)
C
C   >>>>>>>>>>>>>>>>>>>>>>>>>>>>>>>>>>>>>>>>>>>>>>>>>> LOPT CONTROL
C
    GO TO (78,78,79,79,78),LOPT
C
```

```
C       >>>>>>>>>>>>> DETERMINATION OF THE WIDTH OF THE ACTIVE ZONE FROM
C       >>>>>>>>>>>>>>>>>>> THE RATIO OF RECIRCULATED MASS TO TOTAL MASS
C
   79 GO TO (96,97),METOP
   96 WRITE(6,15)
      GO TO 98
   97 WRITE(6,16)
   98 WRITE (6,33)
      QA = Q * FACTER *TD / CTOT
      WA = QA * TDA / L / D
      CALL DSBETA(TDA,EA,FP1,WA,BETA,DS)
C
C >>>>>>>>>>>>>>>>>>>>>>>>>>>>>>>>>>>>>>>>>>>>>>>>>>>>>>>>>>> PLOT COMMANDS
C
      CALL FINITE(BETA,DS,EA,FINAL,260,65,COUT,XT,C,IAXIS,IPLOT,ITER)
      IGRAPH = IGRAPH + 1
      IGRD2 = IGRAPH / 2
      IF ( IGRD2*2.NE.IGRAPH ) WRITE(6,20)
C
C       >>>>>>>>>>>>>>>>>>>>>>>>>>>>>>>>>>>>>>>>>>>>>>>>>>>>> METOPT CONTROL
C
   78 GO TO (60,60,73,60),METOPT
C
C >>>>>>>>>>>>>>>>>>>>>>>>>>>>>>>>>>>>>>>>>>>>>> FERRARA AND HARLEMAN'S METHOD
C
   60 READ (5,8) IFER
      READ (5,3) DS,DDS,NDS
      IIFER = 0
      IF ( NDS.EQ.0 ) GO TO 74
      DSI = DS
      DS = DSI - DDS
      DO 72 II = 1,NDS
      DS = DS + DDS
C
C       >>>>>>>>>>>>>>>>>>>>>>>>>>>>>>>>>>>>>>>>>>>>>>>>>>>>>>>>> IFER CONTROL
C
   74 GO TO (81,82,83,86,77),IFER
   86 IIFER = 1
   81 FP1 = FP11
      TDA = TDA1
      LEAOP = 1
      IF (IIFER.EQ.1) IFER = 2
      WRITE(6,15)
      WRITE(6,17)
      GO TO 85
   82 FP1 = FP12
      TDA = TDA2
      LEAOP = 1
      IF (IIFER.EQ.1) IFER = 3
      WRITE(6,16)
      WRITE(6,17)
      GO TO 85
   83 WRITE(6,19)
      WRITE(6,17)
      TDA = (TDA2 + TDA1) / 2.0
```

```
      LEADP = 2
      IF (IIFER.EQ.1) IFER = 1
   85 CALL BETADS (EA,BETA,DS,LEADP,FP1,TOA)
C
C  >>>>>>>>>>>>>>>>>>>>>>>>>>>>>>>>>>>>>>>>>>>>>>>>>>>>>>>>>>>> PLOT COMMANDS
C
      CALL FINITE(BETA,DS,EA,FINAL,260,65,COUT,XT,C,IAXIS,IPLOT,ITER)
      IGRAPH = IGRAPH + 1
      IGRD2 = IGRAPH / 2
      IF ( IGRD2*2.NE.IGRAPH ) WRITE(6,20)
      IF (IIFER.LQ.0) GO TO 72
C
C     >>>>>>>>>>>>>>>>>>>>>>>>>>>>>>>>>>>>>>>>>>>>>>>>>>>>>>>>>>>> IFER CONTROL
C
      GO TO (72,82,83,77,77),IFER
   72 CONTINUE
   77 WRITE(6,31) ((FINAL(M,N),N=1,4),M=1,MCOUNT)
C
C     >>>>>>>>>>>>>>>>>>>>>>>>>>>>>>>>>>>>>>>>>>>>>>>>>>>>>>>>>>>> PLOT COMMANDS
C
      IF (PLOTOP .NE. 1) GO TO 100
      CALL PLOT (0.0,0.0,999)
  100 STOP
C     ****************************************************************
C     *                                                  INPUT FORMATS*
C     ****************************************************************
    1 FORMAT (3X,I2,4X,F6.2,8X,F6.5,8X,3(F4.2,5X))
    2 FORMAT (/,8(12(F4.1,1X)/))
    3 FORMAT (7(/),6X,F5.3,5X,F5.3,5X,I1)
    4 FORMAT (5(/),52X,I1,9(/),37X,F5.3,/,26X,E9.3)
    5 FORMAT (11X,A8)
    6 FORMAT (/,22X,I1)
    7 FORMAT (42X,I2)
    8 FORMAT (2(/),39X,I1)
    9 FORMAT (52X,F6.1)
  201 FORMAT (58X,I1)
C     ****************************************************************
C     *                                                 OUTPUT FORMATS*
C     ****************************************************************
   10 FORMAT (/,'INPUT DATA',/,
     C6X,'NUMBER OF DATA POINTS (FLUOROMETER READINGS) = ',I2,/,
     C6X,'TIME INTERVAL = ',F7.4,' SECONDS',/,
     C6X,'FLOW RATE = ',F6.3,' CUBIC METRES PER SECOND',/,
     C6X,'DEPTH OF WATER = ',F5.3,' METRES',/,
     C6X,'WIDTH OF MODEL = ',F4.2,' METRES',/,
     C6X,'LENGTH OF MODEL = ',F4.2,' METRES')
   11 FORMAT (/,/,'FLUOROMETER READINGS',/,8(6X,10(F5.2,1X),/))
   12 FORMAT (/,'ROMBERG TABLEAU FOR NUMERICAL INTEGRATION OF THE'
     C/,'AREA UNDER THE CONCENTRATION VS TIME CURVE')
   13 FORMAT (6X,7(F7.0,1X))
   14 FORMAT (/,'LARGEST DIMENSIONLESS CONCENTRATION IN THE',
     C' INPUT DATA = ',F5.2,'.',/,'IT WAS REACHED AT T/TD = ',
     CF5.3,' .',8(/))
   15 FORMAT (/,/,'D/UL WAS ESTIMATED FROM THE PEAK CONCENTRATION ON '
     C,'THE EXPERIMENTAL CURVE')
```

```
   16 FORMAT (/,/,'D/UL WAS ESTIMATED FROM THE VARIANCE OF THE OUTPUT '
     C,'DYE TRACER CURVE')
   17 FORMAT (/,'WA WAS ESTIMATED FROM THE ENTERED VALUE OF DS')
   18 FORMAT (30X,'RUN NUMBER: ',A8)
   19 FORMAT (/,/,'D/UL WAS CALCULATED FROM FISCHER',1H',',S EQUATION')
   20 FORMAT (4(/))
   21 FORMAT (/,53HWA WAS ESTIMATED FROM FISHER'S EQUATION AND THE ROUGH
     C,'NESS COEFFICIENT')
   22 FORMAT (/,53HWA WAS ESTIMATED FROM FISHER'S EQUATION AND THE SLOPE
     C,' OF THE ENERGY GRADE LINE')
   23 FORMAT (/,25HNORMALIZED CONCENTRATIONS,/,8(8X,10(F5.2,1X),/))
   28 FORMAT('THE DETENTION TIME FOR THE BASIN IS ',F7.1,' SECONDS')
   29 FORMAT(/,'THE VOLUME OF THE BASIN IS ',F6.2,' CUBIC METRES')
   31 FORMAT(10(/),15X,'RESULTS OF TESTS',/,/,9X,'EA',10X,'DS',6X,'BETA'
     C,5X,'ERROR',/,30(6X,E8.3,4X,F6.3,4X,F6.3,4X,F7.3,/))
   32 FORMAT('TIME REQUIRED TO RETURN TO A ZERO DYE CONCENTRATION IS ',
     CF6.0,' SECONDS')
   33 FORMAT(/,'WA WAS ESTIMATED FROM THE RATIO OF THE ACTIVE MASS TO '
     C,'THE TOTAL MASS')
   34 FORMAT(6X,48HTHE VALUE OF MANNING'S ROUGHNESS COEFFICIENT IS ,
     CF5.3,/,6X,38HTHE SLOPE OF THE ENERGY GRADE LINE IS ,E8.3)
      END
C     ##########################################################
C     #                                                  TROMB #
C     ##########################################################
      SUBROUTINE TROMB( NMAX, A, B, F, T, JMAX, DT )

C     THE SUBROUTINE TROMB FIRST APPROXIMATES THE INTEGRAL OF
C     F(X)*DX ON THE INTERVAL USING THE TRAPEZOIDAL RULE
C     WITH REPEATED INTERVAL HALVING.  T(N+1,1) IS THE VALUE
C     OF THE INTEGRAL COMPUTED AFTER THE N(TH) INTERVAL-HALVING
C     OPERATION.  ALL T(N+1,1) VALUES ARE COMPUTED FOR N = 0 TO
C     N = MAX .  B IS THE NUMBER OF ELEMENTS IN F(X) - 1.
C     REMAINING ELEMENTS OF THE ROMBERG TABLEAU ARE THEN ENTERED
C     INTO THE FIRST JMAX COLUMNS OF THE FIRST NMAX+1 ROWS OF THE
C     MATRIX T.

      DIMENSION T(7,7),F(65)
      INTEGER A,B

C     ..... COMPUTE H AND FIRST INTEGRAL APPROXIMATION .....

      H = B - A
      HL = H * DT
      T(1,1) =(F(A) + F(B)) * HL / 2.0

C     ..... HALVE INTERVAL REPEATEDLY, COMPUTE T(N+1,1) .....

      DO 2 N = 1,NMAX
      T(N+1,1) = 0.0
      IFR = H / 2.0**N
      ITN = 2.0**N
      IMAX = IFIX(ITN) - 1
      IFRC = A - IFR
      DO 1 I = 1,IMAX,2
```

```
      IFRC = IFRC + IFR * 2
    1 T(N+1,1) = T(N+1,1) + F(IFRC)
    2 T(N+1,1) = T(N,1)/2.0 + HL * T(N+1,1) / 2.0**N
C
C     ..... COMPUTE ROMBERG TABLEAU .....
C
      DO 3 J = 2,JMAX
      NXMJP2 = NMAX - J + 2
      FORJM1 = 4.0**(J-1)
      DO 3 N = 1,NXMJP2
    3 T(N,J) = (FORJM1*T(N+1,J-1) - T(N,J-1))/(FORJM1 - 1.0)
      RETURN
      END
C     ***************************************************************
C     *                                                        SIMP *
C     ***************************************************************
      SUBROUTINE SIMP (IACT,C,DT,CTOT)
C
C     THIS SUBROUTINE CALCULATES THE AREA UNDER THE CONCENTRATION
C     VERSUS TIME CURVE THAT IS ATTRIBUTED TO OUTFLOW FROM THE ACTIVE
C     ZONE BEFORE ANY RECIRCULATED DYE REACHES THE OUTFLOW
C
      DIMENSION C(67)
      CTOT = 0.0
      IM2 = IACT - 2
      DO 1 I = 1,IM2,2
      J = I
    1 CTOT = CTOT + C(I) + C(I+2) + 4.0 * C(I+1)
      CTOT = CTOT / 3.0
      IF (IM2.EQ.J) GO TO 2
      CTOT = CTOT + (C(IACT) + C(IACT-1)) / 2.0
    2 CTOT = CTOT * DT
      RETURN
      END
C     ***************************************************************
C     *                                                        CMAX *
C     ***************************************************************
      SUBROUTINE CMAX( N, X, J, XMAX)
C
C         THIS SUBROUTINE FINDS THE LARGEST VALUE OF AN ARRAY, "X(N)"
C         AND RETURNS ITS VALUE, "XMAX" ALONG WITH THE LOCATION IN THE
C         ARRAY AT WHICH THIS VALUE WAS FOUND, "J".
C
      DIMENSION X(67)
      XMAX = X(1)
      J = 1
      IF (N .EQ. 1) GO TO 1
      DO 2 I = 2,N
      IF (X(I) .LE. XMAX) GO TO 2
      XMAX = X(I)
      J = I
    2 CONTINUE
    1 RETURN
      END
C     ***************************************************************
```

```
                                                                      DSBETAR
C     *
C     ***********************************************************************
      SUBROUTINE DSBETA (TDA,EA,FP,WA,BETA,DS)
C
C        THIS SUBROUTINE COMPUTES AND PRINTS THE VALUE OF VARIOUS
C        PARAMETERS.
C
      COMMON L,ND,DT,TD,W,D,Q,MANING,V
      REAL L,MANING
      QA = L * WA * D / TDA
      DS = QA / Q
      UA = QA / WA / L
      EA = FP * UA * L
      WRITE (6,171)
  171 FORMAT(/,10X,'FINITE DIFFERENCE SOLUTION',/)
      WRITE (6,1) EA
    1 FORMAT(5X,'THE DISPERSION COEFFICIENT IS ',F8.3,' METRES SQUARED'
     C' PER SECOND')
      WRITE (6,2) DS
    2 FORMAT(5X,'THE DILUTION RATIO IS ',F4.2)
      BETA = WA / W
      WRITE (6,3) BETA
    3 FORMAT(5X,'THE RATIO OF THE VOLUME OF THE ACTIVE ZONE TO THE ',
     C'TOTAL VOLUME IS ',F5.3)
      WRITE (6,4) TDA
    4 FORMAT(5X,'THE DETENTION TIME IN THE ACTIVE ZONE IS ',F6.1)
      WRITE (6,5) UA
    5 FORMAT(5X,'THE FLOW VELOCITY IN THE ACTIVE ZONE IS ',F7.5)
      RHA = WA * D / (WA + 2.0 * D)
      REY = 4.0 * RHA * UA / 1.50E-06
      WRITE (6,6) REY
    6 FORMAT(5X,'THE REYNOLDS NUMBER IN THE ACTIVE ZONE IS ',F8.0)
      RHR = (W - WA) * D / (W - WA + 2.0 * D)
      REYR = 4.0 * RHR * (QA - Q) / D / (W-WA) / 1.50E-06
      WRITE (6,9) REYR
    9 FORMAT(5X,'THE REYNOLDS NUMBER IN THE RECYCLE ZONE IS ',F8.0)
      RH = W * D / (W + 2.0 * D)
      RY = 4.0 * RH * Q / D / W / 1.50E-06
      WRITE (6,7) RY
    7 FORMAT(5X,'THE REYNOLDS NUMBER FOR THE ENTIRE BASIN IS ',F8.0)
      FRO = Q / D / W / SQRT(9.81 * D)
      WRITE (6,8) FRO
    8 FORMAT(5X,'THE FROUDE NUMBER FOR THE ENTIRE BASIN IS ',F8.6)
      RETURN
      END
C     ***********************************************************************
C     *                                                              BETADSR
C     ***********************************************************************
      SUBROUTINE BETADS (EA,BETA,DS,LEADP,FP1,TLA)
C
C        THIS SUBROUTINE COMPUTES AND PRINTS THE VALUE OF VARIOUS
C        PARAMETERS.
C
      COMMON L,ND,DT,TD,W,D,Q,MANING,V
      REAL L,MANING
```

```
      WRITE (6,171)
  171 FORMAT(/,10X,'FINITE DIFFERENCE SOLUTION',/)
      QA = Q * DS
      BETA = TDA * QA / V
      WA = W * BETA
      UA = QA / WA / D
      GO TO (9,14), LEADP
   14 EA = 1.101126 * UA * MANING * WA**2.0 * ((WA+2.)*D)/WA/D)**(7./6.
      GO TO 12
    9 EA = FP1 * UA * L
   12 WRITE (6,1) EA
    1 FORMAT(5X,'THE DISPERSION COEFFICIENT IS ',E9.3,' METRES SQUARED'
     C' PER SECOND')
      WRITE (6,2) DS
    2 FORMAT(5X,'THE DILUTION RATIO IS ',F4.2)
      WRITE (6,3) BETA
    3 FORMAT(5X,'THE RATIO OF THE VOLUME OF THE ACTIVE ZONE TO THE ',
     C'TOTAL VOLUME IS ',F5.3)
      WRITE (6,4) TDA
    4 FORMAT(5X,'THE DETENTION TIME IN THE ACTIVE ZONE IS ',F6.1)
      WRITE (6,5) UA
    5 FORMAT(5X,'THE FLOW VELOCITY IN THE ACTIVE ZONE IS ',F7.5)
      RHA = WA * D / (WA + 2.0 * D)
      REY = 4.0 * RHA * UA / 1.50E-06
      WRITE (6,6) REY
    6 FORMAT(5X,'THE REYNOLDS NUMBER IN THE ACTIVE ZONE IS ',F8.0)
      RHR = (W - WA) * D / (W - WA + 2.0 * D)
      REYR = 4.0 * RHR * (QA - Q) / D / (W-WA) / 1.50E-06
      WRITE (6,19) REYR
   19 FORMAT(5X,'THE REYNOLDS NUMBER IN THE RECYCLE ZONE IS ',F8.0)
      RH = W * D / (W + 2.0 * D)
      RY = 4.0 * RH * Q / D / W / 1.50E-06
      WRITE (6,7) RY
    7 FORMAT(5X,'THE REYNOLDS NUMBER FOR THE ENTIRE BASIN IS ',F8.0)
      FRD = Q / D / W / SQRT(9.81 * D)
      WRITE (6,8) FRD
    8 FORMAT(5X,'THE FROUDE NUMBER FOR THE ENTIRE BASIN IS ',F8.6)
      RETURN
      END
C     ******************************************************************
C     *                                                          FINITE*
C     ******************************************************************
      SUBROUTINE FINITE(BETA,DS,EA,FINAL,N,M,COUT,XT,C,IAXIS,IPLOT,ITER)
      DIMENSION ALPHA(260),DD(260),CC(260),COUT(67),FINAL(30,4),C(67),
     CXT(67)
      COMMON L,ND,DT,TD,W,D,Q,MANING,V,MCOUNT,PLOTOP
      REAL L
      INTEGER PLOTOP
      ITERXM = ITER * M
      DELTAX = L / FLOAT(N)
      DELTAT = FLOAT(ND) * DT / FLOAT(M) / FLOAT(ITER)
      CINM = TD / DELTAT / DS
      CINMP1 = 0.0
      CCM = 0.0
      CMASSP = 0.0
```

```
      COUTM = 0.0
      COTMP1 = 0.0
      DO 1 I = 1,N
    1 CC(I) = 0.0
      WA = W * BETA
      U = DS * Q / WA /D
      QA = U * D * WA
      CALL COALFA (DELTAX,DELTAT,EA,U,ALPHA,AD,EE,CF,N)
      COUT(1) = 0.0
      DO 2 I = 2,M
      DO 2 III = 1,ITER
      CALL MATDD(N,CC,DD,AD,BE,CF,CINM,CINMP1)
      CALL SDCC(ALPHA,DD,CC,AD,CF,N)
      CALL CORR (CC,N,WA,D,CINMP1,CINM,COUTM,COTMP1,CMASSP,C,DS,DELTAT,
     CDELTAX)
      COUTM = COTMP1
      COTMP1 = CC(N)
      COUT(I) = (COTMP1 + COUTM) / 2.0
      CCM = (CCM*V*(1.-BETA)+(COUT(I)-CCM)*(DS-1.)*Q*DELTAT)/V/(1.-BETA
      CINMP1 = CINM
    2 CINM = (DS-1.0) * CCM / DS
      WRITE (6,26) (COUT(I),I=1,ND)
   26 FORMAT (/,23HCOMPUTED CONCENTRATIONS,/,8(6X,12(F5.2,1X),/))
      IF (PLOTOP .NE. 1) GO TO 3
      IF(QA.LT.0) GO TO 3
      CALL FLIPLT(XT,C,IAXIS,COUT,ND,IPLOT,BETA,DS,EA,PLOTOP)
    3 CALL ERROR(C,COUT,ND,ERR)
      MCOUNT = MCOUNT + 1
      FINAL(MCOUNT,1) = EA
      FINAL(MCOUNT,2) = DS
      FINAL(MCOUNT,3) = BETA
      FINAL(MCOUNT,4) = ERR
      RETURN
      END
C     ******************************************************************
C     *                                                          COALFA *
C     ******************************************************************
      SUBROUTINE COALFA(DX,DT,D,U,ALPHA,A,E,C,N)
      DIMENSION ALPHA(200)
      C = DT * D / DX ** 2.0
      S = DT * U / DX
      A = C + S
      B = 2.0 * (1.0 + C) + S
      E = 2.0 * (1.0 - C) - S
      B1 = B - C
      ALPHA(1) = B1
      NM1 = N - 1
      DO 1 I = 2,NM1
    1 ALPHA(I) = B - A * C / ALPHA(I-1)
      ALPHA(N) = B1 - A * C / ALPHA(N-1)
      RETURN
      END
C     ******************************************************************
C     *                                                          MATDD *
C     ******************************************************************
```

```
      SUBROUTINE MATDD(N,CC,DD,D,E,F,CINM,CINMP1)
      DIMENSION CC(260),DD(260)
      NM1 = N - 1
      DO 1 I = 2,NM1
    1 DD(I) = D * CC(I-1) + E * CC(I) + F * CC(I+1)
      DD(1) = F * CC(2) + (E + F)* CC(1) + (D - F) * (CINM + CINMP1)
      DD(N) = D * CC(N-1) + (E+F) * CC(N)
      RETURN
      END
C     ##################################################################
C     #                                                          SDCC  #
C     ##################################################################
      SUBROUTINE SDCC(ALPHA,DD,CC,A,C,N)
      DIMENSION ALPHA(260),DD(260),CC(260),SD(260)
      SD(1) = DD(1)
      DO 1 I = 2,N
    1 SD(I) = DD(I) + A * SD(I-1) / ALPHA(I-1)
      CC(N) = SD(N) / ALPHA(N)
      IF (CC(N)) 4,4,5
    4 CC(N) = 0.0
    5 NM1 = N - 1
      DO 2 I = 1,NM1
      CC(N-I) = (SD(N-I) + C * CC(N+1-I)) / ALPHA(N-I)
      IF (CC(N-I)) 3,3,2
    3 CC(N-I) = 0.0
    2 CONTINUE
      RETURN
      END
C     ##################################################################
C     #                                                          CORR  #
C     ##################################################################
      SUBROUTINE CORR(CC,N,WA,D,CINMP1,CINM,COUTM,COUTMP1,CMASSP,Q,DS,
     CDELTAT,DELTAX)
      DIMENSION CC(260)
      CSUM = 0.0
      DO 1 J = 1,N
    1 CSUM = CSUM + CC(J)
      CMASS = CSUM * DELTAX * WA * D
      CTRUE = CMASSP + (CINM+CINMP1-COUTM-COUTMP1) * Q * DS * DELTAT /2.
      IF (CTRUE .LE. 0.0) GO TO 4
      IF (ABS(CMASS - CTRUE) / CTRUE .LE. 0.000001) GO TO 2
      DO 3 I = 1,N
    3 CC(I) = CC(I) * CTRUE / CMASS
      GO TO 2
    4 CTRUE = 0.0
    2 CMASSP = CTRUE
      RETURN
      END
C     ##################################################################
C     #                                                          ERROR #
C     ##################################################################
      SUBROUTINE ERROR (A,B,N,ERR)
      DIMENSION A(67),B(67)
      S = 0.0
      DO 1 I = 1 ,N
```

```
      1 S = S + (ABS (A(I)-B(I)) ) **2.0
        ERR = (S / (N - 1))**0.5
        RETURN
        END
C       ************************************************************
C       #                                                    AXSET#
C       ************************************************************
        SUBROUTINE AXSET(XT,C,I,ND,IPLOTO)
        DIMENSION XT(67),C(67)
        I = I + 1
        IF (I .NE. 1) GO TO 1
        I = 1
        CALL PLOT (3.0,3.0,-3)
        GO TO 5
      1 IF (I .GT. 8) GO TO 2
        CALL PLOT (24.0,0.0,-3)
      5 CALL AXIS (0.0,0.0,6HT / T ,-6,18.0,0.0,XT(ND+1),XT(ND+2))
        CALL SYMBOL (-0.5,9.5,0.28,95,90.0,-1)
        CALL AXIS (0.0,0.0,6HC / C ,6,18.0,90.0,C(ND+1),C(ND+2))
        CALL SYMBOL (9.5,-1.0,0.28,84,0.0,-1)
        CALL FLINE (XT,C,ND,1,0,1)
        CALL GRID (9.0,14.0,2.0,1.0,4,4)
        CALL SYMBOL (9.25,17.375,0.25,29HSYMBOL     EA       DS      BETA,
       C0.0,29)
        GO TO 3
      2 IPLOTO = 0
      3 RETURN
        END
C       ************************************************************
C       #                                                    FLIPLT#
C       ************************************************************
        SUBROUTINE FLIPLT (XT,C,IAXIS,COUT,ND,IPLOT,BETA,DS,EA,IPLOTO)
        DIMENSION XT(67),C(67),COUT(67)
        IPLOT = IPLOT + 1
        IF (IPLOT .LT. 3) GO TO 1
        IPLOT = 0
        CALL AXSET (XT,C,IAXIS,ND,IPLOTO)
        IF (IPLOTO.NE.1) GO TO 5
      1 I = IPLOT + 1
        CALL FLINE (XT,COUT,ND,1,1,IPLOT)
        GO TO (2,3,4),I
      2 CALL SYMBOL(10.0,16.5,0.30,0,0.0,-1)
        CALL NUMBER(11.4,16.375,0.25,EA,0.0,3)
        CALL NUMBER(13.5,16.375,0.25,DS,0.0,2)
        CALL NUMBER(15.5,16.375,0.25,BETA,0.0,2)
        GO TO 5
      3 CALL SYMBOL(10.0,15.5,0.30,1,0.0,-1)
        CALL NUMBER(11.4,15.375,0.25,EA,0.0,3)
        CALL NUMBER(13.5,15.375,0.25,DS,0.0,2)
        CALL NUMBER(15.5,15.375,0.25,BETA,0.0,2)
        GO TO 5
      4 CALL SYMBOL(10.0,14.5,0.30,2,0.0,-1)
        CALL NUMBER(11.4,14.375,0.25,EA,0.0,3)
        CALL NUMBER(13.5,14.375,0.25,DS,0.0,2)
        CALL NUMBER(15.5,14.375,0.25,BETA,0.0,2)
      5 RETURN
        END
```